2002

Dynamic nonlinear optical characterization of asymmetric pentaazadentate porphyrin -like metal complexes for optical power limiting application.

Clare Chisu Byeon
University of Alabama at Birmingham

DYNAMIC NONLINEAR OPTICAL CHARACTERIZATION OF ASYMMETRIC PENTAAZADENTATE PORPHYRIN-LIKE METAL COMPLEXES FOR OPTICAL POWER LIMITING APPLICATION

by

CLARE CHISU BYEON

A DISSERTATION

Submitted to the graduate faculty of The University of Alabama at Birmingham,
in partial fulfillment of the requirements for the degree of
Doctor of Philosophy

BIRMINGHAM, ALABAMA

2002

ABSTRACT OF DISSERTATION
GRADUATE SCHOOL, UNIVERSITY OF ALABAMA AT BIRMINGHAM

Degree Ph.D. Program Physics

Name of Candidate Clare Chisu Byeon

Committee Chair Christopher M. Lawson

Title Dynamic Nonlinear Optical Characterization Of Asymmetric Pentaazadentate Porphyrin-Like Metal Complexes For Optical Power Limiting Application

We introduce a new class of two-dimensional conjugated ring nonlinear optical materials, the asymmetric pentaazadentate porphyrin-like metal complexes [(*R*-APPC)M]Cl_n, for optical power limiting (OPL) application. Series of [(*R*-APPC)M]Cl_n complexes with variability in the phenyl substituents, in the bridging aromatic group in the ring, and in the metal center are characterized for third-order nonlinear optical properties and dynamic photophysical properties.

Degenerate four-wave mixing of [(*R*-APPC)M]Cl_n shows large molecular second-order hyperpolarizabilities, γ, even greater than those of metallophthalocyanines, a well known class of optical limiting materials. The effects on γ due to the structural changes are discussed along with the effect on the linear absorption spectra.

Optical limiting performances of the series are investigated using nonlinear transmission measurements at 532 nm with 5 ns pulses. The results exhibit low limiting threshold fluence and limiting throughput fluence comparable to silicon naphthalocyanine and lead phthalocyanine. The effects of structural variations on nonlinear absorption properties are discussed.

Because excited state absorption is the dominant nonlinear optical process for this series, the dynamic nonlinear properties are discussed from the results of time-resolved

degenerate four-wave mixing (TRDFWM). It is found that at least two different dynamic processes are observable in TRDFWM at 532 nm using a mode-locked picosecond laser. One is a fast process between singlet excited states limited by excitation pulse width (~40 ps), and another is a relatively slower process involving intersystem crossing to the triplet excited state from the singlet excited state.

To understand excited state mechanism further, the lifetime of the singlet excited state has been measured for each complex in the series using the time-correlated single photon counting (TCSPC) method with a femtosecond Ti:Sapphire laser and a fast microchannel plate photomultiplier. The TCSPC results show that the lifetimes of [(*R*-APPC)M]Cl_n are all less than 1 ns. From the previously reported triplet quantum yields, the intersystem crossing rates are found to be quite fast (<1 ns).

These results suggest that [(*R*-APPC)M]Cl_n complexes are very promising candidates for OPLs because these complexes have large optical nonlinearities and exhibit higher flexibility in structures.

DEDICATION

To the ultimate wholeness.

ACKNOWLEDGMENTS

There are many people who helped me through out my graduate study, and I feel deeply grateful for all their support and cooperation.

First of all, many thanks go to my advisor, Dr. Chris Lawson. He has been a great provider and given me every opportunity to be trained as a good independent scientific researcher. I owe him a lot for that.

I would also like to thank Drs. Gary Gray, Ryoichi Kawai, Jimmy Mays, Sergey Mirov, and Thomas Nordlund for serving as members of the dissertation committee. Their resourceful advice and constant encouragement made me come this far. I owe many thanks to them.

Special thanks go to Dr. Wenfang Sun, who supplied the nonlinear optical materials used in this research. Without her, my work was not possible. She also has been a good friend and a helpful chemistry teacher to me.

I also thank Mike Mckerns for his support on various parts of my research, especially for all those discussions, all those arguments, and all the rest.

I cannot forget to acknowledge Dr. David Smith of NASA's Marshall Space Flight Center. He served as a technical advisor when I was a NASA graduate student research program fellow. I can never forget his kindness and warm welcome whenever I visited Marshall Space Flight Center in Huntsville, AL.

I thank Dr. David Shealy, the department chair; Dr. Yogesh Vorha, the graduate program director; and all the rest of faculty in the department. They have given me a chance to start my graduate study, supported me in various ways, taught me courses, and believed in me for these unusually long years of my graduate study.

I would also like to mention the former and current staffs in the department: Kathy Baier, Sharon Bankston, Ginger Hughes, Fay Decastra, Ken Nelson, and Jerry Sewell. These are the people who make my days go smoothly. I express my gratitude to them.

I also thank Neil Jenkins, a former officemate, and Hyunbin Kim and Brian Geislinger, the current officemates, for being with me, laughing with me, eating lunch together, and just watching me live every day with joy and anger, excitement and disappointment, and all the rest. I owe them a great deal of appreciation. I also cannot forget the rest of my fellow graduate students in the department.

As always, I thank my parents, Mr. Yong Suk Byeon and Mrs. Byung Yon Byeon, for their continuous support. They put forth every effort to move the whole family to this blessed country so that I could have a better education and a better life. I can never thank them enough.

Finally, there are people, one big one and two little ones, who have endured as much as I have all these years. They are my family: my wife Lauren Sungsil; my son, Jason Hangyeol; and my newly born daughter, Elaine Yeseul. They are my undying inspiration. For all those moments that I could not be with them, I am forever in debt to them. I cannot thank them enough for their patience, for their support, and just for being home waiting for me.

TABLE OF CONTENTS

TABLE OF CONTENTS (Continued)

Page

CHAPTER

LIST OF TABLES

LIST OF FIGURES

LIST OF FIGURES (Continued)

Figure *Page*

LIST OF ABBREVIATIONS

APPC	Asymmetric pentaazadentate porphyrin-like metal complex
DFWM	Degenerate four-wave mixing
ESA	Excited state absorption or excited state absorber
FWHM	Full width half maximum
IRF	Instrument response function
MCP PMT	Microchannel plate photomultiplier
Nc	Naphthalocyanine
Nd:YAG	Neodymium-doped yttrium aluminum garnet ($Y_3Al_5O_{12}$)
NLO	Nonlinear optics
OPL	Optical power limiting or optical power limiter
PbPc	Lead phthalocyanine
$PbPc(CP)_4$	Lead(II) tetrakis(4-cumylphenoxy) phthalocyanine
Pc	Phthalocyanine
PMT	Photomultiplier
RSA	Reverse saturable absorption or reverse saturable absorber
S_1	First singlet excited state
SA	Saturable absorption or saturable absorber
SiNc	Silicon naphthalocyanine
TCSPC	Time-correlated single photon counting

TPA	Two photon absorption
TRDFWM	Time-resolved degenerate four-wave mixing

CHAPTER 1

INTRODUCTION

Overview and Motivation

It can arguably be said that the 20th century has been the century of electrons. Since the initial developments of quantum theory in early years, much successful research has been based on electronic structure of matter, and electrons have been the most interesting particle in science and engineering. As many new applications involving the science of this much-studied particle were developed, the electronics and electric power industries responded with great products for people to make their everyday life easier and more comfortable. Now at the dawn of 21st century and the new millennium, the trend is shifting toward another fascinating particle, *the photon*, or the light particle. Thus, the new field, *photonics*, arises to study and utilize photons and the relationship with matter. Nonlinear optics (NLO) is one of the backbones of photonics.

Nonlinear optics is the field that studies nonlinear optical phenomena in which the optical properties of medium, such as refraction and transmission become functions of the intensity of the light. Light interacts with light via the medium, and the refractive index and consequently the speed of light do change with the light intensity.

After the discovery of the maser[1,2] and laser,[3,4] lasers have become essential tools as powerful coherent light sources in all areas of science and engineering. As more and more intense lasers with high power output became available, researchers started observing new phenomena that could not be observed with less intense, noncoherent light

sources. Among many new discoveries in the early 1960s, observation of the second harmonic generation by the intense laser light marked the beginning of NLO.[5] Since then, materials with fast and large optical nonlinearities have generated much interest for numerous applications, such as photonic switching for telecommunications.[6]

With the development of high power lasers, various third-order nonlinear materials, such as organic and polymer complexes, have particularly attracted great interest for nonlinear optical applications, such as wave mixings, wave guides, optical phase conjugation, and optical power limiting (OPL). The desirable properties of the third-order nonlinear optical materials include a large nonlinearity, inherently fast response times, broadband spectral responses, and ease of processing and synthesis.[7-9] In general, one can design thermally, mechanically, chemically, and optically quite stable organic systems. The versatility in synthesis gives far greater diversity than most other types of nonlinear materials. Furthermore, the fact that one can control the optical properties of the material by modifying its structure makes organic nonlinear materials the most interesting and exciting class of new optical materials. One can, on the molecular level, engineer, design, and optimize optical properties to perform the particular application. In order to do so, one should first face the challenge of understanding the basic physics of nonlinear optical processes and the mechanisms behind the processes in these organic materials.

In general, an optical electromagnetic field can be completely described by its phase and amplitude. For third-order materials, the third-order susceptibility $\chi^{(3)}$, which is a complex quantity in nature, is the macroscopic physical parameter that describes how the material interacts with the irradiated field by modifying the phase and the amplitude.

The real part of $\chi^{(3)}$ is related to the nonlinear index of refraction and changes the phase of the field, whereas the imaginary part changes the amplitude by nonlinear absorption. Moreover, the real and the imaginary parts are not independent of each other. In addition to $\chi^{(3)}$, the second-order molecular hyperpolarizability, γ, is the microscopic quantity that characterizes the third-order optical nonlinearity. Although the nature of β, the first-order molecular hyperpolarizability, and the optimization of β are well studied in general, the optimization of γ is somewhat more difficult due to more complicated physics involved.

It should be noted that comparison of the third-order nonlinearity among various optical materials in today's literature has some practical difficulties for several reasons. First, the third-order optical nonlinearity can be reported in various forms, such as the bulk property $\chi^{(3)}$, the nonlinear refractive index n_2, or alternatively the corresponding molecular quantity, the concentration-independent microscopic hyperpolarizability, γ. Moreover, the definitions of these quantities depend not only on the unit system of choice (SI vs. esu) but also on how the quantities are defined even within the same unit system (see Appendix). As a result, conversion between different systems of units or between each representation in the same unit system may not be as trivial as one might think. To make the comparison even more difficult, these values are wavelength dependent. To make a legitimate comparison among different materials, one should carefully follow these different definitions and the wavelength dependence of the measurements.

In recent years, organic compounds with extensively delocalized π-conjugated electron systems have received considerable interest for the third-order NLO applications.[10-12] Various organic polymer systems with fairly large third-order optical nonlinearities have been studied.[9,13] For conjugated polymers, where single and multiple

bonds are alternating in chains, it was expected that optical nonlinearity increases with the number of the repeat units.[14] However, the experiments show a more complicated relationship of optical nonlinearity and the chain structure of the polymer systems. Zhao *et al.*[15] performed a systematic study of polarizability and the third-order optical nonlinearity in thiophene oligomers by measuring the second-order molecular hyperpolarizability on the number of repeat units. The results show the rapid increase of γ values of the polymer with the increase in the number of repeat units. Another work on thiophene (2,5-didecylhexathiophene) by Hein *et al.*[16] shows a similar increase of γ up to 5 chain units; the rate of the increase slows down after 5 units. Frazier *et al.*[17] and Porter *et al.*[18] also performed very similar measurements on platinum and palladium poly-ynes. Their results[17,18] suggest that optical nonlinearity generally increases with the number of the repeat units, but only increases to the certain number of the repeat units and with the certain substituents. The experimental work by Flom *et al.*[19] also indicates that the third-order nonlinearity is not simply correlated with the delocalization length of the conjugate systems. Recently, Gubler *et al.*[20] reported the investigation of poly(triacetylene) oligomers with several monomer units using degenerate four-wave mixing (DFWM) and the third harmonic generation. The results show that the chain-length dependence of γ of poly(triacetylene) oligomers follows a power law ($\gamma \propto n^{\alpha}$, n is the number of the chain) for short oligomers and that this power law saturates around n=9-10. The γ values of all these polymers range from about 10^{-36} to 10^{-32} esu.

More interesting groups of complexes are two-dimensional delocalized conjugated π-electron systems.[21] Among those macrocycles, some extensive research have been done on metallophthalocyanines[22,23] and metalloporphyrins[24,25] because of

their relatively large third-order susceptibilities, inherently fast response times, and chemical and thermal stability.

The experimental results of Shirk *et al.*[26] show that the third-order susceptibility of metal-free phthalocyanine (Pc) is enhanced 45 times by inserting a metal ion. These authors[26] reported $\chi^{(3)}$ values for tetrakis(cumylphenoxy) phthalocyanine with Pt ion as high as 2×10^{-10} esu (at 1064 nm), and also reported $\chi^{(3)}$ values for lead phthalocyanine (PbPc) as 2×10^{-11} esu (at 1064 nm) in the same paper. The $\chi^{(3)}$s of bis(phthalocyanine) complexes with various metal centers (Sc, Lu, Yb, Y, Gd, Eu, Nd) were reported by the same group.[27] Their γ values ranged from 15 to 48×10^{-32} esu (at 1064 nm). More recently, other groups[22,25,28-34] reported similar results using various metal centers and substituents in Pc and naphthalocyanine (Nc).

Porphyrin, very similar to Pc in structure, has only four N atoms in its conjugated ring structure; however, there are eight N atoms in Pc. Indeed, Pc is considered to be a porphyrin derivative. For this reason, many of metalloporphyrins are receiving the same type of attention as metallophthalocyanines. Rao *et al.*[24] have performed extensive measurements on $\chi^{(3)}$ of a series of tetrabenzporphyrins with different substituent groups and metal centers, Zn and Mg, and reported $\chi^{(3)}$ values 4 to 5 orders larger than carbon disulfide, a common reference material in third-order NLO. The effects of metal substitution and various axial ligands on the third-order optical nonlinearity of porphyrins were also studied in detail by Kandasamy *et al.*[35]

Metallophthalocyanines and metalloporphyrins in general show large third-order nonlinearities and fast response times. The γ values of these materials can vary with different substituents and metal centers. One of the most popular third-order NLO

applications for these type of materials is OPL. OPL is achieved when a material shows a strong nonlinear absorption, such as reverse saturable absorption (RSA). The transmission of light depends on the intensity or the fluence of input light. At the exposure to low intensity light, an OPL transmits the input light without much loss. At the higher intensity/fluence, however, the output is clamped out due to nonlinear absorption providing the proper protection for optical sensors, especially human eyes.

The need for passive optical limiters to protect human eyes and sensors from intense optical beams has generated much interest in the development of optical limiting materials. Power limiters based on nonlinear absorption, such as diphenyl polyenes,[36] indanthrone dyes,[37] and fullerenes,[38] along with metallophthalocyanines[39-44] and metalloporphyrins, [45,46] have been studied extensively. Metallophthalocyanines and metallonaphthalocyanines are among the most promising materials[38,42,45,47] for use in these devices because of their relatively low linear absorption and high ratios of the excited state to the ground state absorption cross sections (σ_e/σ_g) in the 450~600 nm region. The use of these complexes is limited, however, by their relatively high linear absorption outside of the 450~600 nm region and, in some cases, by the low quantum yields of their triplet excited states. The triplet quantum yield is one of the important parameters in nanosecond excitation because optical limiting occurs mainly due to the nonlinear absorption in triplet-triplet transitions for these materials. Moreover, metallophthalocyanines and metallonaphthalocyanines, like regular metalloporphyrins, have a very rigid ring structure so that any addition of ligands or substituents must be made either axially through the metal center or at the periphery of the ring structure (see FIG. 1). In addition, it is impossible to change the conjugated π-electron structure of

theses complexes. The conjugated π-electron is one of the key variations to manipulate the nonlinear optical properties by the structural modification. Because the ring structure cannot be modified, the size of the metal center is also limited. With large metal centers (Pb, Si), the metal center cannot stay at the same plane with the ring structure, which in general counteracts the increases in the third-order optical nonlinearity. As a result, new types of optical limiters are in high demand today in many areas, such as commercial telecommunication and military applications.

Recently, we began to study a new class of expanded metalloporphyrin complexes, asymmetric pentaazadentate porphyrin-like metal complexes [(*R*-APPC)M]Cl_n, as OPLs.[48,49] These complexes have two-dimensional delocalized conjugated π-electron systems and exhibit strong third-order nonlinearities just like metallophthalocyanines and regular metalloporphyrins.[50] However, unlike metallophthalocyanines and regular metalloporphyrins, the ring structures of these complexes can be readily modified as seen in FIG. 2. Such structural modifications should allow [(*R*-APPC)M]Cl_n complexes with optimal photophysical properties for a variety of applications, such as OPL, to be developed.

The main mechanism contributing to OPL in these complexes is excited state absorption (ESA) or RSA in which the molecules are excited to the higher excited states by the absorption of additional photons after the initial excitation from the ground state to the first excited state (linear absorption). By definition, the ESA cross section must be greater than the ground state absorption cross section ($\sigma_e > \sigma_g$) to achieve an RSA. In general, Pcs and porphyrin derivatives show a mixed form of RSA and two photon absorption.[51] We expect our [(*R*-APPC)M]Cl_n complexes have mainly ESA at 532 nm,

the wavelength at which all of our nonlinear absorption measurements are made. Many ESAs, such as metallophthalocyanines,[39,41,43,52,53] regular metalloporphyrins,[45,46,51,54,55] and expanded metalloporphyrin complexes,[56-58] have been studied as possible candidates for OPLs.

All the materials mentioned previously have relatively high third-order nonlinearities and fairly competitive optical limiting performances. Nevertheless, most research has been focused on reporting the third-order nonlinear susceptibilities or the performance parameters, such as limiting thresholds and clamped limiting throughputs, of many different materials. In today's literature, one can rarely find a report clearly stating a systematic way of enhancing the nonlinearity or optical limiting performance by relating the main parameters, such as nonlinear susceptibility and various photophysical properties involved with the optical limiting performance, to the chemical structure. We know that certain complexes have greater ESA cross sections, longer excited state lifetimes, fast intersystem crossing, or higher triplet quantum yields and that certain complexes perform better optical limiting than others. However, which parameters are the main optimization factors and why certain complexes are better optical limiters than the others are still big mysteries, probably due to the complicated nature of different photophysical and nonlinear optical processes.

The ultimate goal is to develop a better OPL by a systematic optimization of the chemical structure of a series of [(*R*-APPC)M]Cl_n complexes. To do so, it is essential that we know which photophysical properties are the main contributors to OPL and how these properties are related to the variation of the chemical structure, such as in the metal centers and in the conjugated ring structures. Without these kinds of information, the

random trials of different materials, which routinely appear in much current literature, are the only means of developing the desired device.

The main objectives of this dissertation research are to evaluate the optical limiting performance of the preliminary [(*R*-APPC)M]Cl_n complexes and to provide detailed analysis about the effects on linear and nonlinear optical properties due to structural modifications, such as the variation on phenylene substituents, on bridging group in the conjugated ring structure, and on the metal centers. The research activities include several experimental tasks that can provide or estimate some of the basic properties associated with the nonlinear absorption process, such as ESA cross sections, lifetimes of the excited states, and intersystem crossing rates. Moreover, this work also provides the experimental data essential to the numerical fitting of a computational model that is in progress and expected to be complete in the near future.

To date, the third-order nonlinear optical properties of only a few [(*R*-APPC)M]Cl_n complexes, [(C_6H_4-APPC)Cd]Cl, [($OCH_3C_6H_3$-APPC)Cd]Cl, and [(C_6H_4-APPC)Gd]Cl_2, have been reported.[58-60] These studies demonstrated that the complexes have large third-order nonlinear optical susceptibilities at both 532 nm[59] and 1064 nm[60] and that [(C_6H_4-APPC)Cd]Cl has a strong RSA for nanosecond pulses at 532 nm.[58] In addition, photolysis studies revealed that these complexes exhibit high intersystem crossing rates and high quantum yields of triplet excited states.[48] These preliminary results are extremely promising but provide no information about the relationship between ligand structure and nonlinear optical properties of the complexes.

To determine the viability of the series of [(*R*-APPC)M]Cl_n complexes as nonlinear optical materials, it is first necessary to evaluate their linear absorption.

Studies on the effects of alternation of the *R* group and metal ion on the linear absorption of some of these complexes were reported previously.[48,61] The results revealed that the maxima of the linear absorption peaks, mainly the *Q*(0,0) band (transition from the lowest vibrational ground state to the lowest vibrational first excited state), depend on the different secondary phenylene substituents (*R'*, where *R*=*R'*C_6H_3), number of π electrons (18-26), and metal centers (Cd^{2+}, Pd^{2+}, Sm^{3+}). The results also showed that [(*R*-APPC)M]Cl_n complexes can have wider optical windows for the OPL application than the metallophthalocyanines. Recently, we have begun to study the OPL properties of various [(*R*-APPC)Cd]Cl complexes.[61,62] We here investigated the relationship between ligand structure and optical limiting abilities of [(*R*-APPC)Cd]Cl complexes. As will be shown subsequently, variations in the ligand structure have a significant effect on the optical limiting abilities of these complexes, and the nonlinearities of the complexes are sensitive to the nature of the metal centers and ligands. These results suggest that complexes with even larger nonlinearities can be obtained by a judicious choice of ligands and metals.

The large third-order susceptibilities and the competitive preliminary results in optical limiting performance of the series of [(*R*-APPC)M]Cl_n complexes motivated us to investigate further the possibility of structural optimization for developing a better OPLs using these complexes. In this dissertation, we will discuss how nonlinear optical properties and photophysical characteristics are related to the optical limiting performance when the chemical structure is systematically varied. In addition to the basic nonlinear optical properties, such as third-order susceptibility $\chi^{(3)}$, measured by DFWM and thus the second-order molecular hyperpolarizability, γ, the series of

nonlinear optical characterization include OPL performance, measured by nonlinear transmission measurement using a 5 ns *Q*-switched neodymium-doped yttrium aluminum garnet (Nd:YAG) laser; dynamic temporal characteristics of transient excited state population gratings, measured by a separate time-resolved degenerate four-wave mixing (TRDFWM) using a 40 ps *Q*-switched Nd:YAG mode-locked laser; and the singlet excited state lifetime, measurement by time-correlated single photon counting (TCSPC) using a newly purchased femtosecond Ti:Sapphire laser and a fast micro-channel plate photomultiplier (MCP PMT). The series of seven preliminary [(*R*-APPC)M]Cl_n are composed of three types of structural variations; the different secondary phenylene substituents (*R'*=H, OCH_3, NO_2, *R*=*R'*C_6H_3), the bridge groups (R) with different number (18, 22, 26) of conjugated π electrons (*R*=$(NC)_2C_2$, C_6H_4, $C_{10}H_6$), and different metal centers (Cd^{2+}, Pd^{2+}, Sm^{3+}). We will discuss the optical limiting performances, the temporal characteristics of the excited state population gratings, and the lifetime of the first singlet excited states (S_1s) for these seven complexes accordingly. The nonlinear optical characterization presented here is by no means complete; neither do we expect to come up with a perfect optimization method for the best OPL. Our results, however, are a stepping-stone in the progress of gaining a sufficiently good understanding of nonlinear optical characteristics of these materials that optical limiting materials for use in devices can be designed and developed.

Nonlinear Susceptibilities

When an electromagnetic wave propagates through a dielectric medium, the electronic and optical properties of the medium are usually described by the relationship

between the polarization density vector $\mathbf{P}(\mathbf{r},t)$ and the electric field vector $\mathbf{E}(\mathbf{r}, t)$. In a linear medium,

$$\mathbf{P} = \chi \mathbf{E},$$

which indicates that the polarization is proportional to the field. However, at the presence of the highly intense field we can expand $\mathbf{P}$ with higher powers of the field and introduce nonlinear susceptibilities.

$$\begin{aligned} \mathbf{P}_i &= \sum_j \chi^{(1)}_{ij} \cdot \mathbf{E}_j + \sum_{j,k} \chi^{(2)}_{ijk} : \mathbf{E}_j \mathbf{E}_k + \sum_{j,k,l} \chi^{(3)}_{ijkl} : \mathbf{E}_j \mathbf{E}_k \mathbf{E}_l + \cdots \\ &= \mathbf{P}^{(1)} + \mathbf{P}^{(2)} + \mathbf{P}^{(3)} + \cdots. \end{aligned} \tag{1.1}$$

The coefficients $\chi^{(1)}$, $\chi^{(2)}$, and $\chi^{(3)}$ represent the linear, the second- and the third-order susceptibilities and are generally tensors in nature. $\mathbf{P}^{(2)}$ and $\mathbf{P}^{(3)}$ are the nonlinear polarization and are dependent on the higher powers of the fields. In general, the effects due to $\chi^{(2)}$ and $\chi^{(3)}$ are quite small in comparison with the linear susceptibility. Therefore, only in the presence of high magnitude of optical field are the nonlinear optical effects definitely observable, which is why and how the advent of laser physics opened the door to NLO by providing the highly intense optical field sources.

While the polarization $\mathbf{P}$, which is the sum of the individual dipole, and the susceptibilities, χs, describe the macronature of the medium, we can also define corresponding microscopic parameters.

$$\mathbf{P} = \frac{1}{V}\sum_{n=1}^{N} \mathbf{p}_n = \frac{1}{V}\sum_{n=1}^{N} -e\mathbf{x}_n \text{, and}$$

$$\mathbf{p}_i = \sum_j \alpha_{ij} \cdot \mathbf{E}_j + \sum_{j,k} \beta_{ijk} : \mathbf{E}_j \mathbf{E}_k + \sum_{j,k,l} \gamma_{ijkl} : \mathbf{E}_j \mathbf{E}_k \mathbf{E}_l + \cdots, \tag{1.2}$$

where the small $\mathbf{p}_n$ represents the dipole moment of an individual molecule in a volume of interests, V. The corresponding microscopic coefficients α, β, and γ are defined as the linear, the first-order, and second-order molecular hyperpolarizabilities. These higher order molecular hyperpolarizabilities are indeed the fundamental coefficients to quantify the nonlinearity of the materials because they are independent of the concentration or the population.

When the medium has the center of the symmetry under the inversion, such that $\mathbf{r} \rightarrow -\mathbf{r}$ transformation does not change the properties of the medium, the second term in Equations (1.1) and (1.2) must vanish, which means that the medium may not have the symmetry under the inversion to see the second-order nonlinear effects. When there exists the symmetry under the inversion, such as solids in cubic symmetry or liquid medium, the third-order effects are the dominant nonlinear effects.

Nonlinear Absorption and Optical Limiting

An optical limiter is a nonlinear optical device that transmits the low intensity light but blocks the high intensity light via nonlinear absorption. When the strong optical field is propagating through a nonlinear optical medium, the output is clamped out even more due to the nonlinear absorption in addition to the usual linear absorption. The phenomenon in which this intensity -dependent absorption increases is called an RSA, compared with the saturable absorption (SA), where the absorption decreases due to the high input intensity. When the nonlinear absorption occurs, the shape of the output versus the input plot deviates from a straight line. Transmission characteristics of the ideal OPL are illustrated in FIG. 3.

There are two main quantities that characterize the performance of the optical limiter. The limiting throughput fluence ($F_{through}$) is the actual clamped output fluence. Fluence is the optical energy going through a unit of cross-sectional area. It is the optical intensity integrated over the temporal pulse width, such as

$$F(r) = \int I(r,t)dt . \tag{1.3}$$

Fluence is also related to the pulse energy as integration over the whole cross-sectional area,

$$E = \iint F(r)dA. \tag{1.4}$$

The lower the value of $F_{through}$, the better the optical limiter performs. Another important quantity is the limiting threshold fluence, which is the input fluence where the deviation from the linear transmission starts to occur. This threshold value separates the linear transmission region and indicates the region in fluence where the nonlinear transmission occurs. The lower value of F_{th} implies that the device limits the wider range of the fluence.

Two of the most common types of the mechanisms contributing to nonlinear absorption are two photon absorption (TPA) and ESA. Let us assume a simple three level system (see FIG. 4). When the light passes through an optical medium, the change in the intensity can be described as

$$\frac{dI}{dz} = -\alpha I , \tag{1.5}$$

where α is the absorption coefficient.

In a linear medium, α is constant with the field, such as $\alpha = \sigma_g n_g$ (n_g, the steady state population density of the ground state; σ_g the absorption cross section of the ground

state); we can easily get the expression for the output intensity by integrating over the length of the medium.

$$I = I_0 e^{-\alpha L},$$

where I_0 is the input intensity right before the medium and L is the path length of the medium. However, when the absorption is dependent on the intensity, Equation (1.5) should be modified to incorporate with the nonlinear absorption. Equation (1.5) can be rewritten as

$$\frac{dI}{dz} = -\alpha I - \beta I^2 - \sigma_e n_e I . \tag{1.6}$$

The second term in Equation (1.6) corresponds to two photon absorption, and β is the two photon absorption coefficient. The last term corresponds to ESA, and σ_e is the ESA cross section. It should be noted that n_e, the population density of the excited state, is not constant, but is a function of intensity, such as

$$\frac{dn_e}{dt} = \frac{\alpha I}{h\nu} - \frac{n_e}{\tau},$$

where τ is the lifetime of the excited state, ν is the frequency of the excitation light, and h is the Planck constant.

In the next section, we will introduce a new class of nonlinear optical materials that is expected to have great OPL properties, such as large $\chi^{(3)}$, low F_{through} and F_{th}, wide spectral ranges, and fast response.

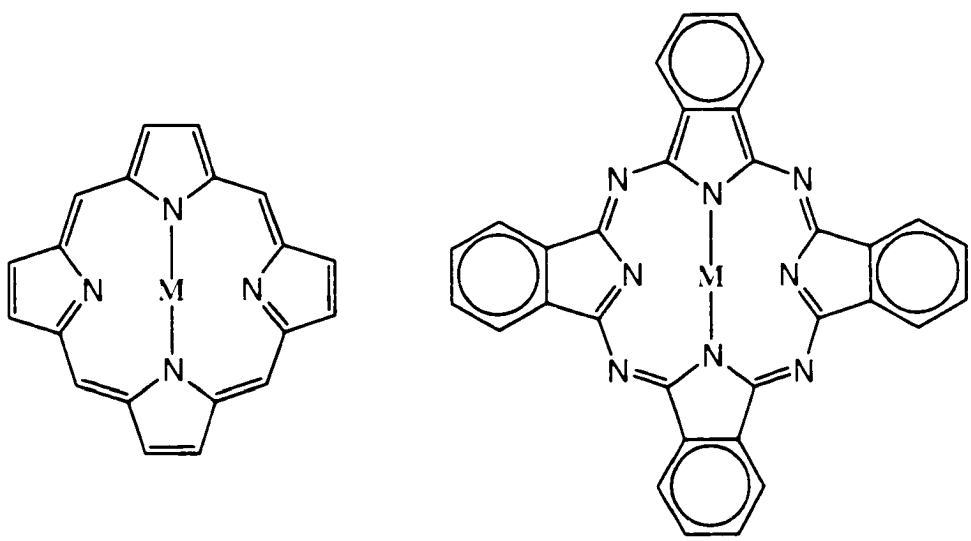

FIG. 1. (a) Metalloporphyrin and (b) metallophthalocyanine. M indicates the metal center.

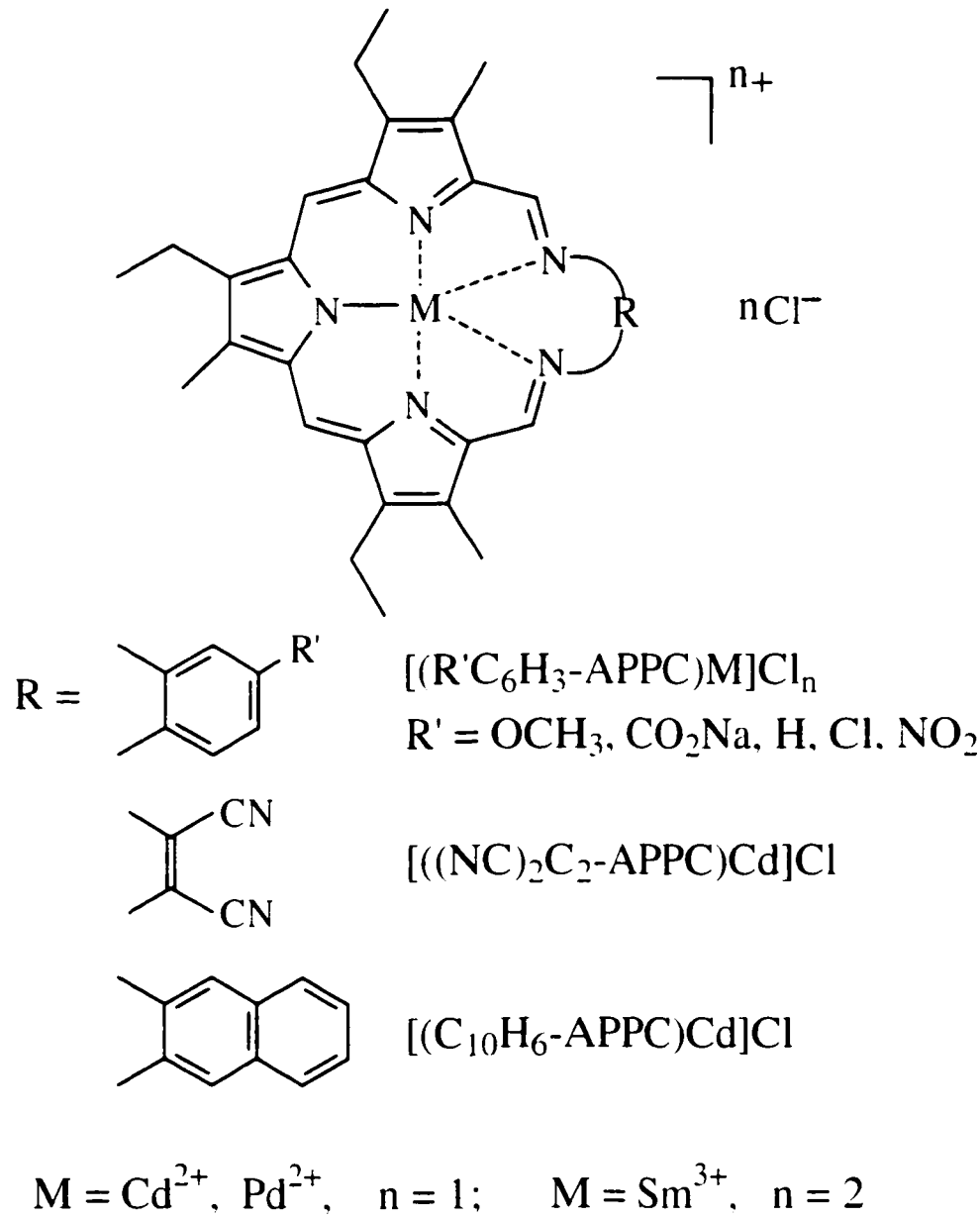

FIG. 2. Chemical structures of [(*R*-APPC)M]Cl_n complexes.

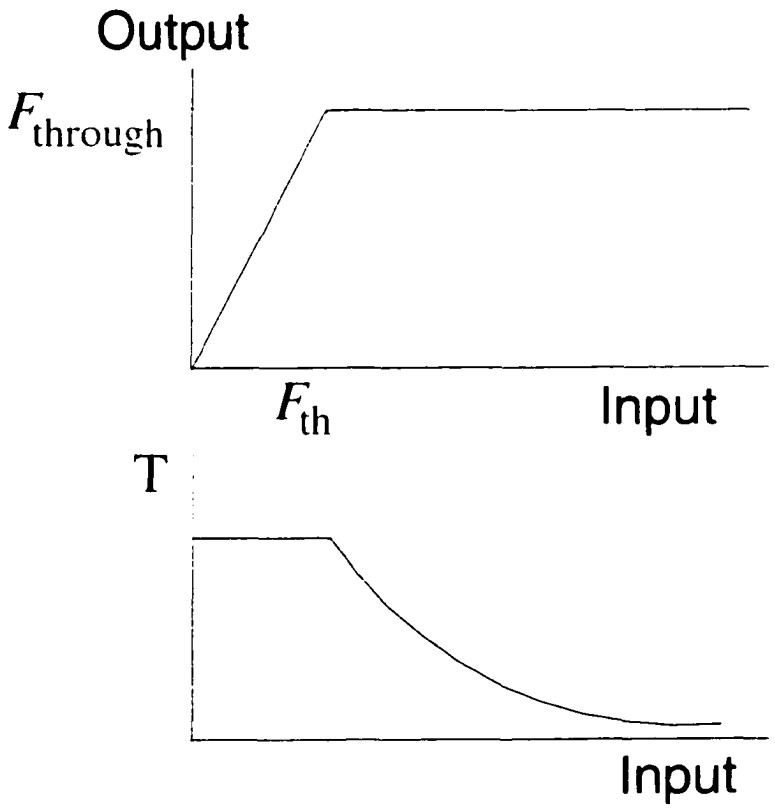

FIG. 3. Ideal optical limiter. The output fluence shows clamping to the throughput fluence, $F_{through}$ after the threshold fluence, F_{th}. The corresponding transmittance, T, is also illustrated as a function of the input fluence.

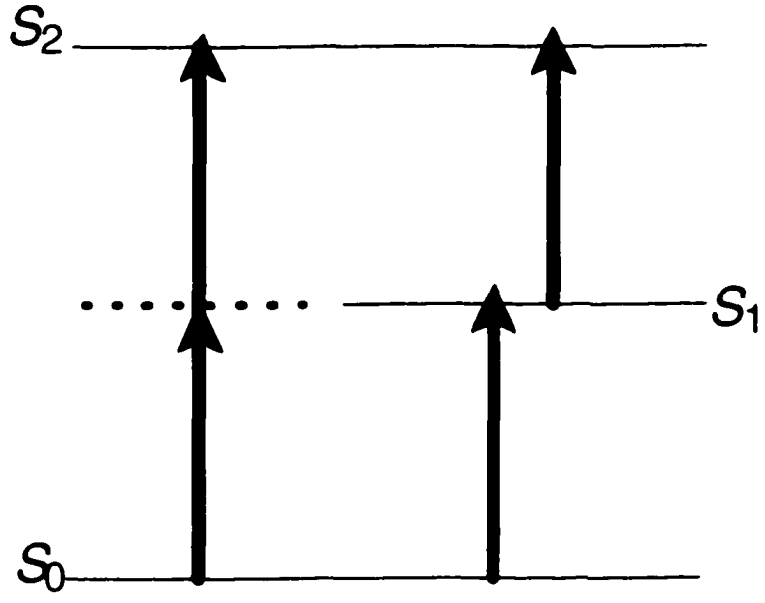

FIG. 4. TPA and ESA. The solid line indicates the presence of an actual state (excited state), and the dotted line indicates a virtual state where two-photon absorption occurs.

CHAPTER 2

ASYMMETRIC PENTAAZADENTATE PORPHYRIN-LIKE METAL COMPLEXES

Structure

The asymmetric pentaazadentate porphyrin-like metal complexes, [(*R*-APPC)M]Cl_n (shown in FIG. 2), are of interest for third-order nonlinear optical applications. The details of the synthesis are well explained in the literature.[48,63] These compounds are stable at room temperature as a solid or in solution in the presence of air. The complexes have two-dimensional delocalized electronic systems and exhibit strong third-order nonlinearities like the metallophthalocyanines and metallonaphthalocyanines. The molecular second-order hyperpolarizabilities for the [(*R*-APPC)Cd]Cl complexes are in the range of 2.6×10^{-31} ~ 1.2×10^{-30} esu, which are significantly larger than those of lead(II) tetrakis(4-cumylphenoxy) phthalocyanine ($PbPc(CP)_4$) and silicon naphthalocyanine (SiNc). [50]

Pc complexes have very rigid ring structures, and the substituents are attached either to the metal center directly as axial ligands or on the periphery of the ring structure. Because the ring is rigidly defined in size, the choices of metal centers in Pc complexes are quite limited. However, unlike metallophthalocyanines and metallonaphthalocyanines, the ring structures of [(*R*-APPC)M]Cl_n complexes can be easily modified so that a more extended conjugate system (18-26 π electrons for our samples) can be obtained. These complexes have more conjugated π electrons than do the

metallophthalocyanines and metalloporphyrins, as well as a variety of metal-to-ligand or ligand-to-metal charge transfer states. In addition, the large core size of the pentaazadentate macrocyclic ligand provides a very stable coordination environment for large metal cations; therefore, the choices for the metal ions are greatly expanded, and nearly coplanar configurations can be formed around the large metal cations. The ability for such structural modifications should allow [(*R*-APPC)M]Cl_n complexes with optimal photophysical properties for a variety of applications to be developed.

Linear Absorption of APPC

To determine the viability of the series of [(*R*-APPC)M]Cl_n complexes as nonlinear optical materials, it is first necessary to evaluate their linear absorption. Studies of the effect of alternation of the *R* group and metal ion on the linear absorption of these complexes were performed, and the results are shown in FIG. 5. The electronic absorption spectrum of [(C_6H_4-APPC)Cd]Cl reveals a strong *Q*(0,0) band absorption at 762 nm and an ~80 nm red-shift with respect to the metallophthalocyanines. Hence, a relatively wide optical window is formed in the 500~660 nm region, wherein RSA may occur. In contrast, the absorption spectra of [($(NC)_2C_2$-APPC)Cd]Cl and [($C_{10}H_6$-APPC)Cd]Cl show a quite different *Q*(0,0) band due to their different numbers of π electrons. Most notably, [($C_{10}H_6$-APPC)Cd]Cl, with its 26 π electrons, exhibits a dramatically bathochromic shift combined with a more extensive window. The absorption spectra of the other four 22 π-electron [($R'C_6H_3$-APPC)Cd]Cl complexes are quite similar to that of [(C_6H_4-APPC)Cd]Cl. Replacing H with the electron donor group, OCH_3, induces a hyperchromic shift of the *Q*(0,0) band to 750 nm; however, replacing H

with the electron withdrawing group, NO_2, induces a bathochromic shift of the $Q(0,0)$ band to 792 nm. In addition, the effect of metal ions on the linear absorption is remarkable. The absorption spectrum of $[(C_6H_4\text{-APPC})Sm]Cl_2$ is quite similar to that of $[(C_6H_4\text{-APPC})Cd]Cl$ and only shows approximately 10 nm bathochromic shifts of the $Q(0,0)$ and B bands. However, the $Q(0,0)$ band of $[(C_6H_4\text{-APPC})Pd]Cl$ exhibits hyperchromic shift to 640 nm, which is probably due to the different coordination geometry of the Pd^{2+} ion and perhaps to the aggregation of complex in solution at high concentration.

Third-order Susceptibilities of APPC

We established a system of three different experiments that are related to the nonlinear optical characterization as illustrated in FIG. 6. The third-order susceptibilities of the complexes were measured by DFWM at 532 nm using the counterpropagating pump geometry described previously,[64] with an additional variable optical delay in the probe beam for alignment purposes. A detailed experimental configuration of DFWM is shown in FIG. 7. The second harmonic of a mode-locked frequency doubled Nd:YAG laser (Continuum PY61) with a temporal pulse width of 40 ps in full width at half maximum (FWHM) and a repetition rate of 10 Hz was used as the light source. The laser intensity can be varied using a half-wave plate and a polarizing cube beam splitter. The main beam was first split into a strong pump beam and a relatively weak probe beam (90:10). Then, the pump beam split again equally into two beams, the forward and the backward. These two beams met at the NLO sample position in counterpropagating fashion. Another 50:50 beam splitter was used to guide the probe beam to the sample

after an optical delay. The optical delay was placed to align all three beams so that they both temporally and spatially overlap at the sample. The beam splitter was used rather than a mirror because the phase conjugate reflection from the nonlinear optical sample is the time reversal of the probe beam, and the phase conjugate beam travels in the opposite direction of the probe beam. The pulse energy of this phase conjugate signal was detected with a silicon joule meter (Molectron J3S-10). The laser intensities at the sample were in the ranges of 26-40 MW/cm^2 in each of the pump beams and 2.9-4.4 MW/cm^2 in the probe beam.

All four beams had same polarizations perpendicular to the plane of incident that was parallel to the optical table. Thus, $\chi^{(3)}$ measured was actually $\chi^{(3)}_{1111}$, a component of $\chi^{(3)}$ tensor [see Equation (1.1)]. Moreover, DFWM actually measures the complex modulus of $\chi^{(3)}$, which is $\sqrt{(\mathrm{Re}\,\chi^{(3)})^2+(\mathrm{Im}\,\chi^{(3)})^2}$. For the rest of this dissertation, $\chi^{(3)}$ is generally used without subscription and the modulus sign for simplicity to represent $\left|\chi^{(3)}_{1111}\right|$ unless a clear representation is required. The same convention goes to $\left|\gamma_{1111}\right|$.

The dependence of the phase conjugate intensity on the incident laser intensity was measured, and a cubic power dependence was observed for CS_2, a reference third-order nonlinear optical material, as well as for all the samples studied. However, when the incident intensity was higher than 90 MW/cm^2, deviations from cubic dependence occurred for all of the [(*R*-APPC)M]Cl$_n$ complexes, indicating the onset of saturation or a competing nonlinear process. FIG. 8 shows the dependence of the phase conjugate intensity on the incident laser intensity for [(C_6H_5-APPC)Cd]Cl, which was typical for the [(*R*-APPC)M]Cl$_n$ complexes.

The $\chi^{(3)}$ for each solution was obtained by comparison of the magnitude of the phase conjugate signal with that of the CS_2 reference using Equation (2.1)[65]:

$$\chi^{(3)}_{sample} = \chi^{(3)}_{ref}\left(\frac{I_{sample}}{I_{ref}}\right)^{1/2}\left(\frac{n_{sample}}{n_{ref}}\right)^{2}\left(\frac{l_{ref}}{l}\right)\left(\frac{\alpha l}{e^{-\alpha l/2}\left(1-e^{-\alpha l}\right)}\right), \qquad (2.1)$$

where I is the intensity of the phase conjugate signal, n is the linear refractive index, l is the sample path length, and α is the linear absorption coefficient of the solution at 532 nm. The subscript ref refers to CS_2, for which a value of $\chi^{(3)}_{xxxx}$=6.8×10^{-13} esu at 532 nm for the 25 ps laser pulse was used.[66]

When a nonlinear optical material is taken into solution, the third-order macroscopic susceptibility of the solution is assumed to be a pairwise addition of the solvent and solute. The molecular second hyperpolarizability, γ_{solute}, can be calculated from[15]

$$\chi^{(3)}_{solution} = L^4\left(N_{solvent}\gamma_{solvent} + N_{solute}\gamma_{solute}\right), \qquad (2.2)$$

where N_{solute}; $N_{solvent}$ are the number densities of molecules of the solute and solvent per mL; and L is the Lorentz local field correction factor, given by $(n^2+2)/3$. We measured $\chi^{(3)}$ values for all samples in methanol or chloroform solution in the concentration range of 10^{-5}-10^{-4} mol/L. The dependence of $\chi^{(3)}$ on the concentration of the solution for [($C_{10}H_6$-APPC)Cd]Cl was typical and is illustrated in FIG. 9. As expected, a linear relationship was observed for all the complexes that were studied, and the γ values of the solutes could be obtained from the slope of the plots.

The calculated γ values for all of the [(*R*-APPC)M]Cl_n complexes as well as those of $PbPc(CP)_4$ and SiNc, two of the metallophthalocyanines that are among the most

promising optical limiting materials, are listed in Table 1. For the [(*R*-APPC)M]Cl_n complexes, the γ values ranged from 1.1×10^{-31}-1.2×10^{-30} esu, varying by a factor of 10 as the conjugated *R* group and metal center were changed. The γ values for all of the [(*R*-APPC)Cd]Cl complexes (2.6×10^{-31}-1.2×10^{-30} esu) were larger than those of PbPc(CP)$_2$ and SiNc. The largest γ was observed for the 26 π-electron complex, [($C_{10}H_6$-APPC)Cd]Cl, and was a factor of 7 larger than those of PbPc(CP)$_2$ and SiNc. This value was also quite comparable with some of the extremely large values reported for *meso*-substituted tetrabenzoporphyrins (5×10^{-31}-1.0×10^{-29} esu).[24]

The typical range of measurement uncertainties was 15% to 20% on $\chi^{(3)}$ values when the pulse energy of the phase conjugate signal was averaged from the collection of 50-100 data points. The γ values were obtained from the slope of $\chi^{(3)}$ values in different concentrations. Thus, the uncertainty on a γ value is related to the linear fitting confidence, which was typically greater than 0.95. It was estimated that the uncertainty of the γvalues would be less than 10%.

The γ values of the [(*R*-APPC)M]Cl_n complexes are highly dependent on the nature of the *R* group. For the three complexes, [(C_6H_2-APPC)Cd]Cl, [($C_{10}H_6$-APPC)Cd]Cl, and [($(NC)_2C_2$-APPC)Cd]Cl, which have the same metal center but different conjugated *R* groups with varying numbers of conjugated π electrons, the γ value of the complex increases as the number of conjugated π electrons increases. (γ increases by a factor of 3.5 going from the 18 π-electron system to the 26 π-electron system.) As expected, the more delocalized π-electron system has the largest γ value.

TABLE 1. Linear absorption cross section and molecular second-order hyperpolarizability of [(*R*-APPC)M]Cl_n complexes at 532 nm.

Complexes	γ 10^{-31} (esu)	λ_{max} (nm)	σ_0 10^{-20} (cm^2)	γ/σ_0 10^{-14} (esu·cm^{-2})
[($OCH_3C_6H_3$-APPC)Cd]Cl [a]	2.6	750.5	470	5.5
[($CO_2NaC_6H_3$-APPC)Cd]Cl [a]	4.3	769.5	2100	2.0
[(C_6H_4-APPC)Cd]Cl [a]	4.8	762.5	780	6.2
[(ClC_6H_3-APPC)Cd]Cl [a]	5.6	768.0	880	6.4
[($NO_2C_6H_3$-APPC)Cd]Cl [a]	7.5	792.5	1600	4.6
[($C_{10}H_6$-APPC)Cd]Cl [a]	12.0	861.5	1300	9.2
[($(NC)_2C_2$-APPC)Cd]Cl [b]	3.4	693.0	1300	2.6
[(C_6H_4-APPC)Pd]Cl [b]	1.1	643.5	1100	1.0
[(C_6H_4-APPC)Sm]Cl_2 [a]	1.4	774.5	1400	1.0
PbPc($CP)_4$ [b]	1.6	713.0	320	5.0
SiNc [b]	1.7	774.0	770	2.2

a. In methanol.
b. In chloroform.

Changing the phenyl ring substituent of [($R'C_6H_3$-APPC)Cd]Cl complexes also affects the γ value of the complex, with the γ value increasing by a factor of 2.9 as the R' group is varied in the sequence R' = OCH_3, CO_2Na, H, Cl, NO_2. There appears to be a correlation between electron donor/acceptor abilities of the R' groups and the γ values of the complexes as shown by linear correlation between the γ values of the complexes and the Hammett sigma parameters (σ_p)[67] of the R' groups (shown in FIG. 10, r=0.97).

Variation in the metal center also has a significant effect on the γ values of the complexes. For the three complexes with identical ligands, [(C_6H_4-APPC)Cd]Cl, [(C_6H_4-APPC)Pd]Cl, and [(C_6H_4-APPC)Sm]Cl_2, the γ value changes by a factor of 4.4 as the metal center is varied. This variation in the γ values may be due to the differences in both the electron configurations and the coordination geometries of the metals.

As we reported previously,[62] the linear absorption peaks of most of the [(*R*-APPC)M]Cl_n complexes appear at ~420 nm (*B* band) and ~760 nm (*Q* band), providing a broad optical window from 500 nm to 680 nm. However, there still is considerable absorption at 532 nm for all of the [(*R*-APPC)M]Cl_n complexes; thus, it is necessary to evaluate the contribution of the linear absorption to the third-order nonlinearities of these complexes. If the linear absorption dominates the nonlinearity, there should be a very strong correlation between the γ value and the linear absorption crosssection, σ_0, at 532 nm. This likelihood is not the case for the [(*R*-APPC)M]Cl_n complexes because the ratio γ/σ_0 for these complexes, listed in Table 1, vary by a factor of 9, indicating that there is no general correlation between γ and σ_0 for these complexes. This lack of correlation implies that linear absorption is not the dominant factor contributing to the γ value of the [(*R*-APPC)M]Cl_n complexes.

The third-order nonlinearity of a sample may originate from electronic, orientational, acoustic, or thermal processes.[68,69] Measurement of the individual components of the $\chi^{(3)}$ tensor, especially the value of the ratio $\chi^{(3)}_{1111}/\chi^{(3)}_{1122}$ for perpendicular and parallel probe polarizations with respect to the pump beam, can help to identify the molecular origin of $\chi^{(3)}$. In an isotropic solution, the ratio $\chi^{(3)}_{1111}/\chi^{(3)}_{1122}$ is 1/3

for an instantaneous electronic $\chi^{(3)}$ but is 3/4 for nuclear reorientation.[70-73] In this work, the ratios of $\chi^{(3)}_{xxyy}/\chi^{(3)}_{xxxx}$ for [(C_6H_4-APPC)Cd]Cl, [($C_{10}H_6$-APPC)Cd]Cl, and CS_2 were measured. For CS_2, in which $\chi^{(3)}$ is dominated by an molecular orientational effect, the ratio of $\chi^{(3)}_{xxyy}/\chi^{(3)}_{xxxx}$ was found to be 0.74, in good agreement with the reported ratio of 0.70,.[70] which is much closer to 3/4 than 1/3 as expected. In contrast, for each [(*R*-APPC)Cd]Cl complex, this ratio was observed to be about 0.3, which strongly suggests that the nonlinearities of the [(*R*-APPC)M]Cl_n complexes are predominantly electronic in origin.

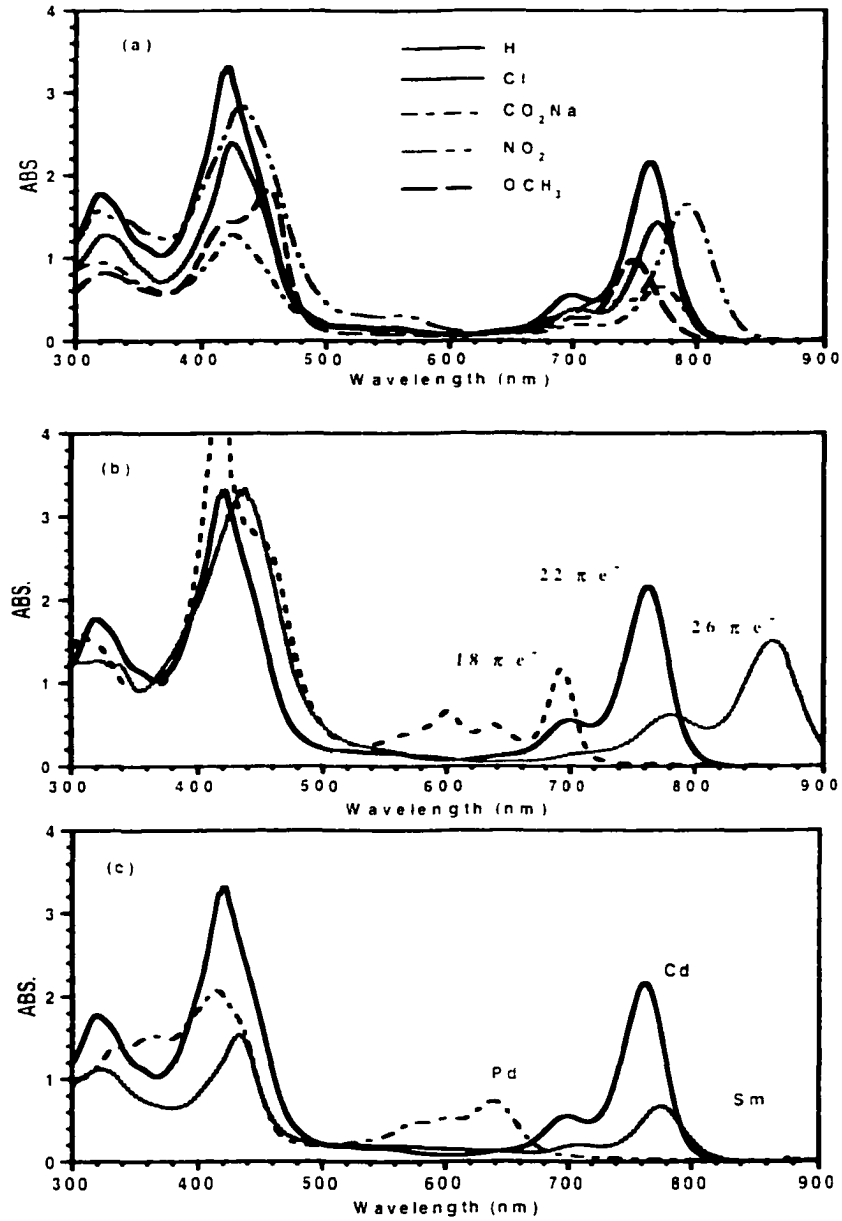

FIG. 5. Linear absorption spectra of [(*R*-APPC)M]Cl_n. (a) Varying the secondary substituent *R'* of [(*R'*C_6H_3-APPC)Cd]Cl, (b) varying the bridge group *R* with different number of π electrons- 18 for $(CN)_2C_2$, 22 for C_6H_4 and 26 for $C_{10}H_6$ of [(*R*-APPC)Cd]Cl, (c) varying the metal center M. We use a Shimadzu UV-3101 PC UV-VIS-NIR Scanning Spectrometer. All samples are prepared in methanol solution of 3.4×10^{-4} mol/L in a 2 mm quartz cell, except [($(CN)_2C_2$-APPC)Cd]Cl and [(C_6H_4-APPC)Pd]Cl are in chloroform.

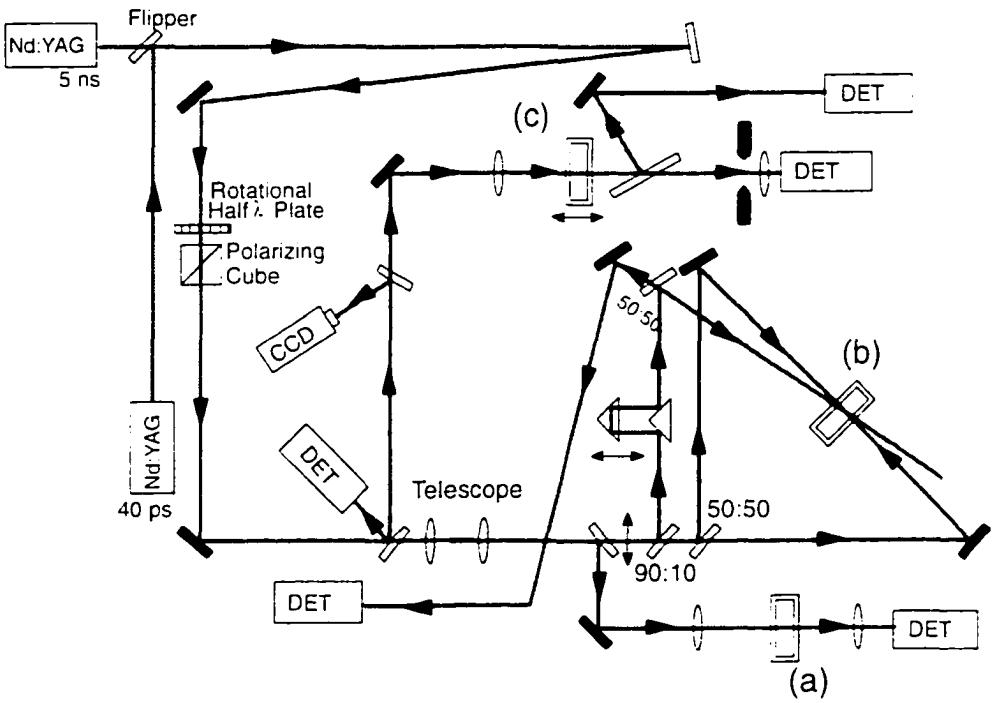

FIG. 6. Nonlinear optical characterization. (a) Nonlinear transmission/absorption, (b) DFWM, (c) Z-scan. The light source can be interchangeable between nanosecond pulse and picosecond pulse using a flipping optics.

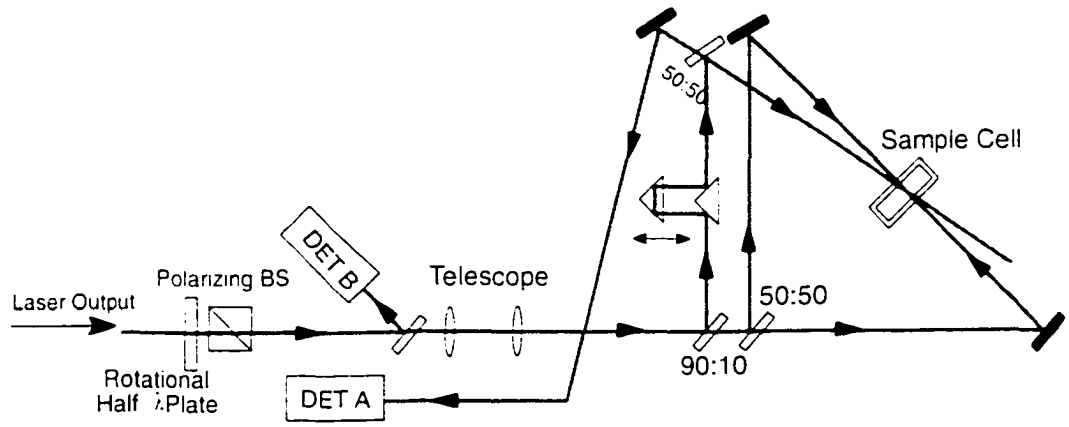

FIG. 7. DFWM in backward geometry.

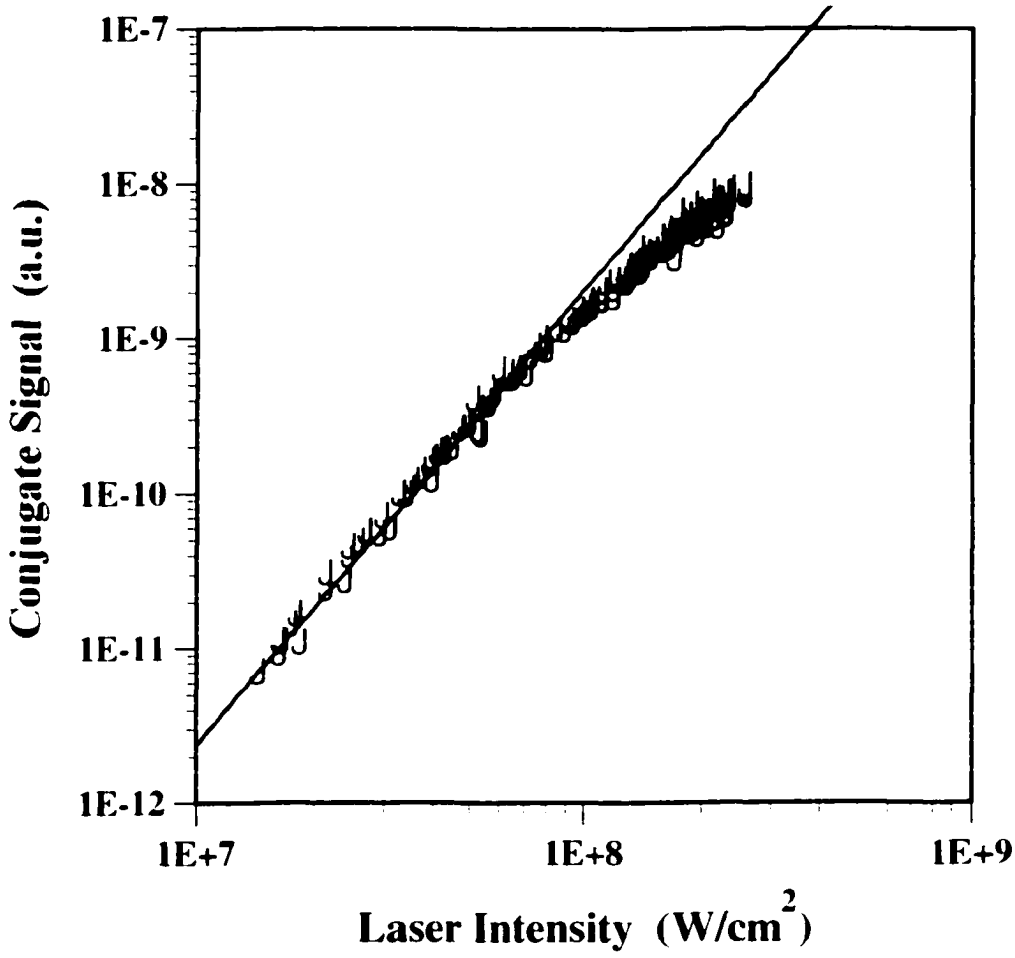

FIG. 8. Dependence of phase conjugate signal on the laser intensity for the 4.02×10^{-4} mol/L [(C_6H_4-APPC)Cd]Cl complex in methanol.

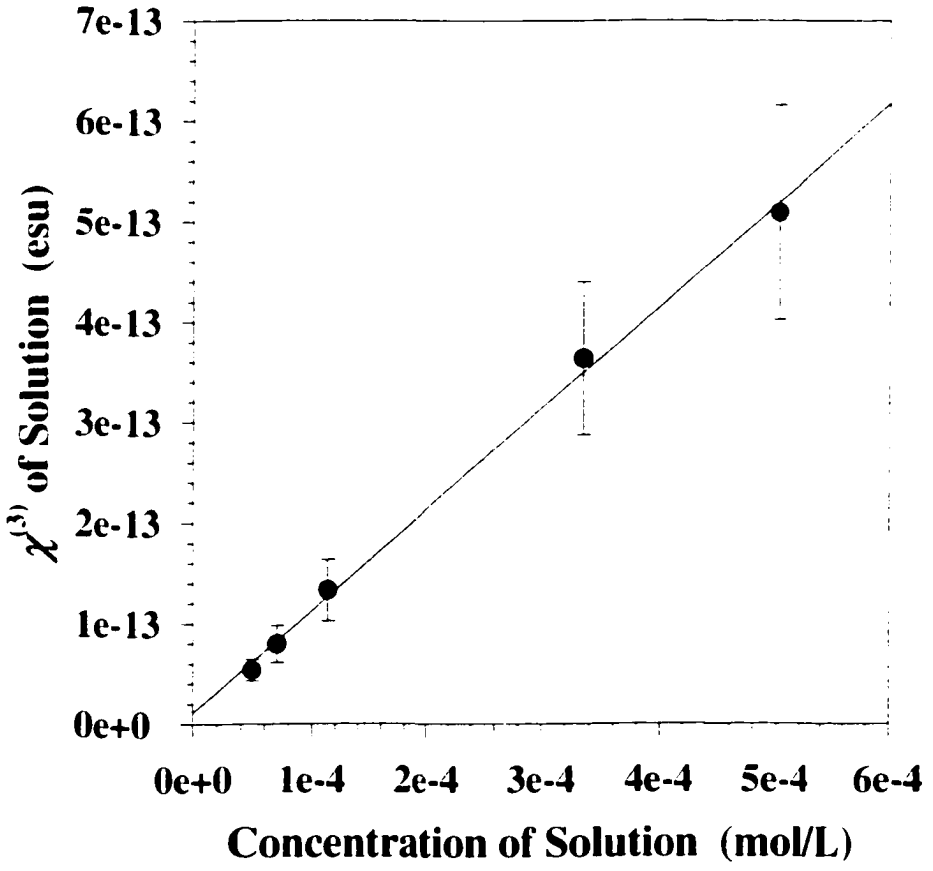

FIG. 9. $\chi^{(3)}$ values versus concentration curve for complex $[(C_{10}H_6\text{-APPC})Cd]Cl$ in methanol. The linear coefficient of confidence r=0.999.

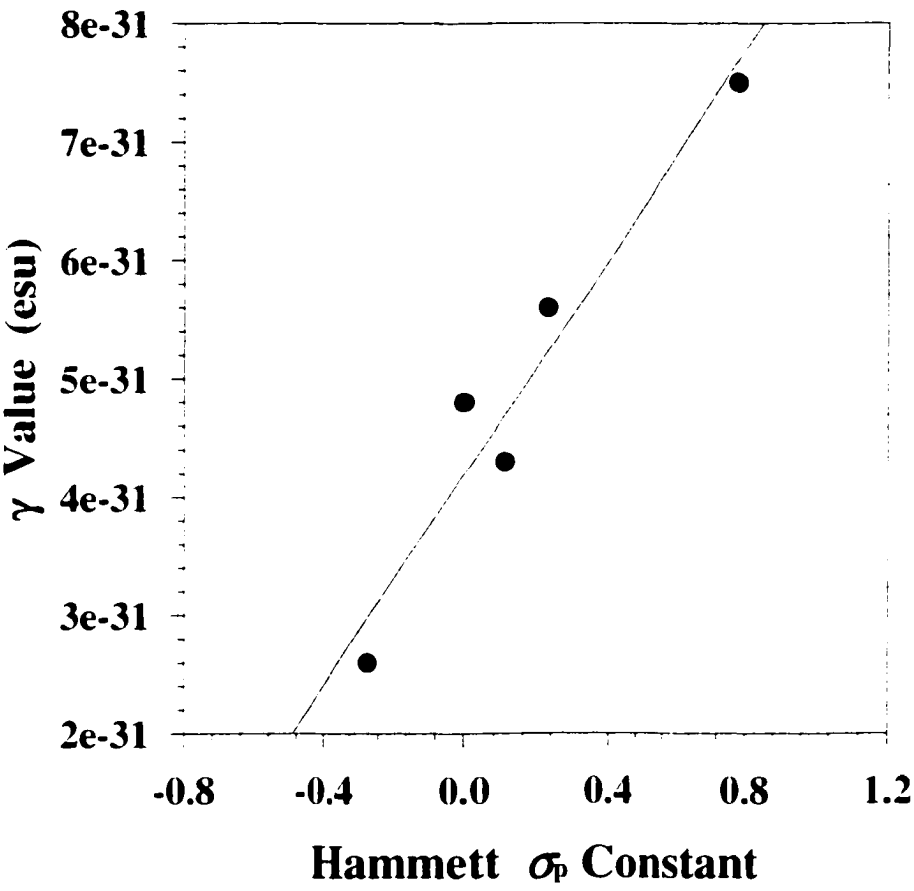

FIG. 10. Linear correlation between the γ values and Hammett σ_p constants for the [($R'C_6H_3$-APPC)Cd]Cl complexes (r=0.97).

CHAPTER 3

OPTICAL LIMITING OF THE APPC COMPLEXES

Experimental Description

The nonlinear transmission measurement was performed using the second harmonic of the nanosecond *Q*-switched Nd:YAG laser (Spectra Physics GCR 230). The pulse width was about 5 ns (FWHM), and the repetition rate was 10 Hz. A wedged window was used to reflect a small portion of the main beam (see FIG. 6). In this manner, most of the pulse energy is transmitted through the sample, which is in solution in a 2 mm thick quartz cell.

As illustrated in FIG. 11, the pulse energy of the reflected beam was measured simultaneously with the transmitted energy using pyroelectric joule meters (Molectron J4-09 series), which were connected to a personal computer through GPIB. When, using a VI in Labview software (National Instrument), the measurement started, the half-wave plate was manually rotated to vary the pulse energy going into the sample. The reference and the transmitted pulse energy were measured and recorded through GPIB and Labview. When the measurement was completed, the recorded transmitted pulse energy was normalized with the reference energy to minimize effects due to energy fluctuation of laser pulses. This procedure recorded typically 100-200 data points covering a couple of orders of magnitude of variance in pulse energy. The fluence was calculated after measuring the beam diameter at the sample using a small adjustable iris. The typical

beam diameter, defined as 87% transmittance, was about 6-7 mm without any focusing lens.

Initially, without a focusing lens, we could measure the linear transmittance in most of the data set and see some deviation from constant transmittance due to nonlinear absorption at the high fluence. Nonetheless, high enough fluences were not obtained to see stronger nonlinear absorption effects. To see significant nonlinear absorption at higher fluence, we placed a focusing lens to generate more concentrated pulse energy at the sample (see FIG. 11). The laser pulses were focused at the center of 2 mm path-length solution cell by a 25 cm focal-length lens (*f*/38) giving an Airy spot radius of ~150 μm. OPL was obtained again by varying the input energy (E_{in}) with a half-wave plate and polarizing cube beam splitter while monitoring input energy (E_{in}) and output energy (E_{out}) with two energy detectors. The transmitted energy was collected by a 2.54 cm focal-length lens located to relay the collected energy to a nominal spot size of ~4 mm on the detector window of 8 mm diameter.

The solutions of nine different [(*R*-APPC)M]Cl_n complexes in methanol (CH_3OH) or chloroform ($CHCl_3$) were prepared at the same concentration, 3.4×10^{-4} mol/L, with the internal transmittance ranging from 51% to 80%.

To get the fluence from the measured value of the energy, it is necessary to know the spot size or, to be more accurate, the spatial profile of the beam. Determining the beam diameter is not a trivial matter. To start, there is no definitive universal definition of the beam width. Some use $1/e^2$ of the irradiance profile. Another common definition is 87% of the energy transmission. There are others. Sometimes some of the definitions are equivalent (or even exact). For example, for a "perfect" Gaussian spatial profile, $1/e^2$

of the irradiance profile is the same value as 87% of the energy transmission. However, in general, none of these definitions can describe the spatial beam diameter in a universal way. The validity of each definition has its own limitation depending on the actual spatial profile of the laser beam.

Another practical difficulty is that most of these definitions and formulas for calculating the spot size are only useful for centro symmetric and diffraction-limited beams, which are difficult to achieve in cost-effective ways. For example, assume that the spatial beam profile is perfect Gaussian and the beam is perfectly collimated as illustrated in FIG. 12. In addition to this ideal beam, assume that the focusing lens is diffraction limited. The focused spot size, the beam waist, is mathematically well defined.

$$\omega_0 = \frac{\lambda f}{\pi \omega_1}, \qquad Z_R = \frac{\pi \omega_0^2}{\lambda}. \tag{3.1}$$

The Rayleigh range Z_R is defined as the distance from the beam waist ω_0 to the transverse plane where the beam area is doubled, or equivalently the intensity becomes a half as in focal plane. The collimated beam length, or confocal length, is arbitrarily defined as $2Z_R$ including the both sides from ω_0. The beam diameters are all defined as $1/e^2$ of the irradiance or 87% of the energy transmission for this ideal Gaussian diffraction-limited case. However, if the spatial profile is not perfect Gaussian, the optics are not perfectly diffraction limited, and/or the beam is not perfectly collimated, then the above expressions are no longer valid, and $\omega_0 > \frac{\lambda f}{\pi \omega_1}$.

As a result, direct scanning of the spatial beam profile using CCDs or knife-edge techniques has provided the most accurate methods for measuring the beam size.

However, each method has its own limitations. It is not safe to use CCDs at focused high fluence laser beams because of detector damage problems. The knife-edge technique is a well-known and very reliable method,[74-80] but a precision translation stage is required when measuring a very small spot, such as the focused spot of a high power laser. In addition, knife-edge techniques raise some safety issues when scanning a tightly focused spot with a metal blade. Furthermore, neither method is a real time measurement.

We have developed a new method to directly measure the fluence from the fluence-dependent transmittance using nonlinear optical materials. This method is quite useful to characterize the optical limiting properties of the material. In addition, the method provides us another way to measure the beam diameter safely anywhere in real time, even at the focused spot, because we can deduce the effective spot size from the fluence.

The new method is based on the following argument. Assume a laser beam in which both the temporal and spatial profiles are Gaussian.

$$I(r,t) = I_0 e^{-2\frac{r^2}{\omega^2}} e^{-2\frac{t^2}{\tau^2}} \tag{3.2}$$

For this beam, τ is the Gaussian half width, and is related to τ(FWHM) as

$$\tau(\text{FWHM}) = 2\tau(\text{Gaussian HW})\sqrt{\frac{\ln 2}{2}} = 1.177\tau(\text{Gaussian HW}).$$

Then, integrating over the pulse width as in Equation (1.3), we can write

$$F(r) = F_0 e^{-2\frac{r^2}{\omega^2}}$$

Integrating over the area gives

$$E = \iint_{Area} F_0 e^{-2\frac{r^2}{\omega_0^2}} r dr d\varphi = \frac{\pi\omega_0^2}{2} F_0 = A_{eff} F_0 . \qquad (3.3)$$

The above expression gives a relationship between the pulse energy and the peak fluence.

Practically, we first measure the transmittance without the focusing lens while varying the intensity using the rotational half-wave plate. The transmittance is simply the normalized ratio of the readings on two detectors in FIG. 11, provided the proper normalization for the reflection loss from the cell. Because we do not use the focusing lens, the beam diameter at the sample is fairly large (approximately a few millimeters), and the fluence is not very high. The beam diameter is easily and fairly accurately measurable by taking 87% of transmittance using an adjustable aperture. The fluence is well defined in this low fluence range, at which we start to see some nonlinear absorption at the high energy end and mostly linear absorption in the low energy region. We plot the transmittance *T vs. Fluence*.

Next, we place the focusing lens and measure the transmittance while varying the intensity. Stronger nonlinear absorption is then observed throughout the whole range, and we plot the transmittance *T vs. Energy*. We compare both plots and concentrate on the region where the overlapping of the transmittance occurs. The region of the same transmittance will be the high fluence end on *T vs. Fluence* without the focusing lens and the low energy end on *T vs. Energy* with the focusing lens. Because transmittance is a unique function of the input fluence, the input fluence must be the same at this overlapping region in *T vs. Energy* as at the overlapping region in *T vs. Fluence*.

Because there exists a unique value for the focused spot size, we can match these two plots using a numerical fitting procedure with the effective area as a fitting

parameter. First, we fit the data in the overlapping region of *T vs. Fluence* to a reasonable mathematical function. The critical point here is that the functional form is of no importance as long as it fits well only to the data in overlapping region. We should not try to fit the whole curve because that can only be done by numerically solving the whole six-level rate equations (see Chapter 5). In addition, the rate equations can only be solved after complete fluence measurement data are obtained. Applying the fitting function to data only in the overlapping region allows us to use some of the simple fitting functions shown below. When the overlapping region is small, and the data points are compact enough, the simplest form will be a linear function.

$$T(F) = a + bF .$$

If it shows a little curve, either

$$T(F) = \frac{1}{a + bF} \quad \text{or} \quad T(F) = a \exp^{nF}$$

will be fairly good functions to fit.

Once we have a well-defined fitting function for *T vs. Fluence*, the same function is used with the exact parameters to fit the data in the overlapping region of *T vs. Energy* with the effective area as the fitting parameter. In other words,

$$T(F) = T\left(\frac{Energy}{A_{eff}}\right).$$

After A_{eff} is obtained, A_{eff} is applied to the data in the whole region of *T vs. Energy*. This procedure will give the second set of *T vs. Fluence*. Finally, the two *T vs. Fluence* plots can be combined to yield the complete plot of the nonlinear transmittance as a function of the input fluence for a wider dynamic range (several orders of magnitude) of the input fluences. The result is shown in FIG. 13.

In summary, the new method utilizes the uniqueness of $T(F)$ of nonlinear optical materials. High fluence on the small focused spot or anywhere else, for that matter, can be directly measured without knowing the beam diameter. The method is simpler, faster, safer, and less expensive than the knife-edge technique; furthermore, it produces real time data.

Optical Limiting Performance

In FIG. 14 to FIG. 16, the transmitted fluences of the nine complexes are shown as a function of the incident fluence. A clear RSA in the 0.01 J/cm^2 to 3.5 J/cm^2 range is exhibited by all of the complexes, with [((NC)$_2$C$_2$-APPC)Cd]Cl yielding results most comparable with those obtained with SiNc and PbPc (shown in FIG. 17 and FIG. 18). This complex has an optical limiting threshold (F_{th}), defined as the incident fluence at which the center of the data band begins to deviate from the extrapolated linear transmission line,[81] of 2.6 mJ/cm^2. As the input fluence increases above 0.01 J/cm^2, the output-input curve bends farther away from the linear transmission line until reaching a maximum output energy, where clamping occurs. The value of the limiting throughput ($F_{through}$) is 0.31 J/cm^2 for incident fluences higher than 0.8 J/cm^2. The transmission for this complex drops to a value less than 0.09 as incident fluence is increased to 3.5 J/cm^2 (see FIG. 18). The thresholds and the limiting throughputs of the other complexes, PbPc, and SiNc are given in Table 2.

As seen in FIG. 14, variations in phenylene substituents of the [(R'C$_6$H$_3$-APPC)Cd]Cl complexes have significant effects on both the linear absorption and opticallimiting properties of the complexes at 532 nm. As expected, there is a roughly

inverse linear relationship between the linear absorptions of the complexes and their limiting throughputs. However, the limiting throughputs of the complexes are also influenced by the electron donor/acceptor properties of the R' group. This influence is exemplified by the fact that two complexes with the same linear absorption at 532 nm, [($CO_2NaC_6H_3$-APPC)Cd]Cl and [(ClC_6H_3-APPC)Cd]Cl, have quite different limiting throughputs. The limiting thresholds, F_{th}, of the [($R'C_6H_3$-APPC)Cd]Cl complexes also change as the R' group is varied, but the uncertainty in these numbers precludes any discussion of whether these changes are related to the linear absorption.

TABLE 2. The linear absorption coefficient, the optical limiting threshold, and the limiting throughput of the nine [(R-APPC)M]Cl_n complexes.

Samples	α_0 (cm^{-1})	T_{lim} [c]	F_{th} (mJ/cm^2)	$F_{through}$ (J/cm^2)
[($OCH_3C_6H_3$-APPC)Cd]Cl [a]	1.12	0.28	1.5	1.13
[($CO_2NaC_6H_3$-APPC)Cd]Cl [a]	2.00	0.26	2.5	0.90
[(C_6H_4-APPC)Cd]Cl [a]	2.15	0.16	1.8	0.56
[(ClC_6H_3-APPC)Cd]Cl [a]	2.00	0.24	1.8	0.77
[($NO_2C_6H_3$-APPC)Cd]Cl [a]	3.37	0.10	1.4	0.40
[(C_6H_4-APPC)Pd]Cl [b]	2.23	0.14	3.0	0.48
[(C_6H_4-APPC)Sm]Cl_2 [a]	1.93	0.42	150.0	1.42
[($(NC)_2C_2$-APPC)Cd]Cl [b]	2.39	0.09	2.6	0.31
[($C_{10}H_6$-APPC)Cd]Cl [a]	2.31	0.13	3.0	0.44
PbPc [b]	0.87	0.11	4.0	0.39
SiNc [b]	1.86	0.09	3.5	0.28

a. In methanol.
b. In chloroform.
c. The limiting transmittance at 3.5 J/cm^2.

In contrast to the effects of variations of the phenylene substituents, *R'*, variations in the conjugated bridging group, *R*, can independently influence the linear and nonlinear absorptions. The three compounds with different conjugated bridging groups, [(C_6H_4-APPC)Cd]Cl, [($(NC)_2C_2$-APPC)Cd]Cl and [($C_{10}H_6$-APPC)Cd]Cl, have similar linear transmissions at 532 nm but show different optical limiting thresholds and limiting throughputs (FIG. 15). Particularly good limiting properties are exhibited by [($(NC)_2C_2$-APPC)Cd]Cl, probably due to the strong electron-withdrawing ability of the –CN group. A similar result is seen for [($C_{10}H_6$-APPC)Cd]Cl due to the effect of the conjugated napthlene group.

Variation in the metal cation has a much larger effect on the optical limiting properties than does variation of the phenylene substituents and conjugated bridging group. FIG. 16 clearly demonstrates this fact. At similar linear transmittance, [(C_6H_4-APPC)Pd]Cl shows the lowest limiting throughput, while [(C_6H_4-APPC)Sm]Cl_2 has the highest limiting threshold and limiting throughput. The high limiting threshold and limiting throughput is connected with the lower yield of the triplet excited state ($\phi_t \approx 0.26$) and the relatively short lifetime of the lowest triplet excited state ($\tau_t \approx 0.55$ μs).

A figure of merit for RSA molecules involving an excited triplet state can be defined as $\sigma_t/\sigma_g \approx \ln T_{sat}/\ln T_{lin}$,[40] where T_{sat} is the value of the transmission for which the slope of the transmission versus input fluence line approximates zero. The conditions for this figure of merit are that the pulse width is longer than the intersystem crossing time, the incident fluence exceeds the saturable fluence $F_{sat} = h\nu/\sigma_g\phi_t$, and the quantum yield of triplet excited state is quite high. These conditions are met by the [(*R*-APPC)M]Cl_n complexes. These complexes exhibit F_{sat} values that range from 0.04 J/cm^2 to 0.12

J/cm^2, implying that for fluences between 0.3~3.5 J/cm^2, the ground state will be greatly bleached. Furthermore, the small intersystem crossing time and the high quantum yields of the triplet excited states[39] for these molecules indicate that the excited state is distributed mainly to the lowest triplet excited state over the duration of one laser pulse in nanosecond pulse regime.

In our current experimental setup, the damage threshold for the optical cell limits the maximum fluence, and we are unable to reach saturable transmission for the complexes. Hence, we can only calculate lowest bounds for the σ_t/σ_g values of the [(*R*-APPC)M]Cl_n complexes (Table 3). Nevertheless, these σ_t/σ_g values are extremely promising because they closely approach those obtained with SiNc and PbPc (32 and 23, respectively).[42] The great ease of structural modification of our complexes may allow for values of σ_t/σ_g that surpass those of the complexes measured in this work. Moreover, the complexes in this work already exhibit higher quantum yields of triplet excited states than does SiNc, as well as F_{th} and $F_{through}$ values that are comparable with those of SiNc and PbPc.

TABLE 3. The photophysical properties and the ratio of lowest triplet excited state to ground state absorption cross section (σ_t/σ_g) for nine [(*R*-APPC)M]Cl_n complexes.

Samples	ϕ_t	F_{sat} (J/cm^2)	σ_g (10^{-17} cm^2)	σ_t/σ_g
[($OCH_3C_6H_3$-APPC)Cd]Cl [a]	0.89 [c]	0.076	0.55	>5.7
[($CO_2NaC_6H_3$-APPC)Cd]Cl [a]	0.47 [c]	0.080	0.99	>3.4
[(C_6H_4-APPC)Cd]Cl [a]	0.91 [c]	0.037	1.10	>4.3
[(ClC_6H_3-APPC)Cd]Cl [a]	0.78 [c]	0.048	0.99	>3.6
[($NO_2C_6H_3$-APPC)Cd]Cl [a]	0.60 [c]	0.038	1.62	>3.4
[(C_6H_4-APPC)Pd]Cl [b]	—	—	1.14	>4.3
[(C_6H_4-APPC)Sm]Cl_2 [a]	0.26 [c]	0.122	0.95	>2.3
[($(NC)_2C_2$-APPC)Cd]Cl [b]	—	—	1.18	>5.0
[($C_{10}H_6$-APPC)Cd]Cl [b]	0.32 [c]	0.102	1.14	>4.4
PbPc [b]	0.92 [d]	0.091	0.43	>12.7
SiNc [b]	0.20 [e]	0.177	0.92	>6.5

a. In methanol.
b. In chloroform.
c. Ref. 49.
d. Ref. 40.
e. Ref. 82.

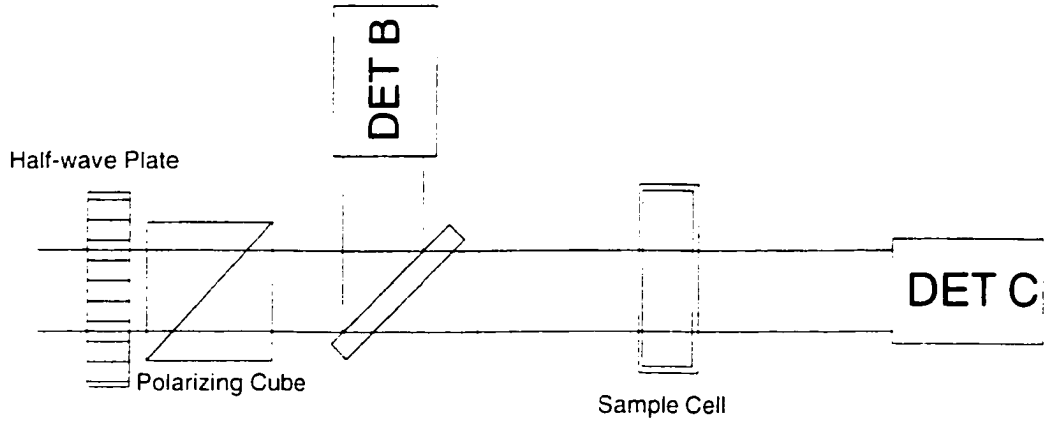

FIG. 11. Nonlinear transmission measurement.

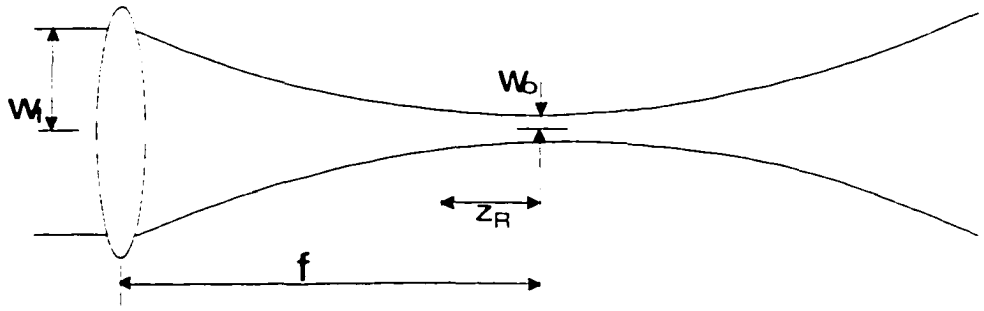

FIG. 12. Focusing of perfect Gaussian beam with diffraction-limited optics.

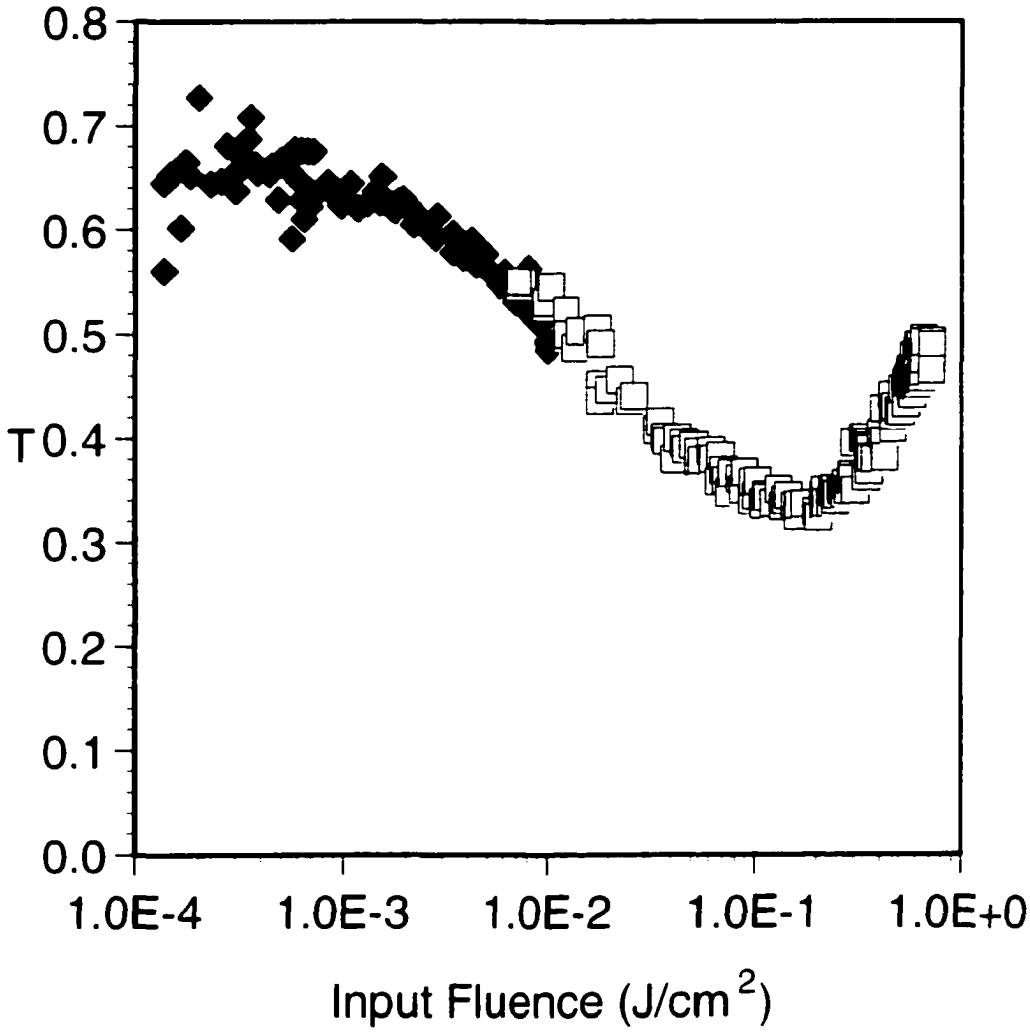

FIG. 13. Nonlinear transmission of [(C_6H_4-APPC)Cd]Cl as a function of the input fluence. The filled symbols represent the data points collected without the focusing lens, while the empty squares represent the data collected with the focusing lens. The light source is *Q*-switched mode-locked Nd:YAG laser with 40 ps pulse width and 10 Hz repetition rate.

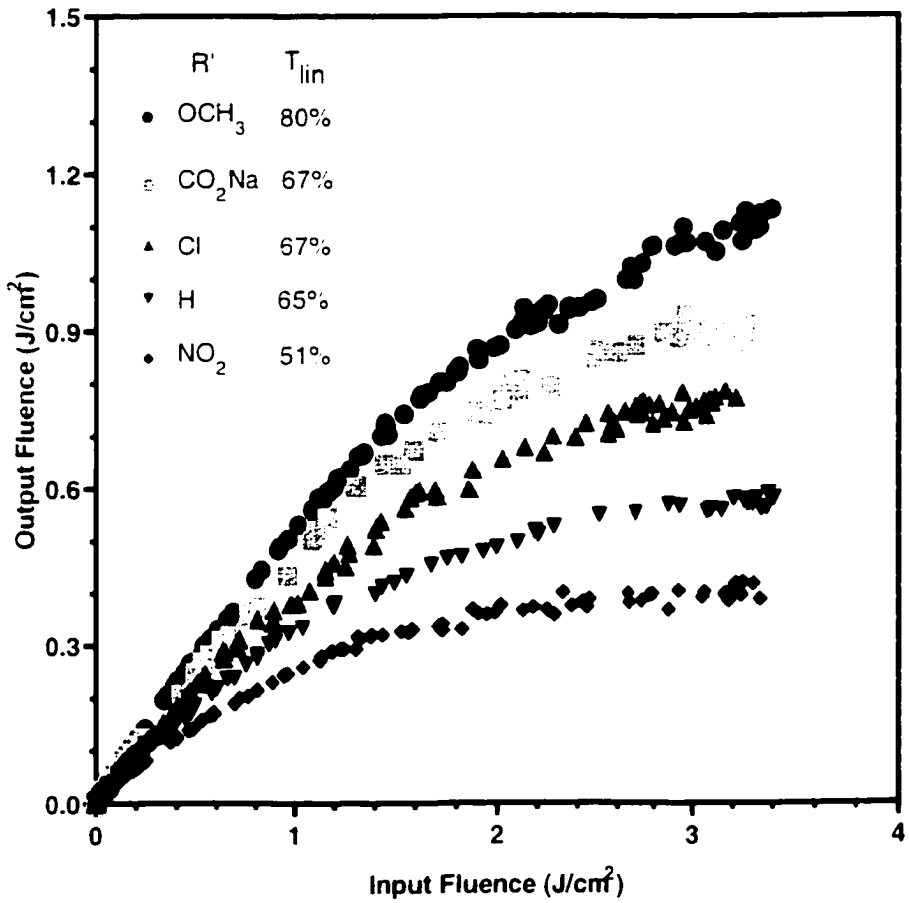

FIG. 14. Input versus output fluences of [($R'C_6H_3$-APPC)Cd]Cl series. The excitation laser pulse width is 5 ns at 532 nm. The concentration is 3.4×10^{-4} mol/L in 2 mm cell. Complexes are dissolved in methanol.

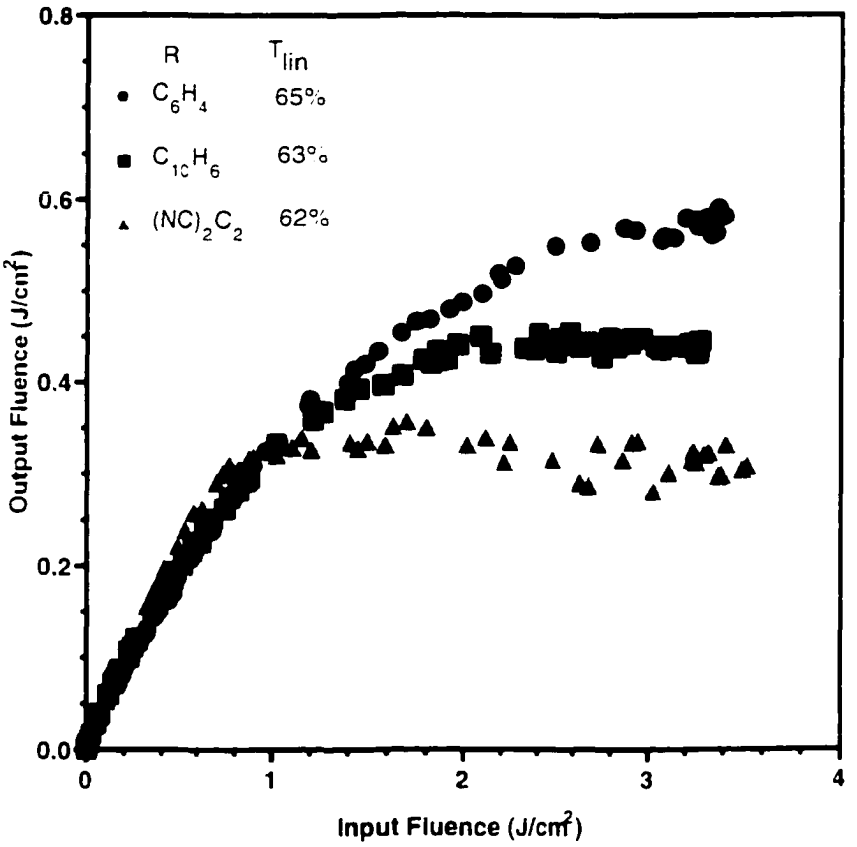

FIG. 15. Input versus output fluences of [(*R*-APPC)Cd]Cl complexes with different numbers of π-electrons- 18 for [$(NC)_2C_2$-APPC)Cd]Cl, 22 for [$(C_6H_4$-APPC)Cd]Cl, and 26 for [$(C_{10}H_6$-APPC)Cd]Cl. The excitation laser pulse width is 5 ns at 532 nm. The concentration is 3.4×10^{-4} mol/L in 2 mm cell. Complexes are dissolved in methanol except for [$(NC)_2C_2$-APPC)Cd]Cl in chloroform.

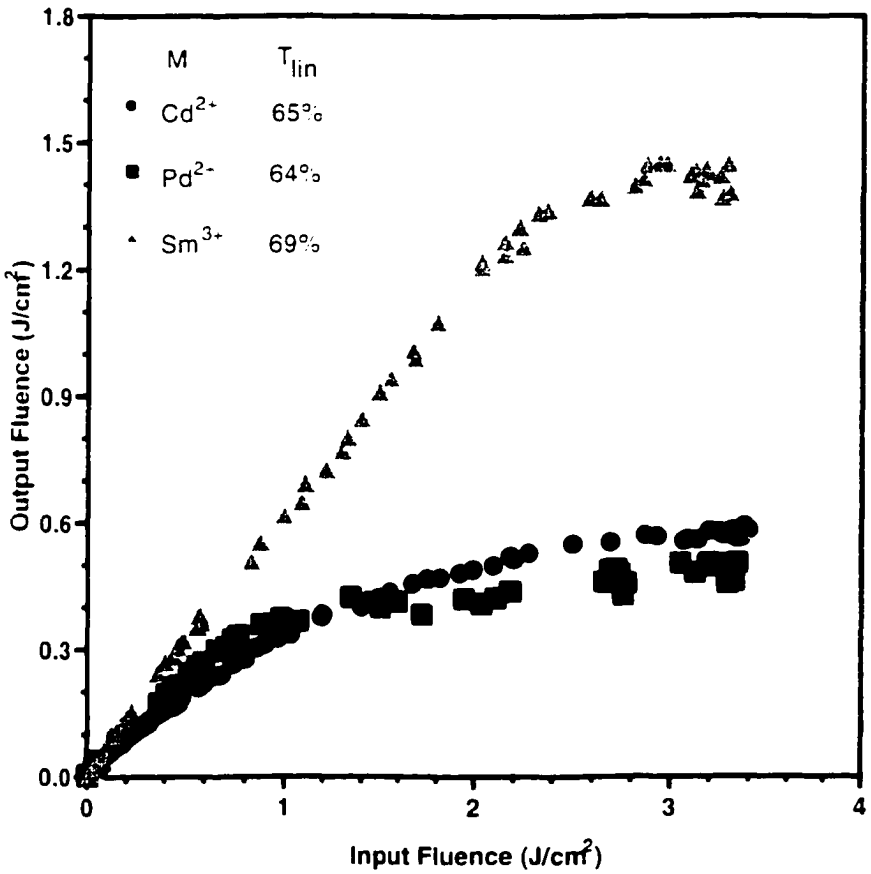

FIG. 16. Input versus output fluences of $[(C_6H_4\text{-APPC})M]Cl_n$ series with different metal centers. The excitation laser pulse width is 5 ns at 532 nm. The concentration is 3.4×10^{-4} mol/L in 2 mm cell. Complexes are dissolved in methanol except for $[(C_6H_4\text{-APPC})Pd]Cl$ in chloroform.

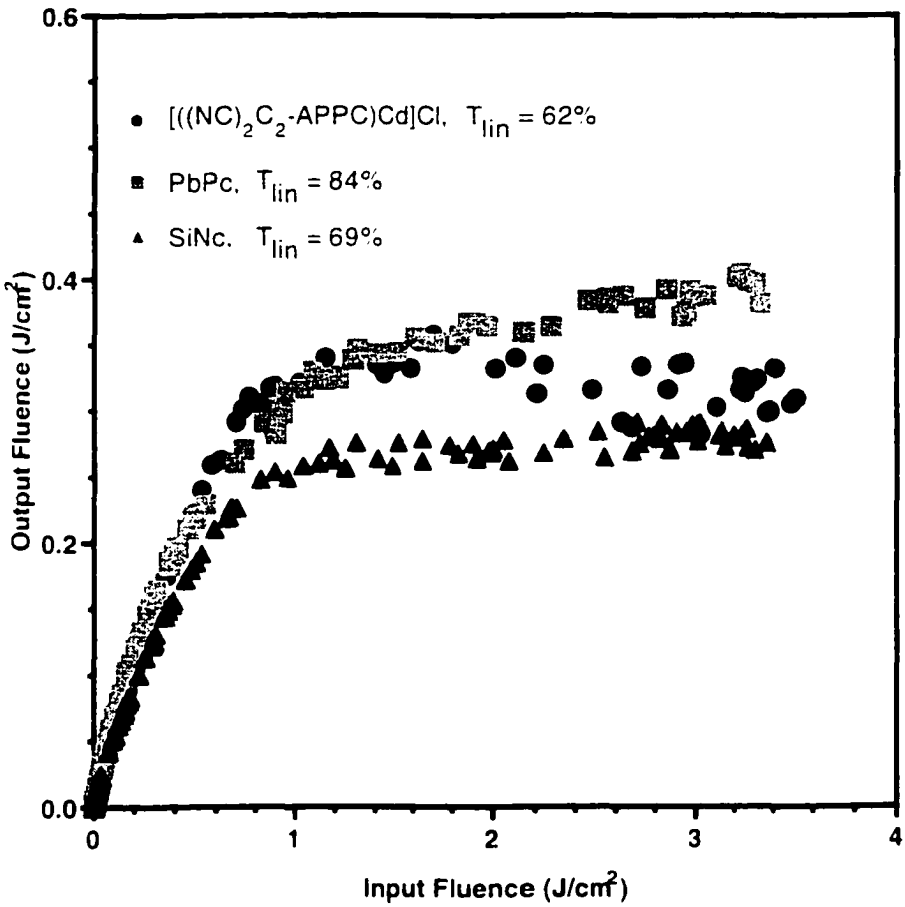

FIG. 17. Comparison of [((NC)$_2$C$_2$-APPC)Cd]Cl with PbPc and SiNc at the same concentration of 3.4×10^{-4} mol/L in 2 mm cell. The excitation pulse width is 5 ns at 532 nm. Complexes are dissolved in chloroform.

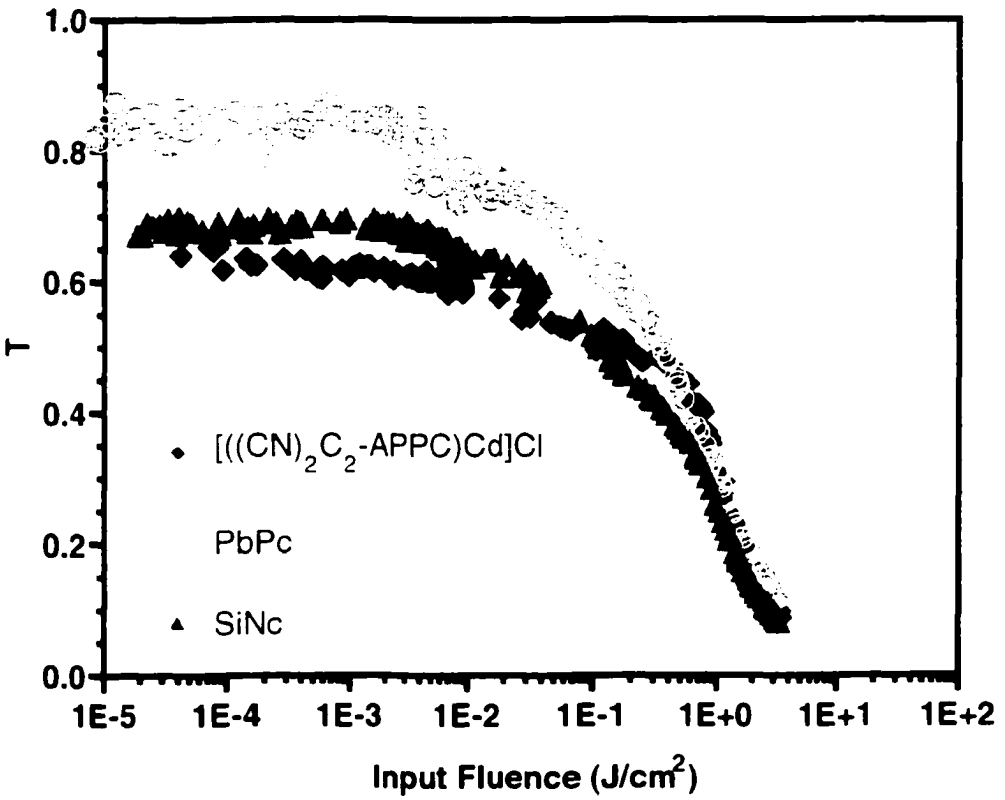

FIG. 18. Comparison in optical limiting performance of [((CN)$_2$C$_2$-APPC)Cd]Cl to SiNc and PbPc.

CHAPTER 4

TIME-RESOLVED DEGENERATE FOUR-WAVE MIXING

Experimental Description

We prepared a separate DFWM setup in addition to the normal DFWM shown in FIG. 6 and FIG. 7. The second setup was needed because TRDFWM required a different geometrical configuration when we introduced various delay elements for time-resolved measurements. In addition, some of the beam splitters must be replaced to accommodate different beam-splitting ratios. The actual experimental configuration is illustrated in FIG. 19. The main beam from the *Q*-switched mode-locked Nd:YAG picosecond laser (Continuum PY61) passes through variable attenuation elements (see FIG. 6) and splits into three beams just like the ordinary DFWM. However, for TRDFWM, an adjustable delay mechanism is adapted on the backward pump beam. The delay element consists of a right angle prism that utilizes a total internal reflection and a micrometer-equipped translation stage. The right angle prism is a very convenient optical element with which one can align the beam parallel to the direction of the translation of the prism by optimizing the energy of the retro reflection. This way, the spatial misalignment can be minimized for the full translation range of 50 mm. The full translation range gives a total time delay up to ~300 ps on the backward pump beam. The zero delay position is set near to one end rather than to the center of the translation stage in order to provide the maximum positive delay of 300 ps. The other delay element on the probe beam is only for the alignment purpose and is fixed throughout the procedures to maximize the spatial

and temporal overlapping of all three beams. Unlike the regular backward geometry DFWM (FIG. 7), where there are two strong counter-propagating pump beams and a weak probe beam, TRDFWM consists of strong forward and probe beams with a weak backward pump beam. The backward beam is attenuated using a beam splitter, and the input energy is monitored by the reflection from this beam splitter. The relatively stronger forward and probe beams interact with each other, forming the transient diffraction grating at the nonlinear optical sample, and the weak backward pump beam diffracts off this transient grating, giving out the phase conjugate signal of the probe beam. The phase conjugate signal, the forth beam, of the probe beam generated from the wave mixing of all three beams is monitored while varying the delay of the backward pump beam with respect to the forward and probe beams. The adjustable delay of the backward beam with respect to the forward and probe beams works as time gating via overlapping of different parts of the pulse in the temporal domain. This delayed pulse essentially takes a picture of the time evolution of this dynamic transient grating formed at the sample path length because all beams must not only spatially but also temporally overlap each other if wave mixing is to occur. The angle between the forward beam and the probe beam is about 7°, and the beam diameter is adjusted to about less than 2 mm by an appropriate telescope system.

The experimental procedures are as follows. First, the reference nonlinear material, CS_2, is measured. The phase conjugate signal of the probe beam is then collected while varying the delay on the backward pump beam. The micrometer in the prism translation stage is manually turned in steps by hand to give an optical delay. The actual optical delay is twice the micrometer displacement, thus giving the amplitude of

the phase conjugate signal as a function of the delay in time. Then, the procedure is repeated for the sample. Because the sample, one of a series of [(*R*-APPC)M]Cl_n complexes, has some linear absorption at this wavelength despite not being near the absorption maxima, the path length of the sample cell should be 2 mm or less in our geometry to minimize the saturation effects due to the possible linear and nonlinear absorption outside the spatially overlapping region. The cubic power relationship of the phase conjugate signal to the input intensity is verified by measuring the amplitude of the phase conjugate signal while varying the energy of the pulse.

For TRDFWM measurement, the solutions of [(*R*-APPC)M]Cl_n are prepared at varying concentrations so that they exhibit the same linear absorptions. The linear transmittances of these solutions were all 95% at 532 nm. All pulse energy measurements are done using Molectron joule meters Model J4-09 and J3S-10. The silicon-based J3S-10 series detector is used to measure the phase conjugate signal, which is typically a few hundred picojoules to a few nanojoules. To reduce the ever-present background scattering light going into the detector, this sensitive silicon detector is covered with dark cardboard and a small adjustable iris is placed in front of the detector window. Typical backgrounds are less than 100 pJ at low energies and up to 300 pJ at high energies even with these precautions. On each scan with a fixed energy, this background scattering light is measured by blocking one of the beams, preferably the forward pump beam. It is observed that the background stays fairly constant for each scan and can be subtracted from the total reading to get the actual phase conjugate signal. Typical reading of the phase conjugate signal is up to a few nanojoules. Any reading above 6 nJ is disregarded due to the limitations of linear response on the J3S-10 joule

meter. All the readings are recorded using a VI in LABVIEW software via GPIB. The VI is programmed to collect 30-50 data points at each delay position. The average is calculated from these points to minimize the effect due to laser pulse fluctuation. After the background is subtracted, the data points are normalized to the cubic power of the monitored input energy, ensuring the third-order effects because the phase conjugate signal is proportional to the cubic power of the input energy.

Dynamic Nonlinearity of APPC

The cubic power relationship of the phase conjugate signal to the input intensity for CS_2 is observed throughout the whole intensity regime. For the [(*R*-APPC)M]Cl_n samples, there are significant deviations from the cubic power relationship. A fitting function of the form $I_{pcs}=cI^b$, with the value b less than 3; sometimes even less than 2 is observed. This result may be due to some higher order saturation effects on nonlinearity resulting from linear and nonlinear absorption even at the low intensity regime.[83] The phase conjugate intensity is proportional not only to the cubic power of the excitation intensity but also to the fifth power, such that $I_{pcs}=cI^3+c'I^5$. This behavior is not unusual for this class of materials.[59] The same kinds of results were reported for the various similar classes of compounds.[25]

For TRDFWM, the measurements from CS_2 indicate that there is no significant transient effect of nonlinearity (FIG. 20) as indicated by an almost symmetric bell-shaped Gaussian. The response of the phase conjugate signal as a function of the temporal delay is almost the same as the expected autocorrelation of the excitation pulse width (~40 ps). As expected, the dynamic nonlinear response of CS_2, represented by the time evolution of

the phase conjugate signal, is sufficiently fast that the response is only limited by the pulse width. The response of CS_2 is consistent with the facts that there is no linear absorption for CS_2 at this wavelength (532 nm), and that the nonlinearity is predominantly due to molecular reorientation rather than electronic excitation. Any deviation from the autocorrelation of pulse width would result from the overall rotational reorientation time of CS_2, which is about 2 ps.[73] It should also be noted that any asymmetry is related to the difference between the rising time and the falling time in nonlinearity of CS_2.[84]

For [(C_6H_5-APPC)Cd]Cl, the transient response of nonlinearity is far different than for the nonabsorbing CS_2 sample (see FIG. 21). First, the transient response is not a symmetric bell shape due to some sort of decay mechanism. In addition, the transient response is not a single exponential decay; instead, there are at least two distinct dynamics present. One is a relatively faster process limited by the laser pulse width, and the other is a significantly slower process. It is very possible there may also be some sort of intermediate process.

Furthermore, as seen in FIG. 22, the response of [($OCH_3C_6H_5$-APPC)Cd]Cl is dependent on the input photon flux as previously reported in literature.[59] The faster process appears to be limited by the pulse width. Thus, the time scale of the process must be shorter than the 40 ps pulse width. As the photon flux varies, the two processes compete with each other, and the faster process becomes dominant as the photon flux increases. The dominance of the faster process results in a faster overall decay. We have previously reported another APPC complex that exhibits this kind of fluence-dependent dynamics.[85]

This unique fluence-dependent response can be explained as follows. The molecules in the first singlet excited state (S_1) are excited to the upper excited states (ESA) when there is enough photon flux. Then, the molecules will relax back to S_1. The time scale of this mechanism is expected to be very fast (picosecond regime or faster). Eventually, the population in S_1 relaxes to the first triplet excited state via intersystem crossing. These molecules are excited to the upper triplet states (ESA). This process is slower, hundreds of picoseconds, and gives the long tail on TRDFWM signal. As the photon flux increases, the probability of excitation to the singlet upper states from S_1 increases, causing a higher fraction of the excited state molecules in S_1 to undergo the faster process; the overall decay becomes more rapid. Many porphyrin and Pc complexes and organic polymers show a very similar behavior.[59,85-88]

Among seven [(*R*-APPC)M]Cl_n complexes that we measured (FIG. 21 to FIG. 27), only two complexes, [(C_6H_4-APPC)Cd]Cl and [($OCH_3C_6H_3$-APPC)Cd]Cl, show such a long-lived tail. These two complexes differ from the others in that both of them have high triplet quantum yields (0.91 and 0.89, respectively; see Table 3). The complex with the next highest triplet quantum yield among the seven complexes is [($NO_2C_6H_3$-APPC)Cd]Cl with a triplet quantum yield of 0.6; this complex does not show the long-lived tail. These data support the contention that the origin of this long-lived process is directly related to the triplet quantum yield. The very similar dependence of TRDFWM signature on the triplet quantum yield was also reported in the case of SiNc and PbPc, with a triplet quantum yield of 0.20 and 0.92, respectively.[23]

Among the series of [(*R*-APPC)M]Cl_n, [($C_{10}H_6$-APPC)Cd]Cl and [($(NC)_2C_2$-APPC)Cd]Cl show the best optical limiting performance (comparable with SiNc and

PbPc). However, TRDFWM results for these two complexes do not show any special characteristic signatures (see FIG. 24 and FIG. 25), leading us to believe that there is no direct correlation between the TRDFWM results and the OPL performances in the nanosecond regime. Both of these complexes show no tail that indicates any kind of slow transient effects; during the picosecond pulse duration (~40 ps), most nonlinear processes are expected to be faster than the pulse width. It should be noted that the triplet quantum yield of these complexes is expected to be quite low, which is in good agreement with the triplet quantum yield of [($C_{10}H_6$-APPC)Cd]Cl (0.32; see Table 3).

In general, the phase conjugate signal in DFWM is generated from the intensity-dependent nonlinear refractive index grating. This purely nonresonance process is related to the real part of $\chi^{(3)}$, which has no relationship to nonlinear absorption. When the material exhibits significant linear absorption, the population grating is formed in addition to the nonlinear refractive index grating. This population grating contributes to the phase conjugate signal and the nonlinear absorption, especially in the case of ESA. For our measurement of TRDFWM, the linear absorption was about 5% and the intensity of the pump and probe beam was significantly lower than the level that we observed optical limiting in nonlinear transmission measurement. Thus, it is possible that our TRDFWM signature was dominantly from the nonresonance refractive index grating instead of the population grating. This nonresonance process of nonlinear refractive index grating is indeed a very fast process and can contribute to the phase conjugated signal limited by the pulse width of 40 ps. This dominance of the nonresonance refractive index grating over the population grating may explain why most [(*R*-

APPC)M]Cl_n complexes did not show the slowly decaying tail, which is related to the excited state population grating.

Although the TRDFWM results do not allow the OPL performances of the complexes in the nanosecond regime to be predicted, these results still provide some very useful insights about dynamic properties of these complexes. For example, the triplet quantum yield values for [(C_6H_4-APPC)Pd]Cl and [($(NC)_2C_2$-APPC)Cd]Cl have not been reported; however, the results from TRDFWM suggest that those values are expected to be low.

There have been a few attempts to quantify the TRDFWM signatures of a similar class of OPL material. A numerical modeling of the transient index grating formed in nonlinear optical material during DFWM was suggested by some authors.[59] Nonetheless, it is not clear why the arbitrary fitting parameters were used in their model. These authors[59] succeeded in generating the shape of TRDFWM signature showing a multidecaying process in which each excited state, with an arbitrary weight, contributed to the overall transient response, but failed to relate their purely numerical model to the actual physical data. Another, much simpler approach is more common. Some authors[25,89] used a multiexponential function to fit the decaying part of TRDFWM results. The multiexponential function consisted of a laser pulse limited short lifetime decay and one or two relatively slower decays with unknown decaying constants. There are several issues with this type of approach that need some attention. First, the part limited by the laser pulse is not an exponential decay but is close to the autocorrelation of the excitation pulse and is a bellshaped Gaussian as has been seen in the case of CS_2 (FIG. 20). Second, the number of the fitting parameters must be considered. Even with a double

exponential function, there are at least three parameters: the weights of each decay and an unknown decay constant that is slower than the excitation pulse width by an order of magnitude. When this approach was used on our data, it was observed that the fitting was not very sensitive to these parameters, especially the slower decay constant. The uncertainties on these values are quite large; hence, the goodness and the sensitivity of fitting are not reliable. Currently, only qualitative analysis on TRDFWM is a reliable means of relating the measurement results to the physical parameters and hence to understanding the physics. In the future, though, it is anticipated that TRDFWM signature may be modeled numerically by solving the whole set of four coupled nonlinear Helmholtz equations using coupled-wave theory.[96] Although requiring significant computational resources, this approach should be the most nearly correct.

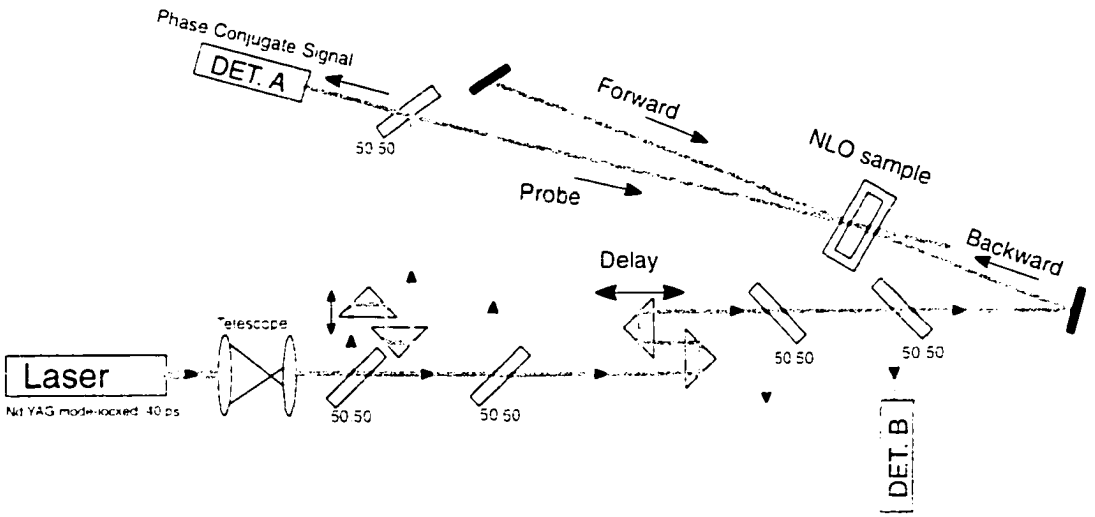

FIG. 19. TRDFWM experimental configuration. The pulse width is ~40 ps, and the repetition rate is 10 Hz. The actual beam splitting ratio of Forward: Probe: Backward: Monitor is 67:61:14:11.

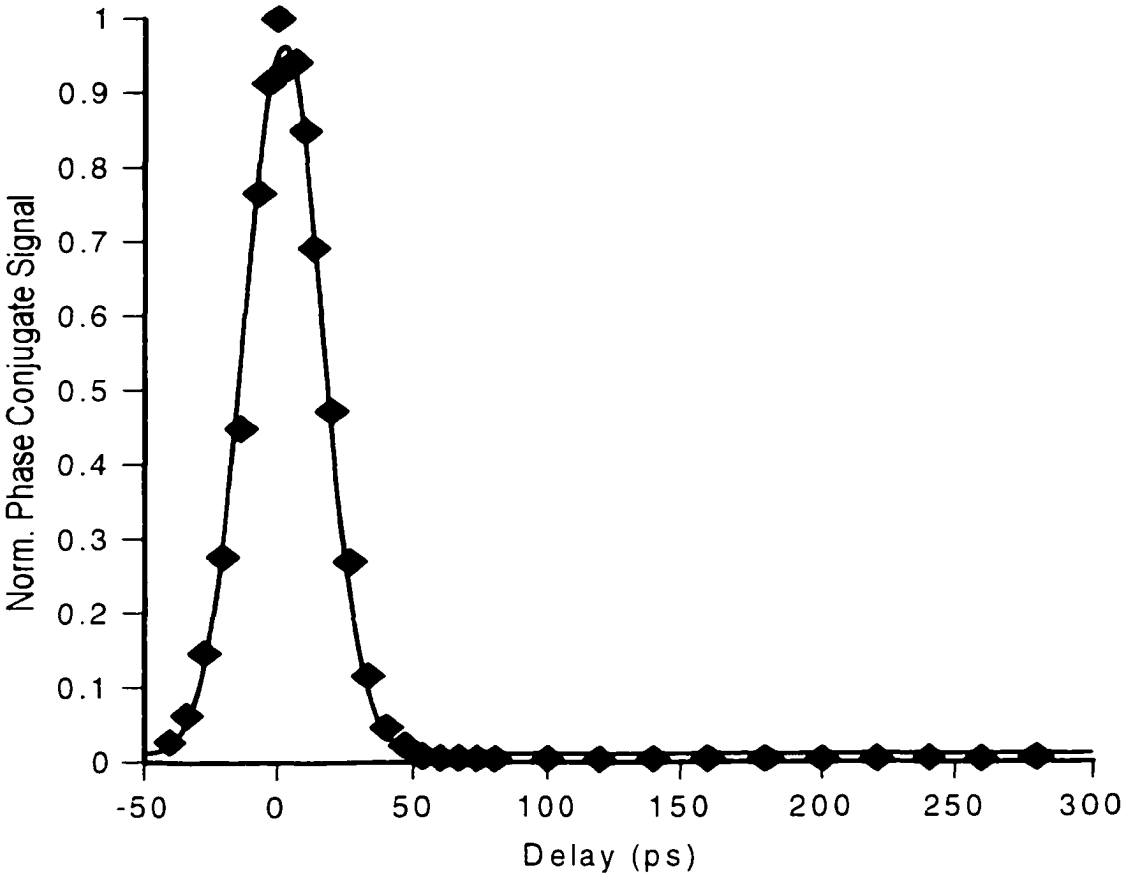

FIG. 20. TRDFWM response of CS_2 in a 1 mm quartz cell at 532 nm. The laser pulse width is 40 ps, and the repetition rate is 10 Hz. The solid line is the fitting to a Gaussian function.

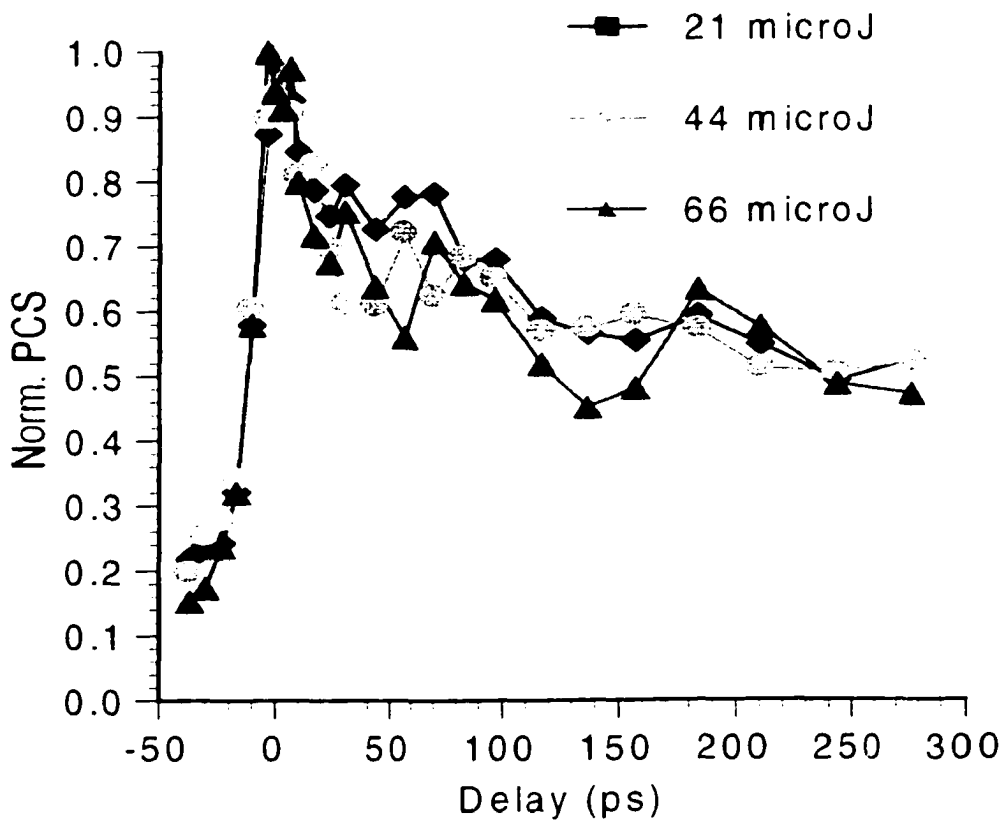

FIG. 21. TRDFWM response of [(C_6H_4-APPC)Cd]Cl in a 1 mm quartz cell at 532 nm. The solution is prepared in 8.02×10^{-5} mol/L in methanol.

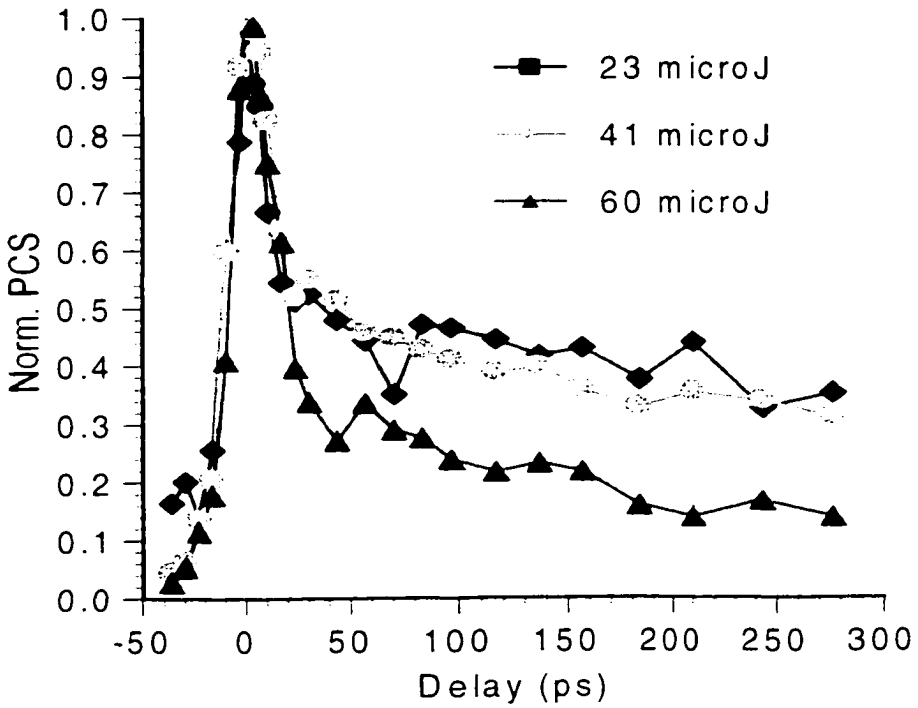

FIG. 22. TRDFWM response of [(OCH$_3$C$_6$H$_3$-APPC)Cd]Cl in a 1 mm quartz cell at 532 nm. The solution is prepared in 1.27×10^{-4} mol/L in methanol.

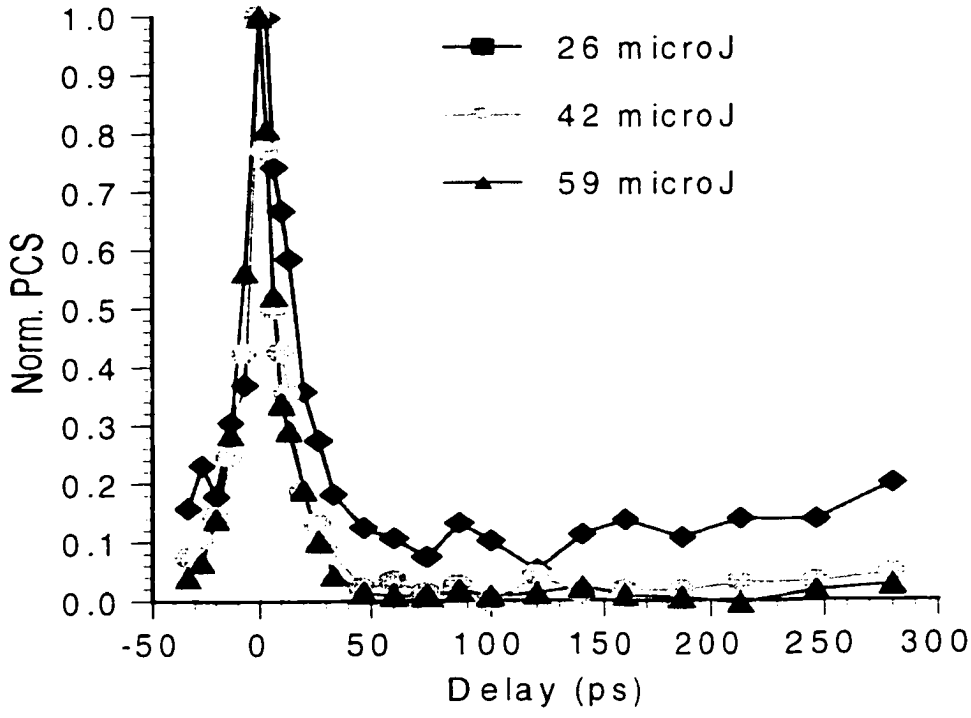

FIG. 23. TRDFWM response of $[(NO_2C_6H_3\text{-}APPC)Cd]Cl$ in a 1 mm quartz cell at 532 nm. The solution is prepared in 6.51×10^{-5} mol/L in methanol.

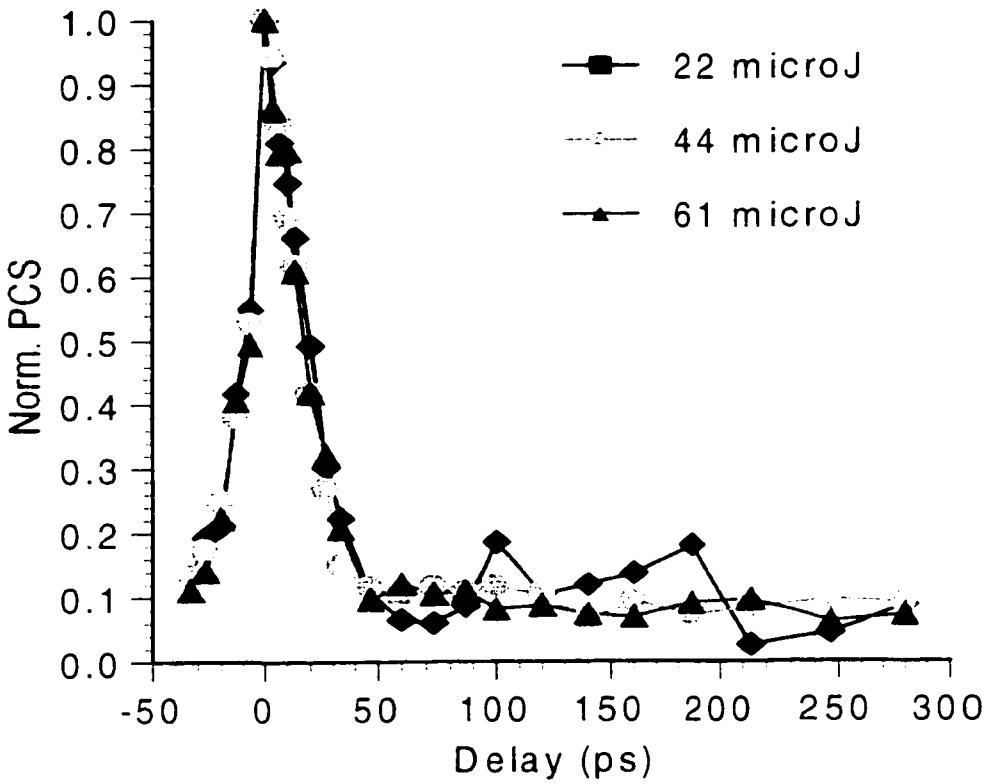

FIG. 24. TRDFWM response of $[((NC)_2C_2\text{-APPC})Cd]Cl$ in a 1 mm quartz cell at 532 nm. The solution is prepared in 5.31×10^{-5} mol/L in chloroform.

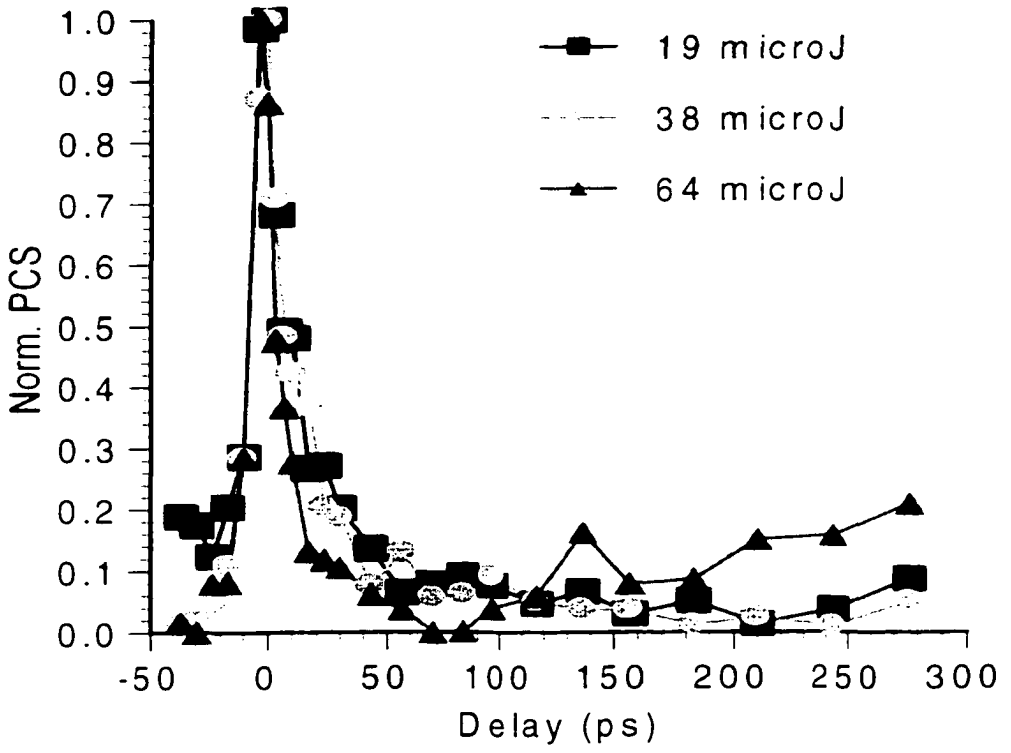

FIG. 25. TRDFWM response of [($C_{10}H_6$-APPC)Cd]Cl in a 1 mm quartz cell at 532 nm. The solution is prepared in 3.55×10^{-5} mol/L in methanol.

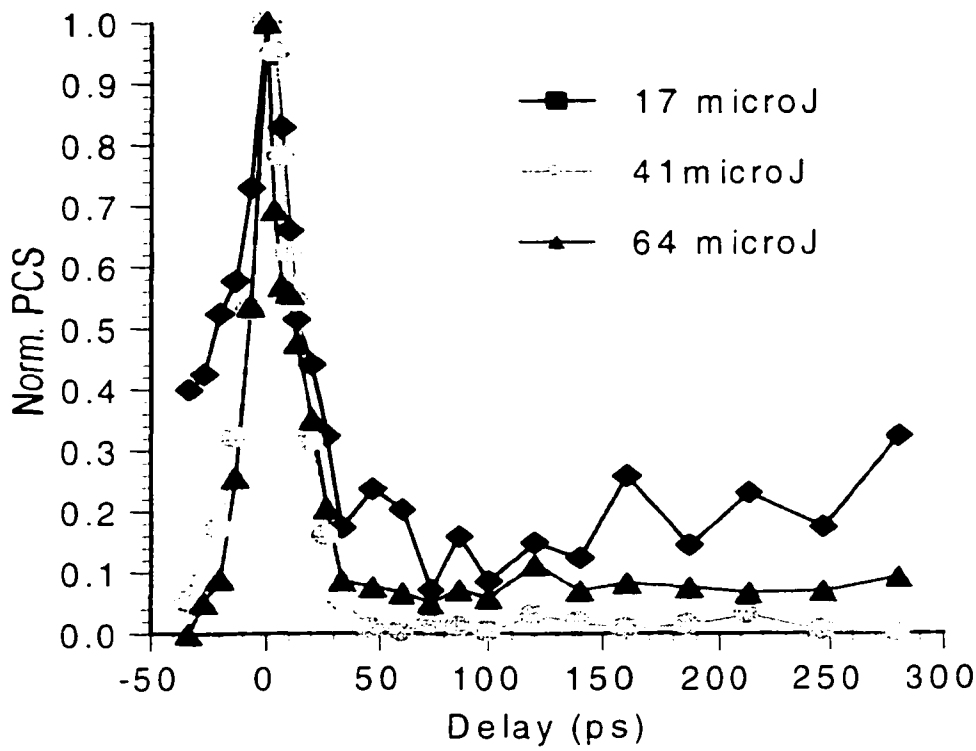

FIG. 26. TRDFWM response of [(C_6H_4-APPC)Pd]Cl in a 1 mm quartz cell at 532 nm. The solution is prepared in 4.72×10^{-5} mol/L in chloroform.

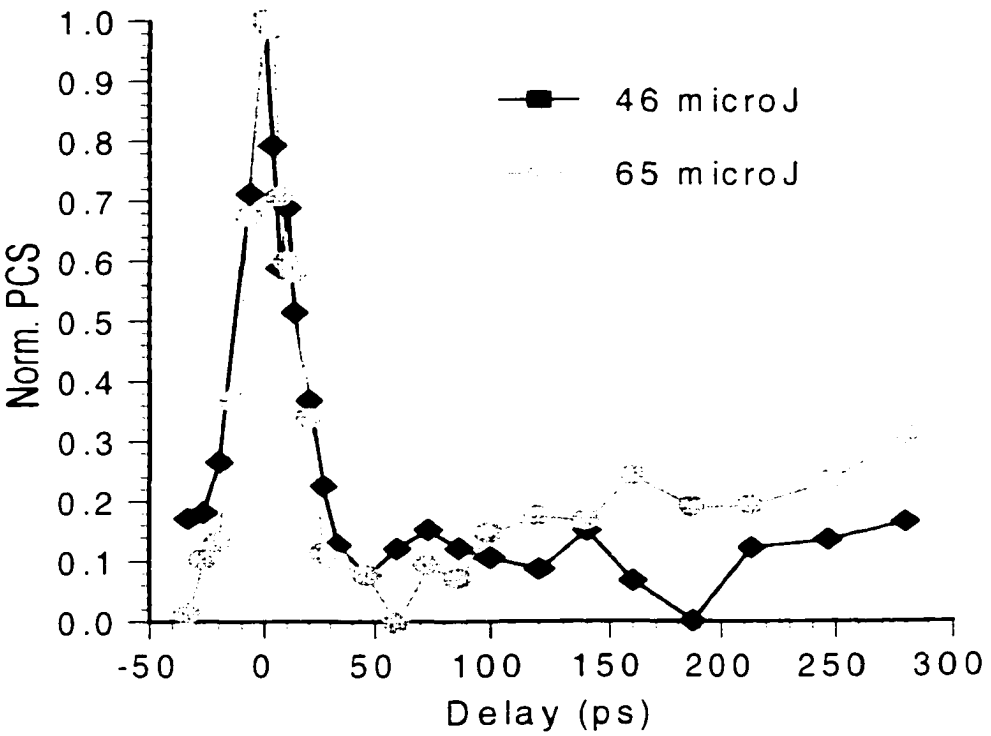

FIG. 27. TRDFWM response of $[(C_6H_4\text{-}APPC)Sm]Cl_2$ in a 1 mm quartz cell at 532 nm. The solution is prepared in 2.50×10^{-5} mol/L in methanol.

CHAPTER 5

EXCITED STATE LIFETIME OF THE APPC COMPLEXES

Six-Level System and Rate Equations

The dynamic processes such as absorption and emission of light between different energy levels are usually illustrated in a Jabłoński diagram named after Alexander Jabłoński, the father of fluorescence spectroscopy.[91] The dynamics of APPC can also be modeled in a six-level system as seen in FIG. 28. The molecules are first excited to the upper vibrational states of S_1 in the presence of excitation light (linear absorption). Then, the molecules collide immediately with surrounding neighbor molecules, quickly losing the energy and stepping down to the lowest vibrational level of the singlet excited state. This process is a nonradiative decay and relatively very fast (subpicosecond time scales). Once in the lowest singlet excited state, the molecules will remain in that state until they either emit the excess of energy in the form of fluorescence radiation and come back down to the ground state or are excited to the upper excited states in the presence of excitation light (ESA). The period during which the molecules stay in the excited state is called the lifetime of the excited state. The lifetime is the key parameter in understanding the dynamics of nonlinear optical phenomena involving excited states. The molecules in the lowest singlet excited state can also go on a different route to the triplet excited state through intersystem crossing (k_{isc}). After arriving in the lowest triplet excited state, the molecules are either excited to upper triplet excited states in the presence of excitation light (ESA) or slowly return to the ground state emitting the excess of energy in the form

of phosphorescence. Phosphorescence is a much slower process than fluorescence because it is a spin forbidden transition. Typical triplet excited state lifetimes of [(*R*-APPC)M]Cl_n are expected to be a few tens of microsecond.[56,57,92]

The dominant nonlinear mechanism in [(*R*-APPC)M]Cl_n is ESA. With nanosecond excitation, the ESA of [(*R*-APPC)M]Cl_n is expected to occur mostly in the triplet excited state. The measurements of the lifetime of the singlet excited states and the TRDFWM responses (see Chapter 4) would give some insights into the temporal dynamics of nonlinear responses for [(*R*-APPC)M]Cl_n and how these dynamic parameters are interrelated to each other. The measurements may also help in optimizing these complexes for better optical limiting performances by providing some knowledge about the parameters that are significant in the desired nonlinear response.

This six-level model can be described with a set of coupled rate equations for the population density (n_i) change in each state. The most important rate equations are for the ground state, S_1, and T_1.

$$\frac{dn_0}{dt} = -\frac{\sigma_0 I}{h\nu} n_0 + \frac{1}{\tau_{s1}} n_{s1} + \frac{1}{\tau_{t1}} n_{t1},$$

$$\frac{dn_{s1}}{dt} = \frac{\sigma_0 I}{h\nu} n_0 - \left(\frac{\sigma_{s1} I}{h\nu} + \frac{1}{\tau_{s1}} + \kappa_{isc} \right) n_{s1} + \frac{1}{\tau_{s2}} n_{s2}, \text{ and}$$

$$\frac{dn_{t1}}{dt} = \kappa_{isc} n_{s1} - \left(\frac{\sigma_{t1} I}{h\nu} + \frac{1}{\tau_{t1}} \right) n_{t1} + \frac{1}{\tau_{t2}} n_{t2}.$$

The equation for the propagation is

$$\frac{dI}{dz} = -(\sigma_0 n_0 + \sigma_{s1} n_{s1} + \sigma_{t1} n_{t1} + \cdots) I,$$

where $n_0(t \to -\infty) = N = n_0 + n_{s1} + n_{t1} + \cdots$, and $n_{s1}(t \to -\infty) = n_{t1}(t \to -\infty) = \cdots = 0$.

Here the internal conversion (nonradiative decay from the lowest singlet excited state to the ground state) is ignored initially for simplicity. The number density of the concentration is represented by N. The rate of intersystem crossing from S_1 to the lowest triplet excited state is k_{isc}. The intrinsic natural fluorescence lifetime of S_1 is denoted by τ_{s1}. The total fluorescence lifetime of S_1 is $(\tau_{s1}^{-1} + k_{isc})^{-1}$. The absorption cross section of each state is indicated by σ_i. The irradiance and the frequency of the irradiance are I and ν, respectively.

As seen in the above rate equations, the lifetime is a very fundamental parameter for the dynamic nonlinear process, along with the ESA cross sections. Absorption cross sections can be estimated by OPL measurements (see Table 1). To get more accurate values of σs, however, the rate equations have to be solved numerically, and the solution must fit the experimental data from nonlinear absorption measurements. This numerical fitting requires accurate measures of the lifetimes of S_1.

TCSPC Measurement

Fluorescent lifetime measurement, one of the most common experimental techniques in spectroscopy, is used in various fields, such as biology, chemistry, and physics. Fluorescence is the emissions of radiation when molecules in the excited state give up the energy and return to the lower state with the same spin, usually to the ground state. The lifetime of the excited state can be measured using laser excitation fluorescence. The relaxation of the excited state is monitored by TCSPC.[93,94]

The basic general theory behind fluorescence lifetime measurement is not complicated. A molecule is first excited by light. When decaying, the molecule gives off

fluorescence. Thus, one could retrace the decay by measuring the intervals between the excitation and the fluorescence. This measurement requires sophisticated timing equipment and a selective variety of optics. Especially in the case of a fast decay (less than a nanosecond), careful attention must be paid to every component to ensure the best temporal accuracy.

The detailed experimental configuration for TCSPC is illustrated in FIG. 29. The excitation light source is a femtosecond Ti:Sapphire laser (Coherent Mira 900) that is optically pumped by a diode-pumped solid state laser with an output power of 10 watts (Coherent Verdi V10). The Ti:Sapphire laser gives out very short pulses (less than 200 fs) and has a broad gain band that is tunable from 700 to 1000 nm in wavelength. This laser is an ideal excitation source for fast decaying lifetime measurements.

The repetition rate of the laser is 76 MHz, which corresponds to the pulse spacing of 13 ns. This high repetition rate is not desirable for our current timing electronics system. The maximum repetition rate that our electronics can handle is about 4 MHz. The high repetition rate of the Ti:Sapphire laser is lowered to 3.8 MHz (20 fold) using a pulse picker (Coherent 9200). This particular pulse picker utilizes Bragg diffraction of an acousto-optic cell made of TeO_2. The particular pulse in the pulse train is diffracted off the acousto-optic cell according to the desired repetition rate that can be adjusted from 4 KHz to 4 MHz. In principle, the output pulse energy should not decrease after the pulse picker; only the average output power should decrease. For this particular acousto-optic cell, the diffraction efficiency is greater than 60%. After the pulse picker, the frequency of the laser is doubled using second harmonic generation. For our lifetime measurements, the fundamental wavelength of the laser was tuned to 810 nm, which is

near the gain peak of Ti:Sapphire laser (780 nm). When the fundamental output of the laser is frequency doubled, the excitation source has a wavelength of 405 nm with a 3.8 MHz repetition rate.

The samples are placed in a 10 mm standard quartz fluorometer cell (Starna 23-I-10). The fluorescence band of [(*R*-APPC)M]Cl_n is expected to occur in the 750-1000 nm range. The fluorescence decay is expected to be a few hundred picoseconds. Typical photomultipliers (PMTs) used in fluorescence lifetime measurements have instrument responses of a few hundred picoseconds to a few nanoseconds, and these responses are not appropriate for the lifetime measurement of [(*R*-APPC)M]Cl_n. The MCP PMT from Hamamatsu (R3809-59) has a very fast instrument response time (<30 ps, the fastest in the current market) and a broad spectral response down to 1200 nm. Because this PMT has a significant responsivity in infrared, it must be cooled in order to reduce the dark current and for the fastest instrument response. We purchased a liquid-cooled thermoelectric housing (Products For Research PC352CE) especially designed for this MCP PMT. Before the PMT is used for measurement, this thermoelectric cooler must be turned on at least for 2 hours to cool down the PMT at 40°C below the ambient temperature. A continuous flow of regular tap water at about 10 gallons per hour was used as the cooling liquid. A high voltage power supply (Standford Research PS 350) is used to set a negative bias voltage of –3000 V in the PMT.

For collection of fluorescence data, a 2 inch diameter double convex lens with focal length of 75 mm is used between the sample cell and the PMT. The PMT has an 11 mm window, and we used a 10 mm sample cell. Thus, 1:1 magnification is optimum. To accomplish this magnification, the sample cell should be at twice the distance (150 mm)

of the focal length on one side of the lens, and the window of the PMT should be at the same distance on the other side. However, in order to allow for a small degree of misalignment, the magnification factor is adjusted to about 1.3 by placing the sample cell at 134 mm from the lens and the PMT window at 170 mm from the lens. To protect this very expensive and very sensitive PMT from any accidental exposure of light, an electrical shutter was attached in front of the window of the thermoelectric cooler housing. A manual switch can open the shutter only when the system is ready to collect the data. A couple of long pass optical filters (Edmund Optics, A32-763, Schott ref. vis GG495, 2 inch x 2 inch) are used right in front of the shutter window to block completely the excitation scattering light. The 50% cutoff wavelength of the filters is 495 nm. The 0.001% critical cutoff wavelength is 450 nm, and wavelength longer than 550 nm passes more than 99% of light. The excitation wavelength is 405 nm, with linewidth about 20 nm or less; the fluorescence band of the [(*R*-APPC)M]Cl_n samples is expected to range from 750 to 1000 nm. The filter will effectively block the scattering light and transmit the most of the fluorescence light.

Because the signal is weak and fast, extensive use is made of fast electronics for cutting down the noise and enhancing the signal. The excitation pulse is detected by a fast silicon-based photodiode (Electro-optic Technology, Inc. ET 2030). The photodiode has rise time and fall time of less than 300 ps and a window of 0.12 mm^2 and is negatively biased. The output of this photodiode is typically about a few hundred millivolts and 1 ns wide (FWHM). The fast pulsed output from the PMT goes through a preamplifier (EG&G Ortec, VT120C) to broaden the pulse enough for the following electronics. A constant fraction discriminator (PRA 1717, EG&G 583) inverts the

portion of the incoming pulse, delays that portion, and recombines with the rest of the pulse to minimize the time jitter due to the pulse height fluctuation. The constant fraction discriminator also sets the discriminator level for the PMT output. More detailed descriptions of the constant fraction discriminator can be found in standard references of TCSPC.[93,94]

In standard mode, the excitation pulse starts the counting and the fluorescence output stops the counting simply because that is what physically happens. The excitation precedes the fluorescence. However, in single photon counting mode, not every excitation produces a fluorescence photon. In fact, it is necessary to reduce the intensity of excitation enough that a fluorescence photon is detected once every 100 excitations or less in order to make sure that every fluorescence photon is indeed a single photon. In other words, the counting rate should be below 1% of the excitation repetition rate. As a result, most cycles in standard mode are wasted without the collection of any photon count; however, noise accumulates. Thus, reverse mode is adopted. In reverse mode, the pulse from fluorescence initiates the counting and the excitation pulse with some fixed delay stops the counting. The delay must be sufficiently long enough to allow 4-5 times of the lifetime to be measured.

A time-to-amplitude converter (PRA 1701) measures the time difference between these two pulses and converts the difference to different voltages. A multichannel analyzer with a personal computer interface (The Nucleus, Inc., PCA II) takes the readings, places them in the corresponding memory bin called a channel, and continues to build a histogram of counts versus, channels until a desired level of maximum counts is reached. In reverse mode, the histogram is horizontally flipped, showing the

fluorescence decay on the left side. In addition, a photon counter (PRA 1770) is used to monitor the excitation rate and the fluorescence signal count rate.

The measured response $F(t)$ is not exactly the fluorescence response $I(t)$. The measured response is actually the convolution of the instrumental response $P(t)$ and the fluorescence response $I(t)$.

$$F(t) = P(t) \otimes I(t) = \int P(t')I(t-t')dt', \tag{5.1}$$

where $I(t)$ is in general a weighted sum of multiexponentials. For our [(*R*-APPC)M]Cl_n complexes, we expect $I(t)$ to be a single exponential decay. The instrument response can be expressed as

$$\Delta t_m = \left[(\Delta t_e)^2 + \sum (\Delta t_i)^2 \right]^{\frac{1}{2}} \approx 90 ps. \tag{5.2}$$

The excitation pulse width at FWHM is represented by Δt_e (~200 fs). The instrument response of the *i*th component in the system at FWHM is represented by Δt_i (for example, PMT ~25 ps). The measured total instrument response at FWHM is Δt_m and is experimentally determined by replacing the sample with a scattering solution.

Before any sample measurement, the instrument response function (IRF) was first measured using a diluted solution of glycogen in water as a scattering sample. The long pass filters were removed during IRF measurement because the scattered light is at the excitation wavelength (405 nm). The procedures can be described as follows. First, the resolution of the channels is set. The resolution of the multichannel analyzer was set to 1 K=1024 channels. The resolution was measured using a time calibrator, a device that electronically generates a start pulse and a stop pulse with variable pulse spacing. The

pulse spacing was selected as 10 ns. The actual channel spacing was counted from the PC display as 521 channels between two pulses, giving a resolution of

$$\frac{10\text{ ns}}{521\text{ channels}} = 19.2\text{ ps/channels.}$$

After the calibration was done, the IRF was measured. The temporal width was found to be about 90 ps, less than 100 ps as expected with this fast MCP PMT with 25 ps response time. The rest of the broadening on IRF was due to the collective sum of the temporal responses of timing electronics [see Equation (5.2)]. According to our measured IRF, our instruments are capable of resolving less than 10 ps (10% of IRF) difference in fluorescence decay, which will be the overall resolution of our system. The typical IRF is plotted in FIG. 30.

After the IRF was consistently measured, the long pass filters were placed back in the position, and sample measurement was begun. Samples were prepared in appropriate solvents as stated in Table 3. Solutions were diluted to the concentration at which the absorbance at the excitation wavelength (405 nm) was 0.1 to 0.2. Because each [(*R*-APPC)M]Cl_n has a different fluorescence quantum yield, the intensity of the excitation light was adjusted for each complex to a counting rate of 2-3 K counts/s. Because the repetition rate of the excitation was 3.8 MHz, the maximum counting rate to ensure a single photon emission was about 40,000 counts/s. However, the MCP PMT also limited the counting rate even further, down to 20,000 counts/s, to avoid any harmful saturation effect. The range of the counting rates was well below all these figures ensuring single photon emissions and the safe use of the MCP PMT.

Singlet Excited State Lifetime of APPC

After data were collected, the binary file generated by the multichannel analyzer was converted to a text file for a deconvolution fitting procedure. A fluorescence decay data analysis software called FluoFit (PicoQuant) was used for fitting. This software can fit fluorescence decay data to a maximum of four exponential functions by reconvolution and has a very good user interface window in which users have full control over the fitting parameters, such as lifetime, background, and shift of IRF. FluoFit also reports the goodness of fit, represented by reduced chi-square, χ_R^2.

$$\chi_R^2 = \frac{1}{N-P}\sum_i \frac{(Decay(i)-Fit(i))^2}{Decay(i)} \tag{5.3}$$

where N is the number of fitted channels, P is the number of fitting parameters, and $Decay(i)$ and $Fit(i)$ are measured intensity and fitted intensity in i^{th} channel, respectively. The value of χ_R^2 close to 1 shows a good fit with fitting parameters that are proper representations of the actual data.[94]

All of the data showed acceptable degrees of χ_R^2, ranging from 1.09 to 2.16. First, attempts were made to fit the data to a single exponential function. With a single exponential function, χ_R^2 was unacceptably large (>10). As a result, the data were fitted to a double exponential function, and the results were significantly better despite a single exponential decay function overwhelming the other as seen in Table 4. The main decay constants initially had very small uncertainties (less than 1%). The values in Table 4 are actually the weighted averages with the second decay constants. The averaging yielded a little larger uncertainty on these values because the second decay constants carried much larger uncertainties, although they are only a few percentage points from the total weight.

The second decay constants in the double exponential function ranged from 1.1 to 1.6 ns for [(*R*-APPC)M]Cl_n complexes, with much larger uncertainties (about 10%) than the first decay constants. It is not clear at this point what the origin of this longer decay could be. Still, the large uncertainties on these values suggest that the origin could be just a noise from the timing electronics. These large uncertainties might explain the large χ_R^2 in the initial single exponential fitting, in which the slowly decaying photons were counted in significant numbers in tails.

TABLE 4. Lifetime of singlet excited states of [(*R*-APPC)M]Cl_n from TCSPC and the deconvolution fitting results.

Sample	τ_1 (ns)[a]	χ^2[b]	Weight (%)[c]	Solvent
[(C_6H_4-APPC)Cd]Cl	0.35	1.58	99.7	CH_3OH
[($OCH_3C_6H_3$-APPC)Cd]Cl	0.29	2.09	99.9	CH_3OH
[($NO_2C_6H_3$-APPC)Cd]Cl	0.33	2.16	99.8	CH_3OH
[($(NC)_2C_2$-APPC)Cd]Cl	0.16	1.20	99.9	$CHCl_3$
[($C_{10}H_6$-APPC)Cd]Cl	0.18	1.25	99.9	CH_3OH
[(C_6H_4-APPC)Pd]Cl	0.37	1.19	96.3	$CHCl_3$
[(C_6H_4-APPC)Sm]Cl_2	0.38	1.09	97.1	CH_3OH
SiNc	1.31	1.68	97.7	$CHCl_3$
$PbPc(CP)_4$	2.18	1.64	98.6	$CHCl_3$

a. These are weighted average values. The uncertainties are about 0.01 ns or less.
b. Reduced χ^2.
c. Weight of the single exponential when fitting to double exponentials.

As we expected, all [(*R*-APPC)M]Cl_n complexes have predominant singlet excited state lifetimes of less than 1 ns. From the triplet quantum yield, the intersystem crossing rate and the corresponding intersystem crossing time were calculated for each complex. The results are shown in Table 5. In addition, the intrinsic natural fluorescence lifetime, sometimes called radiative lifetime, is estimated and reported in the same table. The values of the natural fluorescence lifetimes are only estimates because the internal conversion, the nonradiative decay from the lowest singlet excited state to the ground state, might be significant and thus cannot be ignored in the whole dynamic process. The nonradiative decay does not affect our calculation of the intersystem crossing rate, however, because the measured fluorescence lifetime is the actual lifetime of the lowest singlet excited state and because the triplet quantum yield is defined as the ratio of the intersystem crossing rate to the total decay rate of the lowest singlet excited state that includes the nonradiative decay.

The effects of different secondary phenylene substituents (*R'*=H, OCH_3, NO_2) on the excited state lifetime are small as expected. The overall lifetime does not vary significantly (0.29 ns-0.35 ns). What is interesting is that the trend in the intersystem crossing rate parallels the trend of electron donor/acceptor ability. The electron donor (*R'*= OCH_3) shows the fastest intersystem crossing rate, while the electron acceptor (*R'*= NO_2) shows the slowest. The highest intersystem crossing rate among APPCs may explain the fluence dependence in the TRDFWM result of the [($OCH_3C_6H_3$-APPC)Cd]Cl complex (see FIG. 22), which is not observed in [(C_6H_4-APPC)Cd]Cl with an almost equally high triplet quantum yield. The intersystem crossing times of all three complexes are shorter than a nanosecond, which may explain why these three complexes showed

similar optical limiting performances when exposed to 5 ns pulses despite large differences in the triplet quantum yields (see Chapter 3). The results from OPL and the similar lifetimes of these complexes also suggest that the lowest triplet state absorption cross section of these three complexes, which is one of the most important parameters in optical limiting, would not differ much from one complex to another. This possibility will be verified in the near future when the numerical analysis on the rate equations is completed using the lifetime results of this work.[95] Although their OPL performances are similar, the alternation of the secondary substituents is still an important controlling parameter to adjust the effective spectral window of linear absorption for desired wavelength in OPL.

In the series of different bridging groups [R=$(NC)_2C_2$, C_6H_4, $C_{10}H_6$] with varying numbers of π electrons (18, 22, 26, respectively) in the ring structure, the lifetime varies significantly. Both $(NC)_2C_2$- and $C_{10}H_6$- show much faster overall decays (0.16 ns and 0.18 ns, respectively) in the singlet excited state than does the C_6H_4- complex. It should be noted that these are the two best optical limiters among APPCs that were characterized in this work. Such a short overall lifetime may explain why these two complexes still perform best in optical limiting despite relatively low triplet quantum yields. For example, the $C_{10}H_6$- complex has a triplet quantum yield of only 0.32, which is considerably lower than those of complexes with substituted phenylene groups. However, this complex still shows an intersystem crossing rate close to those of complexes with higher triplet quantum yield. The fact that the $C_{10}H_6$- complex shows better optical limiting performance with an intersystem rate comparable with those of the complexes with higher triplet quantum yield suggests that the triplet absorption cross

section would be relatively larger than the others. In the case of the $(NC)_2C_2$- complex, the value of the triplet quantum yield is not available currently. However, TRDFWM results (see FIG. 24) have suggested that the triplet quantum yield is low because the results did not show the slowly decaying tail. Then, for the same reasoning used in the case of the $C_{10}H_6$- complex, we can predict that the triplet absorption cross section of the $(NC)_2C_2$- complex would be larger than the others.

TABLE 5. Dynamic photophysical parameters of [(*R*-APPC)M]Cl_n.

Complexes	τ_S (ns)[a]	ϕ_T[b]	τ_{isc} (ns)[c]	k_{isc} (10^9 /s)[d]	τ_n (ns)[e]
[(C_6H_4-APPC)Cd]Cl	0.35	0.91	0.39	2.59	>3.90
[($OCH_3C_6H_3$-APPC)Cd]Cl	0.29	0.89	0.33	3.04	>2.66
[($NO_2C_6H_3$-APPC)Cd]Cl	0.33	0.60	0.55	1.83	>0.82
[($(NC)_2C_2$-APPC)Cd]Cl	0.16	--	--	--	--
[($C_{10}H_6$-APPC)Cd]Cl	0.18	0.32	0.56	1.79	>0.26
[(C_6H_4-APPC)Pd]Cl	0.37	--	--	--	--
[(C_6H_4-APPC)Sm]Cl_2	0.38	0.26	1.47	0.68	>0.52
SiNc	1.31	0.20[f]	6.56	0.15	>1.64
PbPc(CP)$_4$	2.18	0.92[g]	2.37	0.42	>27.25

a. $\tau_S = (k_{10} + k_{nr} + k_{isc})^{-1}$

b. $\phi_T = \dfrac{k_{isc}}{k_{10} + k_{nr} + k_{isc}}$, values from Table 3.

c. $\tau_{isc} = k_{isc}^{-1}$.

d. Calculated using b.

e. Intrinsic natural fluorescence lifetime, $\tau_n = k_{10}^{-1}$.

f. In benzene.[82]

g. Pb tetra(t-butyl)Pc in toluene.[40]

Varying the central metal center (M=Pd^{2+}, Cd^{2+}, Sm^{3+}) in the ring structure does affect the lifetime of the excited state. Moreover, the effect on the intersystem crossing rate, equivalently the triplet quantum yield, is quite noticeable. It is well known that heavier atoms (higher in atomic number) have larger effective spin-orbit couplings for π electrons and that this increases the intersystem crossing rate.[42,96] An opposite trend was observed in this study because the Sm^{3+} (atomic number 62) complex shows a considerably slower intersystem crossing rate than does the Cd^{2+} (atomic number 48) complex. This difference is due to the fact that Sm has f-orbitals in the outer shell, while Cd and Pd have d-orbitals. It is expected that the d-orbital electrons of the metal center interact more strongly with the conjugate ring structure of the [(*R*-APPC)M]Cl_n complexes. In fact, as has been seen from optical limiting performances, the [(C_6H_4-APPC)Sm]Cl_2 complex is a much poorer optical limiter than are the [(C_6H_4-APPC)Cd]Cl and [(C_6H_4-APPC)Pd]Cl complexes. Unfortunately, the triplet quantum yield of the [(C_6H_4-APPC)Pd]Cl complex is not available yet. However, just like the case of [(($NC)_2C_2$-APPC)Cd]Cl, the TRDFWM result (FIG. 26) suggests that this triplet quantum yield is between those of [(C_6H_4-APPC)Sm]Cl_2 and [($OCH_3C_6H_3$-APPC)Cd]Cl.

For comparison, the singlet excited state lifetimes of SiNc and PbPc(CP)$_2$ were also measured. These complexes are the best optical limiting materials in the current literature, and their singlet excited state lifetime and the triplet quantum yields in different solvents were previously reported. For SiNc in toluene, the lifetime of singlet excited state was reported as 3.2 ns,[43] and the intersystem crossing time was reported as 16 ns.[44] The lifetime of SiNc in dimethylformanide (DMF) was reported as 8.8 ns.[42] The lifetime of Pb(II)tetra(*t*-butyl)Pc in toluene was measured as 0.35 ns by a picosecond

pump-probe measurement at 700 nm[40] and 0.7 ns by TCSPC.[42] These results suggest that the dynamics of these complexes depend on the solvent. As a result, the triplet quantum yield and the intersystem crossing rates of these complexes reported in Table 3 and Table 5 should be viewed with some caution. Because we used chloroform, these values are only useful for estimation purposes and do not necessarily represent the real values in chloroform. Assuming that the triplet quantum yields do not vary much among different solvents, our values for lifetimes suggest their intersystem crossing rates are quite low. Still, both complexes exhibit the best optical limiting performance at 532 nm which implies that their triplet absorption cross sections would be much larger than those of the APPC complexes in this work.

In addition, the results from the lifetime measurements of the excited state also suggest that the slowly decaying tail of the TRDFWM results is the effect strictly of the high triplet quantum yield alone and that neither the actual value of the lifetime of the excited state nor the intersystem crossing time has a direct relation to the slowly decaying tail. For example, [($NO_2C_6H_3$-APPC)Cd]Cl, [(C_6H_4-APPC)Pd]Cl, [(C_6H_4-APPC)Sm]Cl_n, and SiNc show either comparable or even longer decay of the excited state and slower intersystem crossing times than do [(C_6H_4-APPC)Cd]Cl and [($OCH_3C_6H_3$-APPC)Cd]Cl with high triplet quantum yield. However, none of these complexes shows the slowly decaying tail in TRDFWM that is observed for [(C_6H_4-APPC)Cd]Cl and [($OCH_3C_6H_3$-APPC)Cd]Cl. Meanwhile, $PbPc(CP)_4$, with a high triplet quantum yield of 0.92, shows a similar slowly decaying tail in TRDFWM.[23]

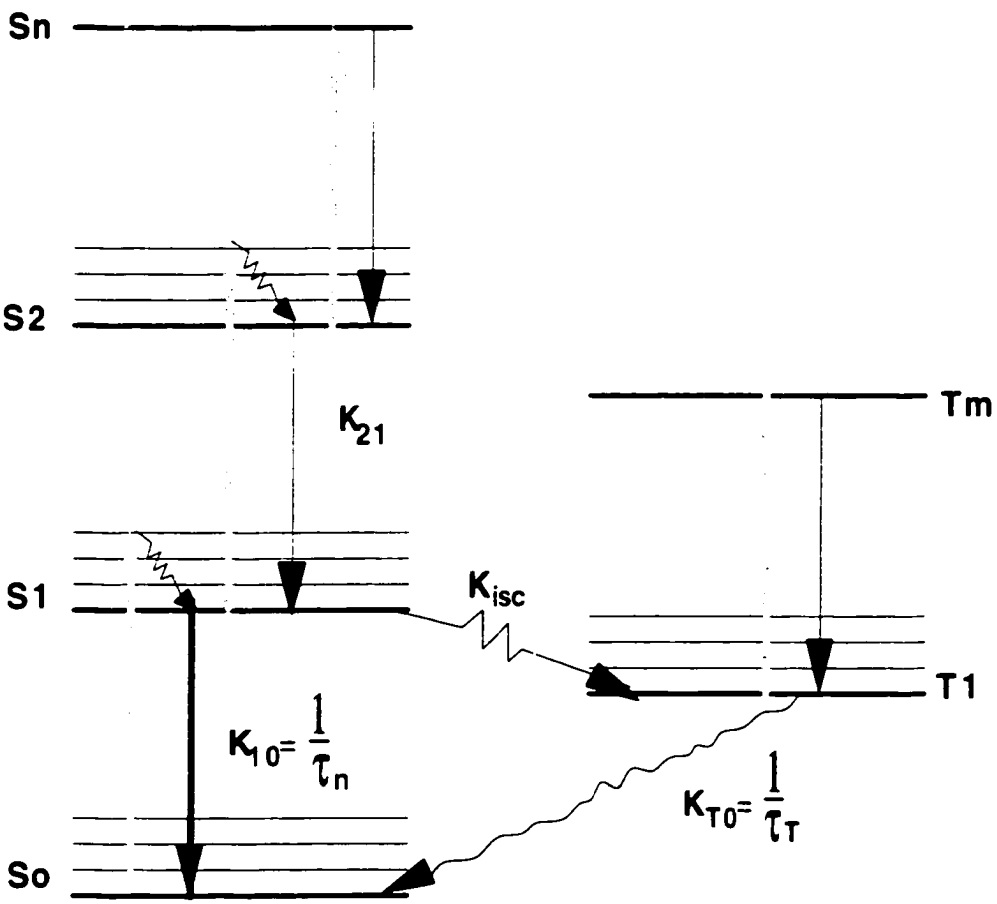

FIG. 28. A six-level Jabłoński diagram of [(*R*-APPC)M]Cl_n.

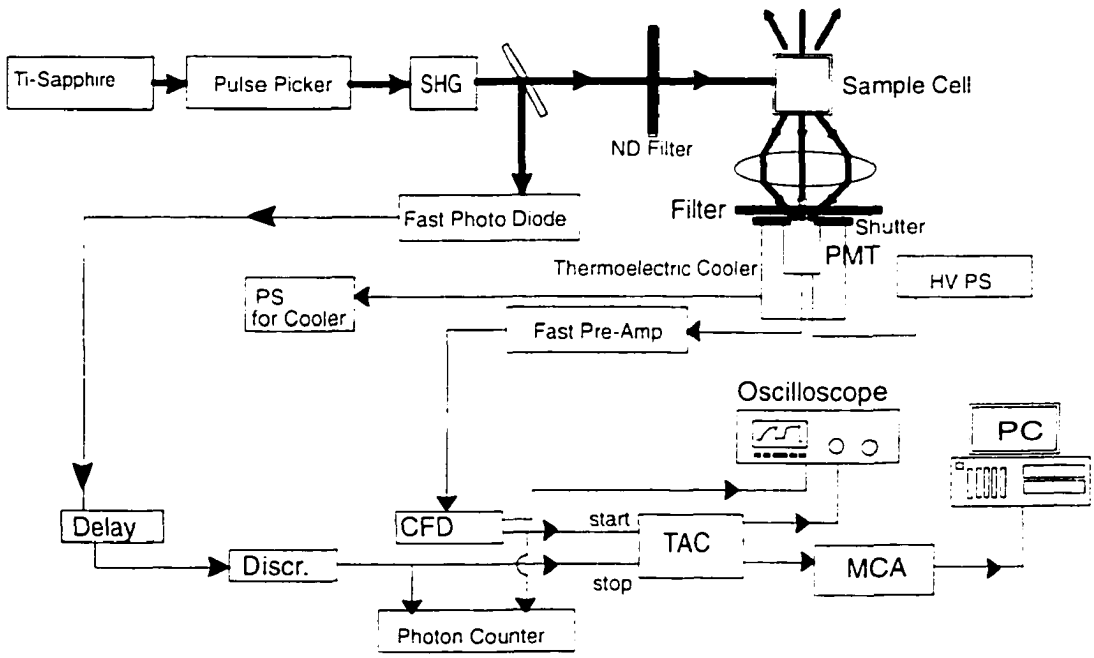

FIG. 29. Experimental configuration of TCSPC measurement.

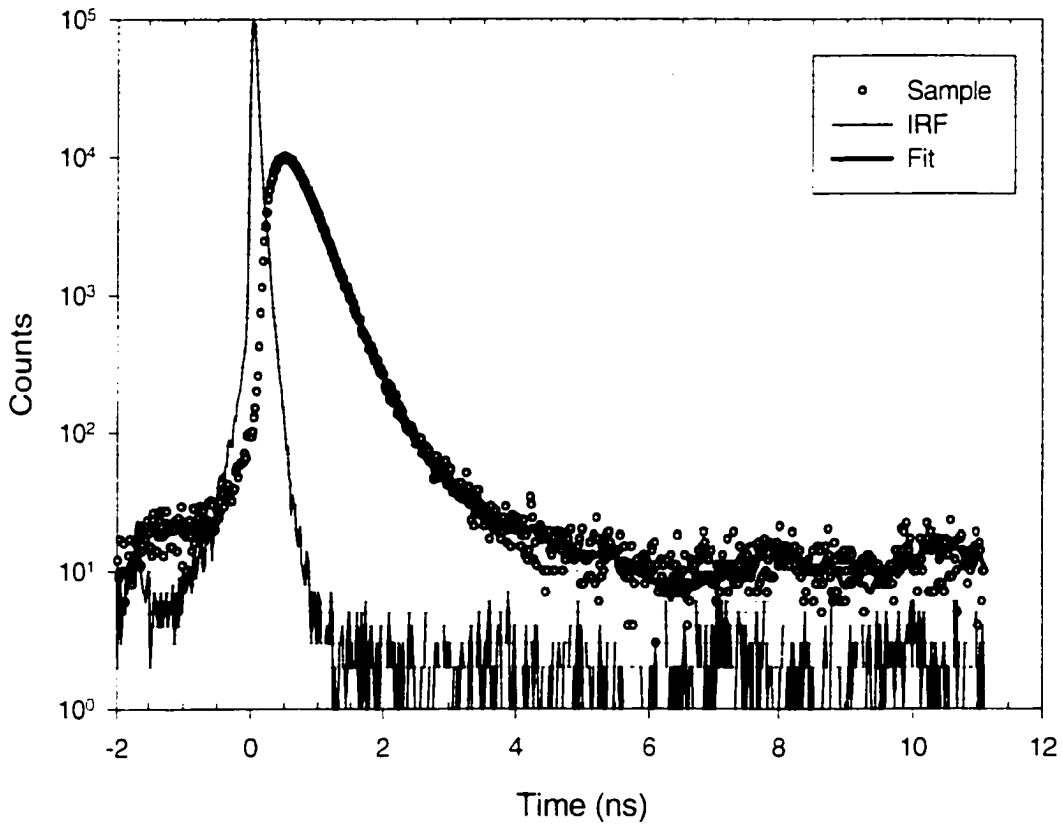

FIG. 30. TCSPC result of [(C_6H_4-APPC)Cd]Cl. The IRF has a response width of ~90 ps (FWHM). The thicker solid line indicates the fitting function of reconvolution with IRF.

CHAPTER 6

CONCLUSIONS

We have introduced a new class of nonlinear optical materials for OPL application. $[(R\text{-APPC})M]Cl_n$ complexes have a two-dimensional delocalized π-electron conjugated ring structure similar to metalloporphyrin and metallophthalocyanine. Unlike metalloporphyrin and metallophthalocyanine, the ring structure of $[(R\text{-APPC})M]Cl_n$ complexes can be easily modified, providing a possibility of optimization in nonlinear optical properties. We reported preliminary results of this possibility by varying secondary phenylene substituents (R'=H, OCH_3, NO_2 in R=$R'C_6H_3$), bridge groups inside the ring structure with different numbers of π electrons (R=C_6H_4, $(NC)_2C_2$, $C_{10}H_6$), and metal centers coordinating with the conjugate ring structure (M=Cd^{2+}, Pd^{2+}, Sm^{3+}).

In general, $[(R\text{-APPC})M]Cl_n$ complexes showed large third-order nonlinearities represented by the second-order molecular hyperpolarizability. The third-order nonlinearities of a series of $[(R\text{-APPC})M]Cl_n$ complexes were investigated by DFWM using 40 ps laser pulses at 532 nm with a repetition rate of 10 Hz. The molecular second-order hyperpolarizabilities for the $[(R\text{-APPC})Cd]Cl$ complexes are in the range of 2.6×10^{-31}-1.2×10^{-30} esu and are significantly larger than those of $PbPc(CP)_4$ and SiNc, two of the best optical limiting materials in current literature. The nonlinearities of the complexes are predominately electronic in origin and are sensitive to the nature of both the metal center and the ligand, suggesting that complexes with even larger molecular

second-order hyperpolarizabilities can be obtained by a judicious choice of ligands and metals.

Nonlinear absorption measurements were performed using a 5 ns pulsed laser at 532 nm with a repetition rate of 10 Hz. Most of these $[(R\text{-APPC})M]Cl_n$ complexes showed quite promising optical limiting performance through ESA. The induced absorption from the $[(R\text{-APPC})M]Cl_n$ complexes is sufficiently fast to provide optical limiting on a nanosecond scale. The optical limiting performance of these complexes is comparable with those of the most promising complexes in the literature. Moreover, these preliminary studies suggest that it will be possible to optimize the optical limiting properties of the complexes by varying the conjugated bridging *R* group and the metal center. Although varying the secondary phenylene substituent did not affect the optical limiting performances considerably, it was found that the secondary substituent could be a good controlling factor to adjust the linear absorption property so that the desired spectral window for optical limiting could be achieved.

The dynamics of nonlinear response was studied by TRDFWM using a 40 ps laser at 532 nm. Time evolution of the phase conjugate signal showed a faster process, indicated by the autocorrelation of the excitation pulse, and a relatively slower process, indicated by a slowly decaying tail. The results showed that the high triplet quantum yield close to 0.9 or above has a very strong correlation to the slowly decaying tail of the phase conjugate signal after the excitation. All other fast nonlinear process such as singlet ESA to the higher excited states, which is faster than the excitation pulse width, were hidden under the autocorrelation of the excitation pulse width. The complex with the fastest intersystem crossing rate showed fluence-dependent dynamics.

The lifetimes of singlet excited states were measured by TCSPC. The results showed that all of our [(*R*-APPC)M]Cl_n complexes have sub-nanosecond singlet excited state lifetimes from 0.16 ns to 0.3 ns. Due to high triplet quantum yield, some of the [(*R*-APPC)M]Cl_n complexes showed intersystem crossing rates greater than 3×10^9 s^{-1}, which is an order of magnitude higher than that of metallophthalocyanine. It is evident that a high intersystem crossing rate is one of the major factors in optical limiting of [(*R*-APPC)M]Cl_n.

This work is by no means a complete characterization of the nonlinear optical properties of [(*R*-APPC)M]Cl_n. As a preliminary study, we only tried several complexes with limited variation to test the possibility of optimization in optical limiting performance by structural modification. We showed that [(*R*-APPC)M]Cl_n complexes allow much more flexibility in structural variation than some of the well known best optical limiting materials. With further development, these complexes may ultimately prove to be an important new class of materials for OPLs.

This work is only a partial step to full characterization that would provide complete information about some of the controlling factors in optimization. The final goal is to develop the best optical limiter good enough to be an actual device. In order to do that, there are several aspects into which we have to look further. First and foremost, the numerical solution of the rate equation must be realized to fit the experimental data of optical limiting results accurately. This realization will give us the values for the ESA cross section, the key parameter in the ESA process, along with the intersystem crossing. In the past, the accurate fitting was not successful because the lifetime values were not available. The present dissertation research has now provided the singlet excited state

lifetime, along with the intersystem crossing rate, which is calculated from the triplet quantum yield. Currently, the numerical fitting of optical limiting results is on the way to completion by another graduate student[95] in our group, and the values of the ESA cross section will be available in the very near future. In addition, transient absorption measurement will be a very valuable tool to probing the absorption characteristics of the excited states experimentally. A transient absorption experiment is a more direct empirical approach to providing the absorption spectrum of the excited states.

Even with the information about the ESA cross section, additional work is also required to develop an actual device. The other work involves the field of chemistry. Once we have extended knowledge about the controlling factors, we have to work with chemists to predict and synthesize the complexes expected to have good optical limiting properties. To do this, another type of computational work is additionally needed to simulate the candidate complexes that have fast intersystem crossing and large ESA cross sections. So far, our complexes showed fast intersystem crossing rates and comparable ESA cross sections. By the judicious choice of the metal centers, the bridge groups, and the secondary substituents, it is expected that the absorption cross sections of the excited state can be enhanced. Among these preliminary [(*R*-APPC)M]Cl_n complexes, [$(NC)_2C_2$-APPC)Cd]Cl and [$(C_{10}H_6$-APPC)Cd]Cl could be the best materials with which to start because these complexes showed the best optical limiting. Especially, [$(C_{10}H_6$-APPC)Cd]Cl attracts particular attention because the complex has most number of π electrons and a wide optical window in the visible spectrum.

In addition, it is evident that the photophysical dynamics of this type of nonlinear material are significantly dependent on solvents, which means that their nonlinear

properties, including OPL performance, may be also dependent on solvents. Thus, the effect of various solvents should be studied to develop better optical limiters; such studies were beyond the scope of this dissertation.

In conclusion, [(*R*-APPC)M]Cl_n complexes are very promising candidates for OPL because of their large nonlinearities and their flexibility in structural modification to enhance the desired optical nonlinearity. Moreover, whatever materials we devise in the future by the structural modification of [(*R*-APPC)M]Cl_n, the series of experimental nonlinear optical characterization methods we developed here are the essential parts in developing effective OPLs.

LIST OF REFERENCES

1. J. P. Gordon, H. J. Zeiger, and C. H. Townes, Phys. Rev. **95**, 282 (1954).

2. J. P. Gordon, H. J. Zeiger, and C. H. Townes, Phys. Rev. **99**, 1164 (1955).

3. A. L. Schawlow and C. H. Townes, Phys. Rev. **112**, 1940 (1958).

4. T. H. Maiman, Nature **187**, 493 (1960).

5. P. A. Franken, A. E. Hill, C. W. Peters, and G. Weinreich, Phys. Rev. Lett. **7** (4), 118 (1961).

6. M. N. Islam, Physics Today **47** (5), 34 (1994).

7. R. A. Hann and D. Bloor, *Organic Materials for Nonlinear Optics*, (The Royal Society of Chemistry, Cambridge, 1989).

8. J. Messier, F. Kajzar, and P. Prasad, *Organic Molecules for Nonlinear Optics and Photonics*, in *NATO ASI Ser. E* (Kluwer Academic publishers, Dordrecht, 1991), Vol. 194.

9. P. N. Prasad and D. J. Williams, *Introduction to Nonlinear Optical Effects in Molecules and Polymers* (John Wiley & Sons, Inc., New York, 1991).

10. J. P. Hermann, Opt. Comm. **9**, 74 (1973).

11. K. C. Rustagi and J. Ducuing, Opt. Comm. **10**, 258 (1974).

12. C. Sauteret, J. P. Hermann, R. Frey, F. Pradere, J. Ducuing, R. H. Baughman, and R. R. Chance, Phys. Rev. Lett. **36**, 956 (1976).

13. G. M. Carter, Y. J. Chen, M. F. Rubner, D. J. Sandman, M. K. Thakur, and S. K. Tripathy, in *Nonlinear Optical Properties of Organic Molecules and Crystals*; edited by D. S. Chemla and J. Zyss (Academic Press, Orlando, 1987), Vol. 2, pp. 85-120.

14. J. P. Hermann, Opt. Comm. **12**, 102 (1974).

15. M. T. Zhao, B. P. Singh, and P. N. Prasad, J. Chem. Phys. **89**, 5535 (1988).

16. J. Hein, H. Bergner, M. Lenzner, and S. Rentsch, Chem. Phys. **179**, 543 (1994).

17. C. C. Frazier, S. Guha, W. P. Chen, M. P. Cockerham, P. L. Porter, E. A. Chauchard, and C. H. Lee, Polymer **28**, 553 (1987).

18. P. L. Porter, S. Guha, K. Kang, and C. C. Frazier, Polymer **32** (10), 1756 (1991).

19. S. R. Flom, G. C. Walker, L. E. Lynch, L. L. Miller, and P. F. Barbara, Chem. Phys. Lett. **154** (3), 193 (1989).

20. U. Gubler, C. Bosshard, P. Günter, M. Y. Balakina, J. Cornil, J. L. Brédas, R. Martin, and F. Diederich, "Scaling Laws of Second-Order Hyperpolarizabilities in Molecular Wires," presented at the Conference on Lasers and Electro-Optics, San Francisco, CA, 2000 (unpublished).

21. N. R. Armstrong, J. Porphyrins Phthalocyanines **4**, 414 (2000).

22. Z. Z. Ho, C. Y. Ju, and W. M. Hetherington III, J. Appl. Phys. **62** (2), 716 (1987).

23. J. S. Shirk, J. R. Lindle, F. J. Bartoli, Z. H. Kafafi, A. W. Snow, and M. E. Boyle, Int. J. Nonlinear Opt. Phys. **1** (4), 699 (1992).

24. D. V. G. L. N. Rao, F. J. Aranda, J. F. Roach, and D. E. Remy, Appl. Phys. Lett. **58** (12), 1241 (1991).

25. R. A. Norwood and J. R. Sounik, Appl. Phys. Lett. **60** (3), 295 (1992).

26. J. S. Shirk, J. R. Lindle, F. J. Bartoli, C. A. Hoffman, Z. H. Kafafi, and A. W. Snow, Appl. Phys. Lett. **55** (13), 1287 (1989).

27. J. S. Shirk, J. R. Lindle, F. J. Bartoli, and M. E. Boyle, J. Phys. Chem. **96** (14), 5847 (1992).

28. H. S. Nalwa, M. K. Engel, M. Hanack, and G. Pawlowski, Appl. Phys. Lett. **71** (15), 2070 (1997).

29. M. A. Diaz-Garcia, J. M. Cabrera, F. Agullo-Lopez, J. A. Duro, G. de la Torre, T. Torres, F. Fernandez-Lazaro, P. Delhaes, and C. Mingotaud, Appl. Phys. Lett. **69** (3), 293 (1996).

30. H. Tajalli, J. P. Jiang, J. T. Murray, N. R. Armstrong, A. Schmidt, M. Chandross, S. Mazumdar, and N. Peyghambarian, Appl. Phys. Lett. **67** (12), 1639 (1995).

31. B. K. Mandal, B. Bihari, A. K. Sinha, M. Kamath, and L. Chen, Appl. Phys. Lett. **66** (8), 932 (1995).

32. H. Hoshi, K. Kohama, S. Fang, and Y. Maruyama, Appl. Phys. Lett. **62** (24), 3080 (1993).

33. H. S. Nalwa and S. Kobayashi, J. Porphyrins Phthalocyanines **2**, 21 (1998).

34. N. Q. Wang, Y. M. Cai, J. R. Heflin, J. W. Wu, D. C. Rodenberger, and A. F. Garito, Polymer **32** (10), 1752 (1991).

35. K. Kandasamy, S. J. Shetty, P. N. Puntambekar, T. S. Srivastava, T. Kundu, and B. P. Singh, J. Porphyrins Phthalocyanines **3**, 81 (1999).

36. T. J. Bunning, L. V. Natarajan, M. G. Schmitt, B. L. Epling, and R. L. Crane, Appl. Opt. **30** (30), 4341 (1991).

37. R. Chari, S. R. Mishra, H. S. Rawat, and S. M. Oka, Appl. Phys. B **62**, 293 (1996).

38. L. W. Tutt and A. Kost, Nature **356**, 225 (1992).

39. D. R. Coulter, V. M. Miskowski, J. W. Perry, T.-H. Wei, E. W. Van Stryland, and D. J. Hagan, Proc. SPIE **1105**, 42 (1989).

40. J. W. Perry, K. Mansour, S. R. Marder, K. J. Perry, J. Alvarez, Daniel, and I. Choong, Opt. Lett. **19** (9), 625 (1994).

41. J. S. Shirk, R. G. Pong, F. J. Bartoli, and A. W. Snow, Appl. Phys. Lett. **63** (14), 1880 (1993).

42. K. Mansour, D. Alvarez, Jr., K. J. Perry, I. Choong, S. R. Marder, and J. W. Perry, Proc. SPIE **1853**, 132 (1993).

43. J. W. Perry, L. R. Khundkar, D. R. Coulter, D. Alvarez, Jr., S. R. Marder, T. H. Wei, M. J. Sence, E. W. Van Stryland, and D. J. Hagan, in *Organic Molecules for Nonlinear Optics and Photonics*, edited by J. Messier, F. Kajzar, and P. Prasad (Kluwer Academic Publishers, Dordrecht, 1991), Vol. 194, p. 369.

44. T. H. Wei, D. J. Hagan, M. J. Sence, E. W. Van Stryland, J. W. Perry, and D. R. Coulter, Appl. Phys. B **54**, 46 (1992).

45. W. Blau, H. Byrne, W. M. Dennis, and J. M. Kelly, Opt. Comm. **56** (1), 25 (1985).

46. G. L. Wood, M. J. Miller, and A. G. Mott, Opt. Lett. **20** (9), 973 (1995).

47. J. Staromlynska, P. B. Chapple, J. R. Davy, and T. J. Mckay, Proc. SPIE **2229**, 59 (1994).

48. W. Sun and D. Wang, Chinese Chem. Lett. **4** (3), 225 (1993).

49. W. Sun and D. Wang, Science in China (Series B) **39** (5), 509 (1996).

50. W. Sun, C. C. Byeon, C. M. Lawson, G. M. Gray, and D. Wang, Appl. Phys. Lett. **74** (22), 3254 (1999).

51. S. Guha, K. Kang, P. Porter, J. F. Roach, D. E. Remy, F. J. Aranda, and D. V. G. L. N. Rao, Opt. Lett. **17** (4), 264 (1992).

52. P. A. Miles, Appl. Opt. **33** (30), 6965 (1994).

53. J. W. Perry, K. Mansour, I.-Y. S. Lee, X.-L. Wu, P. V. Bedworth, C.-T. Chen, D. Ng, S. R. Marder, P. Miles, T. Wada, M. Tian, and H. Sasabe, Science **273**, 1533 (1996).

54. M. J. Miller, A. G. Mott, and G. L. Wood, Proc. SPIE **2853**, 2 (1996).

55. S. R. Mishra, H. S. Rawat, and M. Laghate, Opt. Comm. **147**, 328 (1998).

56. B. G. Maiya, A. Harriman, J. L. Sessler, G. Hemmi, T. Murai, and T. E. Mallouk, J. Phys. Chem. **93**, 8111 (1989).

57. J. Si, M. Yang, Y. Wang, L. Zhang, C. Li, D. Wang, S. Dong, and W. Sun, Opt. Comm. **109**, 487 (1994).

58. J. Si, M. Yang, Y. Wang, L. Zhang, C. Li, D. Wang, S. Dong, and W. Sun, Appl. Phys. Lett. **64** (23), 3083 (1994).

59. J. Si, Y. Wang, J. Zhao, P. Ye, D. Wang, W. Sun, and S. Dong, Appl. Phys. Lett. **67** (14), 1975 (1995).

60. Q. Gong, Y. Wang, S.-C. Yang, Z. Xia, Y. H. Zou, W. Sun, S. Dong, and D. Wang, J. Phys. D: Appl. Phys. **27**, 911 (1994).

61. W. Sun, C. C. Byeon, M. M. McKerns, G. M. Gray, D. Wang, and C. M. Lawson, Proc. SPIE **3472**, 127 (1998).

62. W. Sun, C. C. Byeon, M. M. McKerns, C. M. Lawson, G. M. Gray, and D. Wang, Appl. Phys. Lett. **73** (9), 1167 (1998).

63. J. L. Sessler and A. K. Burrell, "Expanded Porphyrins," in *Macrocycles*, edited by E. Weber and F. Vögtle (Springer, New York, 1991), Vol. 161, pp. 179-273.

64. G. M. Gray and C. M. Lawson, "Structure-Property Relationships in Transition Metal-Organic Third-Order Nonlinear Optical Materials," in *Optoelectronic*

Properties of Inorganic Compounds, edited by D. M. Roundhill and J. P. Fackler, Jr. (Plenum Press, New York, 1999), pp. 1-27.

65. R. G. Caro and M. C. Gower, IEEE J. Quantum Electron. **QE-18**, 1376 (1982).

66. N. Phu Xuan, J. L. Ferrier, J. Gazengel, and G. Rivoire, Opt. Comm. **51** (6), 433 (1984).

67. E. S. Gould, in *Mechanism and Structure in Organic Chemistry* (Holt, Reinhart and Winston, New York, 1962), p. 221.

68. F. W. Deeg and M. D. Fayer, J. Chem. Phys. **91**, 2269 (1989).

69. A. B. Myers and R. M. Hochstrasser, IEEE J. Quantum Electron. **QE-22**, 1482 (1986).

70. W. Hellwarth, Prog. Quant. Electron. **5**, 1 (1977).

71. D. J. McGraw, A. E. Siegman, G. M. Wallraff, and R. D. Miller, Appl. Phys. Lett. **54** (18), 1713 (1989).

72. J. Etchepare, G. G., J. P. Chambert, G. Hamoniaux, and A. Orszag, Opt. Comm. **63**, 329 (1987).

73. S. A. Jenekhe, W.-C. Chen, S. Lo, and S. R. Flom, Appl. Phys. Lett. **57** (2), 126 (1990).

74. J. A. Arnaud, W. M. Hubbard, G. D. Mandeville, B. de la Claviere, E. A. Franke, and J. M. Franke, Appl. Opt. **10** (12), 2775 (1971).

75. D. R. Skinner and R. E. Whitcher, J. Phys. E: Sci. Inst. **5**, 237 (1972).

76. Y. Suzaki and A. Tachibana, Appl. Opt. **14** (12), 2809 (1975).

77. A. H. Firester, M. E. Heller, and P. Sheng, Appl. Opt. **16** (7), 1971 (1977).

78. M. Mauck, Appl. Opt. **18** (5), 599 (1979).

79. J. M. Khosrofian and B. A. Garetz, Appl. Opt. **22** (21), 3406 (1983).

80. G. Brost, P. D. Horn, and A. Abtahi, Appl. Opt. **24** (1), 3840 (1985).

81. A. Hochbaum, Y. Y. Hsu, and J. L. Fergason, Proc. SPIE **2229**, 48 (1994).

82. P. A. Firey, W. E. Ford, J. R. Sounik, M. E. Kenney, and M. A. J. Rodgers, J. Am. Chem. Soc. **110** (23), 7626 (1988).

83. R. L. Sutherland, *Handbook of Nonlinear Optics* (Marcel Dekker, Inc., New York, 1996).

84. Y. Pang and P. N. Prasad, J. Chem. Phys. **93** (4), 2201 (1990).

85. W. Sun, C. C. Byeon, C. M. Lawson, G. M. Gray, and D. Wang, Appl. Phys. Lett. **77** (12), 1759 (2000).

86. Z. Z. Ho and N. Peyghambarian, Chem. Phys. Lett. **148** (2,3), 107 (1988).

87. B. P. Singh, M. Samoc, H. S. Nalwa, and P. N. Prasad, J. Chem. Phys. **92** (5), 2756 (1990).

88. M. K. Casstevens, M. Samoc, J. Pfleger, and P. N. Prasad, J. Chem. Phys. **92** (3), 2019 (1990).

89. P. Yuan, Z. Xia, Y. H. Zou, L. Qiu, J. Shen, Y. Shen, and H. Xu, Chem. Phys. Lett. **224**, 101 (1994).

90. B. E. A. Saleh and M. C. Teich, *Fundamentals of Photonics* (John Wiley & Sons, Inc, New York, 1991).

91. A. Jabłoński, Z. Phys. **94**, 38 (1935).

92. A. Harriman, B. G. Maiya, T. Murai, G. Hemmi, J. L. Sessler, and T. E. Mallouk, J. Chem. Soc.; Chem. Comm. **89**, 314 (1989).

93. D. V. O'Connor and D. Phillips, *Time-correlated Single Photon Counting* (Academic Press, London, 1984).

94. J. R. Lakowicz, *Principles of Fluorescence Spectroscopy*, 2nd ed. (Kluwer Academic Publishers, New York, 1999).

95. M. M. McKerns, *Characterization of Molecular Structure, Excited State Absorption, and Nonlinear Optical Resposnse of Metallotexaphyrin Complexes*, Ph. D. Dissertation, The University of Alabama at Birmingham, (in preparation), 2002.

96. J. H. Brannon and D. Magde, J. Am. Chem. Soc. **102**, 62 (1980).

APPENDIX

UNITS IN NONLINEAR SUSCEPTIBILITY AND NONLINEAR REFRACTIVE INDEX

From Maxwell's equations, the well-known wave equation can be derived for a dielectric medium.

$$\nabla^2\mathbf{E}(\mathbf{r},t)-\frac{1}{c_o^2}\frac{\partial^2}{\partial t^2}\mathbf{E}(\mathbf{r},t)=\frac{1}{c_o^2}\frac{\partial^2}{\partial t^2}4\pi\mathbf{P}(\mathbf{r},t)\ \text{(esu)}$$

$$\nabla^2\mathbf{E}(\mathbf{r},t)-\frac{1}{c_o^2}\frac{\partial^2}{\partial t^2}\mathbf{E}(\mathbf{r},t)=\mu_0\frac{\partial^2}{\partial t^2}\mathbf{P}(\mathbf{r},t)\ \text{(SI)} \qquad \text{(A.1)}$$

Here, c_o is the speed of light in vacuum, and $\mathbf{P}$ is the polarization of the medium such that

$$\mathbf{P}=\frac{1}{V}\sum_i^N\mathbf{p}=\frac{1}{V}\sum_i^N e\mathbf{r}_i,$$

where $\mathbf{p}_i=e\mathbf{r}_i$ is an individual dipole.

In a nonlinear medium, $\mathbf{P}$ can be expanded with higher order terms such that

$$\mathbf{P}_i=\chi_{ij}^{(1)}:\mathbf{E}_j+\chi_{ijk}^{(2)}:\mathbf{E}_j\mathbf{E}_k+\chi_{ijkl}^{(3)}:\mathbf{E}_j\mathbf{E}_k\mathbf{E}_l+\cdots\ \text{(esu)}$$

$$\mathbf{P}_i=\varepsilon_0(\chi_{ij}^{(1)}:\mathbf{E}_j+\chi_{ijk}^{(2)}:\mathbf{E}_j\mathbf{E}_k+\chi_{ijkl}^{(3)}:\mathbf{E}_j\mathbf{E}_k\mathbf{E}_l+\cdots)\ \text{(SI)} \qquad \text{(A.2)}$$

Here, Einstein's double index-sum rule is adopted. It should be noted that there might be different expansion coefficients associated with each higher order term, especially for some authors who use Taylor expansion to expand $\mathbf{P}$ as a power series. For example, $\chi_{ijk}^{(2)}=\frac{1}{2}d_{ijk}$, and many authors use d instead of $\chi^{(2)}$ in the second order term. It should also be noted that some authors prefer to absorb ε_0 into χ in higher order in SI system. In any case, readers should be aware of the several variations in defining the nonlinear susceptibilities in current literature when comparing the nonlinear optical parameters among different authors.

The polarization $\mathbf{P}$ can be divided into linear and nonlinear terms.

$$\mathbf{P}=\mathbf{P}^{lin}+\mathbf{P}^{nl},$$

where $\mathbf{P}^{lin} = \mathbf{P}^{(1)}$ corresponds to the first term on the right side of (A.2) and $\mathbf{P}^{nl} = \mathbf{P}^{(2)} + \mathbf{P}^{(3)} - \cdots$ corresponds to the rest of the higher order terms. As the expanded form of polarization as a function of the field vector is substituted in the wave equation (A.1), the wave equation is now modified with the nonlinear driving term.

$$\nabla^2\mathbf{E} - \frac{1}{c^2}\frac{\partial^2}{\partial t^2}\mathbf{E} = \frac{1}{c_n^2}\frac{\partial^2}{\partial t^2}4\pi\mathbf{P}^{nl} \quad \text{(esu)}$$

$$\nabla^2\mathbf{E} - \frac{1}{c^2}\frac{\partial^2}{\partial t^2}\mathbf{E} = \mu_n\frac{\partial^2}{\partial t^2}\mathbf{P}^{nl} \quad \text{(SI)} \qquad \text{(A.3)}$$

The speed of light from the left side of the original wave equation (A.1) is modified in such a manner that $c(=c_n/n_n)$ is the speed of light in the medium and n_n is the linear index of refraction, which originated from $\chi^{(1)}$. Without the driving nonlinear term on the right side ($\mathbf{P}^{nl}$=0), Equation (A.3) is just another homogeneous wave equation with propagation speed c rather than c_n describing the wave propagation in linear dielectric medium. Thus, we can see that light propagates with slower speed in the linear medium and none of the physics changes. Consequently, no nonlinear effect, such as wave mixing, is possible in the linear medium. It is quite obvious just by looking at the wave equation why presence of the driving nonlinear polarization term is needed to see nonlinear phenomena.

The displacement vector **D** relates the susceptibilities to the index of refraction, n.

$$\mathbf{D} = \varepsilon\mathbf{E} = n^2\mathbf{E} = \mathbf{E} + 4\pi\mathbf{P} \quad \text{(esu)}$$

$$\mathbf{D} = \varepsilon\mathbf{E} = \varepsilon_n n^2\mathbf{E} = \varepsilon_n\mathbf{E} + \mathbf{P} \quad \text{(SI)} \qquad \text{(A.4)}$$

Then, for the third-order materials, the index of refraction is modified with higher order of fields such that

$$n^2 = n_0^2 + 4\pi\chi^{(3)} : \mathbf{EE} \text{ where } n_0^2 = 1 + 4\pi\chi^{(1)} \text{ (esu)}$$

$$n^2 = n_0^2 + \chi^{(3)} : \mathbf{EE} \text{ where } n_0^2 = 1 + \chi^{(1)} \text{ (SI).} \qquad \text{(A.5)}$$

The index of refraction becomes

$$n = n_0(1 + \frac{4\pi\chi^{(3)} : \mathbf{EE}}{n_0^2})^{\frac{1}{2}} \approx n_0 + \frac{4\pi\chi^{(3)} : \mathbf{EE}}{2n_0} \text{ (esu)}$$

$$n = n_0(1 + \frac{\chi^{(3)} : \mathbf{EE}}{n_0^2})^{\frac{1}{2}} \approx n_0 + \frac{\chi^{(3)} : \mathbf{EE}}{2n_0} \text{ (SI).} \qquad \text{(A.6)}$$

Now we introduce the third-order nonlinear index of refraction n_2, sometimes called quadratic refractive index, which is related to the strength of quadratic field as

$$n = n_0 + \Delta n = n_0 + n_2 |\mathbf{E}|^2. \qquad \text{(A.7)}$$

Before we relate the nonlinear index of refraction to the nonlinear susceptibility, we have to consider a few important things, such as multiplication factors and degeneracy factors. We are interested in the third-order effects, so here we consider the case of either third harmonic generation or degenerate four-wave mixing (DFWM) for simplicity and all practical purpose despite the fact that some of the factors might remain the same in nondegenerate cases. As we define the field as real quantities, such as $\mathbf{E}(r,t) = \mathbf{E}_0(r)\cos(\omega t)$ or $\mathbf{E}(r,t) = \frac{1}{2}\mathbf{E}_0(e^{i\omega t} + e^{-i\omega t})$, the product of three degenerate fields yields the different multiplication factor depending on the nonlinear process in which we are interested such that

$$\mathbf{EEE} = \frac{1}{4}\mathbf{E}_0^3\cos(3\omega t) + \frac{3}{4}\mathbf{E}_0^3\cos(\omega t).$$

As we see here, there is a factor of 1/4 for third harmonic generation and a factor of 3/4 for DFWM. In addition, when we contract the tensor in (A.2), there will always be

degeneracy factors associated with the permutation of three different field vectors for different tensor components. For example, if we consider the case where all the three E-fields have the same polarization such that we are interested in $\chi^{(3)}_{1111}$, the degeneracy factor is 6 from the permutation of three different fields ($i = 1,2,3$). Comparing (A.6) and (A.7) and taking these factors into consideration, we get, for DFWM, the expressions for relating n_2 to $\chi^{(3)}$.

$$n_2 = \frac{2\pi\chi^{(3)}}{n_0^2}\cdot\frac{3}{4}\cdot 6 \ (\text{esu})$$

$$n_2 = \frac{\chi^{(3)}}{2n_0^2}\cdot\frac{3}{4}\cdot 6 \ (\text{SI}). \qquad (A.8)$$

In the current literature, we have to be extra cautious in keeping track of these factors because many authors omit either or both of these factors, implying that they are absorbed in χs. Some authors do not specify in their publication how they define the higher order susceptibilities incorporated with these factors. In those cases, it is almost impossible to make a meaningful comparison among any reported susceptibility values unless the value of a common reference material is reported in the same paper.

Sometimes in practice, n_2 is defined with intensity, I, rather than the quadratic field, such that

$$n = n_0 + n_2^I I. \qquad (A.9)$$

It should be noted that some authors use γ in place of n_2^I. In such a case, readers should be aware of the fact that the letter γ also represents the second-order molecular hyperpolarizability. For this reason, using the letter γ for nonlinear refractive index should be avoided to ease the confusion.

Here we have to be a bit more careful with different system of units because the intensity is defined differently in each system. The intensity, sometimes called *irradiance*, is optical power per unit area and is defined as the time average of Poynting vector, **S**. Thus, the intensity is expressed in terms of quadratic field in different ways, depending on the unit system of choice.

$$I = \frac{cn_0}{8\pi}|\mathbf{E}_0|^2 \text{ (esu)}$$

$$I = \frac{1}{2}n_0\varepsilon_0 c|\mathbf{E}_0|^2 \text{ (SI)} \tag{A.10}$$

Notice that some authors use complex amplitude of the field without an additional complex conjugate term, such as $\mathbf{E} = \mathbf{E}_0 e^{-i(\mathbf{k}\cdot\mathbf{r}-\omega t)}$. Then, there will be a factor of $(2)^2$ in (A.10). Using (A.7)-(A.10), the third-order susceptibility can be written in terms of n_2^I rather than n_2.

$$\chi^{(3)} = \frac{cn_0^2}{16\pi^2}\cdot n_2^I \cdot \frac{4}{3}\cdot\frac{1}{6} \text{ (esu)}$$

$$\chi^{(3)} = n_0^2\varepsilon_0 c\cdot n_2^I \cdot \frac{4}{3}\cdot\frac{1}{6} \text{ (SI)} \tag{A.11}$$

Equations (A.10) and (A.11) should be utilized with one important caution. The magnitude of c in esu differs by a factor of 100 from c in SI.

It should be noted that the linear susceptibility, $\chi^{(1)}$, is unitless regardless of the choice of unit system. However, the story is quite different with nonlinear susceptibilities. The higher order nonlinear susceptibilities carry all different units, depending on the order of nonlinearity and the choice of unit system. For example, the

unit of $\chi^{(3)}$ in esu is [cm/statvolts]^2 and in SI is [m/volts]^2. Using 1 statvolt = 299.8 volts, we can generate a conversion factor between $\chi^{(3)}$ in esu and $\chi^{(3)}$ in SI.

$$4\pi\chi^{(3)}_{esu} = (3\times10^4)^2 \cdot \chi^{(3)}_{SI} \tag{A.12}$$

The same story goes with the index of refraction. The linear index of refraction is not only unitless but also universal between the two unit systems. However, all the higher order nonlinear refractive indices carry different units. Then, it is very convenient to have conversion factors handy for each nonlinear refractive index. For example,

$$n_{2esu}(\frac{cm^2}{statvolts^2}) = (3\times10^4)^2 \cdot n_{2SI}(\frac{m^2}{volts^2}). \tag{A.13}$$

In addition to n_2, the relationship of n_2' in esu and in SI will be

$$n'_{2esu}(\frac{cm^2}{erg/s}) = 10^{-3} n'_{2SI}(\frac{m^2}{J/s}). \tag{A.14}$$

GRADUATE SCHOOL
UNIVERSITY OF ALABAMA AT BIRMINGHAM
DISSERTATION APPROVAL FORM
DOCTOR OF PHILOSOPHY

Name of Candidate Clare C. Byeon

Graduate Program Physics

Title of Dissertation Dynamic Nonlinear Optical Characterization of Asymmetric Pentaazadentate Porphyrin-like Metal Complexes for Optical Power Limiting Application

I certify that I have read this document and examined the student regarding its content. In my opinion, this dissertation conforms to acceptable standards of scholarly presentation and is adequate in scope and quality, and the attainments of this student are such that he may be recommended for the degree of Doctor of Philosophy.

Dissertation Committee:

Name	Signature
Christopher M. Lawson, **Chair**	
Gary M. Gray	
Ryoichi Kawai	
Jimmy W. Mays	
Sergey B. Mirov	
Thomas M. Nordlund	

Director of Graduate Program Suma Vohra

Dean, UAB Graduate School

Date 9/11/02